



# LUND UNIVERSITY

## On the Combustion Characteristics of Closely-Coupled LD Diesel Injection Strategies

Denny, Michael

2019

*Document Version:*  
Publisher's PDF, also known as Version of record

[Link to publication](#)

*Citation for published version (APA):*  
Denny, M. (2019). *On the Combustion Characteristics of Closely-Coupled LD Diesel Injection Strategies*. Department of Energy Sciences, Lund University.

*Total number of authors:*  
1

### General rights

Unless other specific re-use rights are stated the following general rights apply:  
Copyright and moral rights for the publications made accessible in the public portal are retained by the authors and/or other copyright owners and it is a condition of accessing publications that users recognise and abide by the legal requirements associated with these rights.

- Users may download and print one copy of any publication from the public portal for the purpose of private study or research.
- You may not further distribute the material or use it for any profit-making activity or commercial gain
- You may freely distribute the URL identifying the publication in the public portal

Read more about Creative commons licenses: <https://creativecommons.org/licenses/>

### Take down policy

If you believe that this document breaches copyright please contact us providing details, and we will remove access to the work immediately and investigate your claim.

LUND UNIVERSITY

PO Box 117  
221 00 Lund  
+46 46-222 00 00

On the Combustion Characteristics of Closely-Coupled LD  
Diesel Injection Strategies



# On the Combustion Characteristics of Closely-Coupled LD Diesel Injection Strategies

by Michael Denny



**LUND**  
UNIVERSITY

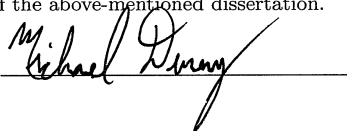
Thesis for the degree of Doctor of Philosophy in Engineering  
Thesis advisors: Dr. Öivind Andersson  
Faculty opponent: Dr. Stephen Busch

To be presented, with the permission of the Faculty of Engineering of Lund University, for public criticism in the M:B lecture hall at the Department of Energy Sciences on Friday, the 26th of April 2019 at 10:15.

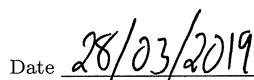
Organization <b>LUND UNIVERSITY</b> Department of Energy Sciences Box 188 SE-221 00 LUND Sweden		Document name <b>DOCTORAL DISSERTATION</b>	
		Date of disputation 2019-04-26	
Author(s) Michael Denny		Sponsoring organization	
Title and subtitle On the Combustion Characteristics of Closely-Coupled LD Diesel Injection Strategies:			
Abstract <p>Multiple-pilot injection strategies with both moderate and short time separations (dwells) are investigated in a light-duty diesel engine. Both conventional and optical engine experiments are performed. By implementing triple-pilot injection strategies with short dwells between the individual injections, combustion noise can be significantly reduced. The sound pressure level was reduced by nearly 4 dB compared to a conventional double-pilot injection strategy. This is significant since every 3 dB is a doubling of sound power. Reducing the combustion noise allowed for combustion to be phased to its peak efficiency point, improving gross efficiency by nearly 4%.</p> <p>A new metric, the ratio of reduced heat release (RRHR) was developed in order to analyze the heat release rate (HRR). This metric quantifies the magnitude of the undulations in the HRR and explains their influence on the combustion noise. It can explain the relative strength of frequency content in the combustion noise, indicate how the HRR should be modified to reduce combustion noise, and predict the total noise level at a specific load-speed point for different injection strategies.</p> <p>The combustion processes of conventional and closely-coupled strategies were studied in an optical engine. It was discovered that contact ignition stabilizes the combustion of subsequent fuel injected into prevailing combustion regions. Where a physical interface between the fuel and combustion region does not occur, that region has a significantly delayed ignition. Closely-coupling injections can lead to lower stability since the injections arrive sooner, at less developed stages of combustion. In this interface, hot combustion products are extinguished and replaced with cool ones which can add to the undulation in the HRR. In order to minimize its effects on combustion noise, this extinguishing phenomenon should be limited.</p> <p>A balance of mixture dilution, injection pressure, short injection separations, and injection rate shaping are utilized to create a quadruple-pilot injection strategy creating a near linear HRR progression and very low noise level.</p>			
Key words Diesel Combustion; Closely-Coupled Pilot Injections; Closely-Spaced Pilot Injections; Combustion Noise; Heat Release Rate Shaping; Multiple-Injection Strategies; Formaldehyde PLIF			
Classification system and/or index terms (if any)			
Supplementary bibliographical information		Language English	
ISSN and key title 0282-1990		ISBN 978-91-7895-064-5 (print) 978-91-7895-065-2 (pdf)	
Recipient's notes		Number of pages 166	Price
		Security classification	

I, the undersigned, being the copyright owner of the abstract of the above-mentioned dissertation, hereby grant to all reference sources the permission to publish and disseminate the abstract of the above-mentioned dissertation.

Signature



Date



# On the Combustion Characteristics of Closely-Coupled LD Diesel Injection Strategies

by Michael Denny



**LUND**  
UNIVERSITY

A doctoral thesis at a university in Sweden takes either the form of a single, cohesive research study (monograph) or a summary of research papers (compilation thesis), which the doctoral student has written alone or together with one or several other author(s).

In the latter case the thesis consists of two parts. An introductory text puts the research work into context and summarizes the main points of the papers. Then, the research publications themselves are reproduced, together with a description of the individual contributions of the authors. The research papers may either have been already published or are manuscripts at various stages (in press, submitted, or in draft).

**Cover illustration front:** Overlaid images of extinction of hotter (gray) combustion by cooler (blue) intermediate combustion products during a fuel injection. The combustion shown in gray is from natural combustion luminescence. The combustion shown in blue is from laser induced fluorescence.

**Funding information:** The thesis work was financially supported through the KCFP Engine research center. This center is funded by several industry partners and the Swedish energy agency, project numbers 22485-3, 22485-4.

© Michael Denny 2019

Faculty of Engineering, Department of Energy Sciences

ISRN: LUTMDN/TMHP-19/1148-SE

ISBN: 978-91-7895-064-5 (print)

ISBN: 978-91-7895-065-2 (pdf)

ISSN: 0282-1990

Printed in Sweden by Tryckeriet i E-huset, Lund University, Lund 2019

*To you, the Reader*





# Contents

List of publications . . . . .	iv
Acknowledgements . . . . .	v
Populärvetenskaplig sammanfattning . . . . .	vii
<b>1 Introduction</b>	<b>1</b>
1.1 Background . . . . .	1
1.2 Motivation . . . . .	2
1.3 Scope and Approach . . . . .	3
<b>2 Diesel Combustion</b>	<b>5</b>
2.1 Emissions From Diesel Engines . . . . .	6
2.1.1 Particulates . . . . .	6
2.1.2 Oxides of Nitrogen . . . . .	6
2.2 Quasi-Steady Conceptual Models . . . . .	7
2.3 Fuel Injection Systems . . . . .	10
2.3.1 Nozzles . . . . .	10
2.3.2 High Pressure Fuel Delivery . . . . .	12
2.4 Pilot Injections . . . . .	13
2.4.1 Effects on Noise, Soot, and NOx . . . . .	14
<b>3 Research Methods</b>	<b>19</b>
3.1 Data Mining . . . . .	19
3.1.1 Response Modeling . . . . .	19
3.1.2 Prediction . . . . .	21
3.2 Engine Experimentation . . . . .	21
3.2.1 Engine Control . . . . .	23
3.2.2 Considerations of Optical Engines . . . . .	24
3.3 Heat Release Analysis . . . . .	26
3.3.1 Calculation of the Heat Release Rate . . . . .	27
3.3.2 Ratio of Reduced Heat Release . . . . .	29
3.4 Noise Analysis . . . . .	31
3.4.1 Sound Pressure Level . . . . .	31
3.4.2 One-third Octave Bands . . . . .	32

3.4.3	Magnitude Spectrum . . . . .	32
3.4.4	Pressure Rise Rate . . . . .	32
3.5	Optical Analysis . . . . .	33
3.5.1	Line-of-Sight Imaging . . . . .	33
3.5.2	Planar Laser Induced Fluorescence . . . . .	33
3.5.3	Image Distortion Correction . . . . .	35
3.5.4	Combustion Area Growth . . . . .	36
3.5.5	Combustion Feature Tracking . . . . .	37
<b>4</b>	<b>Results</b>	<b>39</b>
4.1	Data Mining . . . . .	39
4.2	Investigation into Noise Minimization . . . . .	40
4.2.1	Injection Strategies . . . . .	40
4.2.2	Efficiency and Emissions . . . . .	41
4.2.3	Pressure . . . . .	42
4.2.4	Heat Release . . . . .	44
4.2.5	Conclusions . . . . .	46
4.3	Optical Investigation of the Combustion Progression . . . . .	47
4.3.1	Initial Combustion Development . . . . .	47
4.3.2	Contact Ignition . . . . .	48
4.3.3	Extinguishing of Prevailing Combustion . . . . .	51
4.3.4	Re-entrainment of Combustion Radicals . . . . .	52
4.3.5	Conclusions . . . . .	52
4.4	Investigations on the Extinguishing Phenomenon . . . . .	53
4.4.1	Temporal and Spatial POF Behavior . . . . .	53
4.4.2	Conclusions . . . . .	56
4.5	Minimizing Combustion Noise . . . . .	57
4.5.1	Dwells and Mixture Dilution . . . . .	57
4.5.2	Injection Pressure . . . . .	60
4.5.3	Noise Optimization . . . . .	61
4.5.4	RRHR as a Predictor of Noise . . . . .	63
<b>5</b>	<b>Conclusions</b>	<b>65</b>
<b>6</b>	<b>Future Outlook</b>	<b>69</b>
<b>7</b>	<b>References</b>	<b>71</b>
	<b>Scientific publications</b>	<b>77</b>
	Author contributions . . . . .	77
	Paper I: Impact of Closely-Coupled Triple-Pilot and Conventional Double-Pilot Injection Strategies in a LD Diesel Engine . . . . .	77

Paper II: Optical Investigation on the Combustion Process Differences between Double-Pilot and Closely-Coupled Triple-Pilot Injection Strategies in a LD Diesel Engine . . . . .	77
Paper III: Interaction between Fuel Jets and Prevailing Combustion during Closely-Coupled Injections in an Optical LD Diesel Engine . . . . .	78
Paper IV: Manipulating Heat Release Features to Minimize Combustion Noise . . . . .	78
Paper I: Impact of Closely-Coupled Triple-Pilot and Conventional Double-Pilot Injection Strategies in a LD Diesel Engine . . . . .	79
Paper II: Optical Investigation on the Combustion Process Differences between Double-Pilot and Closely-Coupled Triple-Pilot Injection Strategies in a LD Diesel Engine . . . . .	81
Paper III: Interaction between Fuel Jets and Prevailing Combustion during Closely-Coupled Injections in an Optical LD Diesel Engine	83
Paper IV: Manipulating Heat Release Features to Minimize Combustion Noise . . . . .	85

# List of publications

This thesis is based on the following publications, referred to throughout the text by their Roman numerals:

- I **Impact of Closely-Coupled Triple-Pilot and Conventional Double-Pilot Injection Strategies in a LD Diesel Engine**  
M. Denny, F. Holst, A. Helmantel, H. Persson, P. Tunestål, Ö. Andersson  
*Fuel*, vol. 246, February, pp. 141-148, 2019
  
- II **Optical Investigation on the Combustion Process Differences between Double-Pilot and Closely-Coupled Triple-Pilot Injection Strategies in a LD Diesel Engine**  
M. Denny, A. Matamis, Z. Wang, H. Persson, P. Tunestål, M. Richter, Ö. Andersson  
SAE Technical Paper, 2019-01-0022, 2019
  
- III **Interaction between Fuel Jets and Prevailing Combustion during Closely-Coupled Injections in an Optical LD Diesel Engine**  
M. Denny, A. Matamis, H. Persson, M. Richter, Ö. Andersson  
SAE Technical Paper, 2019-01-0551, 2019. To be published April 2nd, 2019.
  
- IV **Manipulating Heat Release Features to Minimize Combustion Noise**  
M. Denny, L. van den Ende, H. Persson, Ö. Andersson  
Submitted to *Fuel* on March 28th, 2019.

## Acknowledgements

When I stop and consider how it came to be that I'm writing this thesis, I should once again thank my Master's thesis supervisors, Fredrik Ekström and Sören Eriksson, from Volvo Cars. Had they not chosen me as their thesis worker, the chances are slim to none that I would've gone down this road towards a PhD. Without that connection I had to the advanced engine engineering section at Volvo Cars, I would not have been approached by our section manager, Lucien Koopmans, (whom I would also like to thank) about this industrial PhD position. To all those involved in the outline of this project and collaboration, thank you for recognizing in me the ability to tackle such a project, for encouraging me to apply for the position, and for making sure that the content aligned with my strengths to ensure the potential for success.

I am also grateful for having two very insightful, knowledgeable project supervisors to learn from: Håkan Persson, my industrial supervisor, and Övind Andersson, my academic supervisor. Thank you both for your critical feedback and direction throughout the project. Both of you taught me how to properly define, formulate and motivate research questions from a broad, scientific perspective. Early discussions with both of you were critical in getting me up to speed on the current state of the art knowledge of diesel combustion. Prior to this project, my knowledge was centered in SI combustion. I'd also like to thank Per Tunestål, my academic co-supervisor. Your help was very useful in the early PCA investigations and again later on regarding the flame front propagation speeds.

My managers at Volvo Cars, first Bengt Tullgren and now Carolin Wang-Hansen have been very supportive of my project throughout. I want to thank you both for continually following up and making sure that I was getting the support in the project that I needed. I never once felt like my project was on a lower priority than those more directly tied to production.

My more senior optical engines colleagues, Guillaume, Yann, Ted, Slavey, thank you for teaching me about the intricacies and limitations of optical engines. The same goes for my combustion physics colleagues, Zheming, Zhenkan, and Alexios for teaching me about the practical application of optical combustion diagnostics. Alexios and Zhenkan, we have spent many hours in the lab, and Alexios, many hours on the wrong side of midnight writing to meet deadlines. Both of your efforts have been critical to my project and we have made some excellent findings as a result of those efforts, if I do say so myself!

Pablo, not only were you a PhD student, you were the go-to guy for all things

LabView. Your knowledge of that program and its specific application to our test cells was both impressive and invaluable to me setting up my new engine installation. Your generous support of not only my project but other people's projects while you had challenges in your own was greatly appreciated. You often put the needs of others ahead of your own which says a lot of your good nature.

I must also thank the technicians for their support. Every one of you has played a role in my project. Your support was especially helpful since my time in Lund always had to be efficient. A very big recognition goes out to Tomas Lindén especially. Tomas was responsible for building my engine from a new design which had its shortcomings. Tomas, your ability to quickly identify design issues and resolve them with very proper, well considered and fabricated solutions meant a lot for the early success of my already delayed project.

In particular; Pablo, Marcus, Nhut, Sam, Vikram, Sebastian, Martin Tunér and Tomas, our talks about engines, cars, motorcycles, racing and the like were fun on any day, and refreshing when I needed to get my mind off of that day's challenges. In general to all my colleagues past and present at Lund, thank you for the good discussions, mutual commiseration over engine failures and tight paper deadlines, and for the fun times at the many dissertation parties, conference dinners, and Christmas dinners we've shared. Oh, and thank you Öivind for initiating fredagsfika at Lund. I'm not sure how you guys survived without it before.

I would also like to thank my family for their support. To my Mom and Dad, thank you for instilling in me the determination to take on challenges, finish what I started, and do the absolute best I can at whatever I commit to do. To my brothers, Christopher and Alex, thank you for the weekly intercontinental gaming sessions. Not only is it a good way to stay in touch, it provides some much needed stress relief at the end of some very taxing weeks. To my extended family, thank you all for the support and interest you showed in my studies here in Sweden.

# Populärvetenskaplig sammanfattning

Personbilar (allt från små bilar till lätta lastbilar) är ett av de främsta transportsätten i samhällen runt om i världen. De har blivit så utbredda, eftersom de tillåter människor friheten att resa vart och när de vill med bekvämlighets- och komfortnivåer som inte kan matchas av andra transportsätt. Ett alternativ till personbilar är kollektivtrafik. Men även i de storstäder där kollektivtrafiken är som störst är bilismen fortfarande utbredd tack vare de extra friheter och bekvämligheter den erbjuder. På grund av fördelarna och populariteten med detta transportsätt finns det nu i världen cirka 1 miljarder personbilar. I takt med att stora utvecklingsländer fortsätter att växa sig ekonomiskt starkare så kommer det antalet att öka.

Dessa fordon har dock också nackdelar. Förbränningsmotorerna som drivs av dessa fordon avger växthusgaser och vissa utsläpp, nämligen NO<sub>x</sub> och sotpartiklar, som kan orsaka hälsorisker i stora mängder. På grund av dessa nackdelar har vi över de senaste decennierna sett hur världen inför strängare lagstiftning och krav på fordonsutsläpp. Syftet med detta har varit att minska effekterna på den globala uppvärmningen som orsakas av växthusgasutsläpp och att minska hälsorisker som orsakas av luftföroreningar.

En föreslagen lösning för att minska de lokala utsläppen är att istället ha batteridrivna fordon. Stora delar av världen har emellertid inte helt förnybar och miljövänlig elproduktion. Detta flyttar de lokala utsläppen från ett område till ett annat. Det finns också farhågor kring miljöpåverkan av utvinningen av de stora mängderna ädelmetaller som skulle krävas för att producera hundratal miljoner batteripack för dessa elfordon (potentiellt över 1 miljard om man ponerar att byta ut hela världens bilflotta). År 2017 var mindre än 1% av världens fordon helt eldrivna. På grund av denna mycket låga marknadsandel, den långsamma tillväxt som elfordonsmarknaden uppvisar samt de tvivelaktiga lösningar på utsläpps- och växthusgasproblemen som implementeras, är fortsatt forskning och utveckling av förbränningsmotorer fortfarande mycket relevant.

En svårighet i denna utvecklingsprocess av förbränningsmotorer är att olika motoregenskaper ofta konkurrerar med varandra vilket oundvikligen leder till kompromisser. Ett exempel på en sådan situation kan vara bränsleförbrukning kontra utsläpp av NO<sub>x</sub>, sot och buller från dieselmotorer (som driver cirka 40% av personbilarna i Europa). Dessa attribut är ett resultat av förbränningsprocessen som används. Förbränningsbuller är inte bara viktigt för fordonets passagerare, men det förekommer spekulationer om att krav på ljudnivå från förbipasserande fordon även kan komma att implementeras i framtida fordonslagstiftning. Om



man vill förbättra bränsleekonomin och därmed sänka koldioxidutsläppen, resulterar det ofta i högre NO<sub>x</sub>- och bullerutsläpp. För att försöka lindra dessa och relaterade problem har det gjorts hårdvaruframsteg inom bränsleinsprutningstekniken. Dessa framsteg möjliggör nya strategier för bränsleinsprutningen som avsevärt förbättrar förbränningsprocessen. Att förstå hur förbränningsprocessen påverkas med denna nya teknik och hur detta kan förbättra motorns bränsleekonomi och utsläpp är målet med denna avhandling.

Moderna dieselmotorer har redan kapacitet att spruta in bränsle i flera individuella doser per förbränning. Huvuddelen av bränslet levereras i det som kallas huvudinsprutningar. Denna kan föregås och följas av flera mindre insprutningar som kallas pilot- respektive postinsprutningar. Den senaste bränsleinsprutningshårdvaran har gjort det möjligt för dessa insprutningar att vara tidsmässigt mycket närmare varandra än någonsin tidigare. Preliminära studier visade att detta kan leda till mer fördelaktig balansering mellan olika motoregenskaper, men orsakerna bakom dessa resultat var inte klara, och trenderna var inte heller konsekventa.

Genom undersökningarna i denna avhandling upptäcktes att förbränningsgenererat buller kan minskas kraftigt genom att lägga till ytterligare en pilotinsprutning. Samtidigt som tiderna för det två sista pilotinsprutningar och huvudinsprutningen sätts väldigt nära varandra ökas även storleken på samtliga pilotinsprutningar gradvis. Som jämförelse hade tidigare insprutningsstrategier endast två lika stora pilotinsprutningar vid måttliga tidpunkter. Genom att reducera förbränningsbullret öppnas upp möjligheten för att lägga förbränningen vid en mer gynnsam tidpunkt, vilket minskar både koldioxid- och sotutsläppen. NO<sub>x</sub>-utsläppen kan dock öka, men detta kan mildras genom att öka avgasåterledningen (EGR) till motorn. Detta skulle i sin tur kräva en ökning av bränsleinsprutningstrycket för att mildra sotförhöjningen orsakad av EGR-ökningen. Sambandet mellan dessa utsläpp är det som historiskt sett gjorde kompromisserna så svåra. Dessa nya resultat eliminerar inte kompromisserna, men de möjliggör en övergripande bättre balans.

Genom att studera hur den kemiska energin frigjordes när förbränningsprocessen fortskred, upptäcktes det att uppträddandet av denna värmefrigörelse är grundorsaken till förbränningsbullret. Ett nytt sätt att studera denna värmefrigörelsetakt skapades. Denna nya metod gör det möjligt att förstå vilka delar av värmefrigörelsen som leder till signifikanta nivåer av förbränningsbuller och hur man bör modifiera förbränningsprocessen för att minimera den.

Förbränningseffekterna av både konventionella och nya insprutningstrategier studerades i en motor med optisk access. Studierna möjliggjorde undersökning

av skillnaderna mellan dessa alternativ. Resultatet visade att efter de första pilotinsprutningar har börjat brinna, interagerar efterföljande insprutningar med den rådande förbränningen till större eller mindre omfattning beroende på tidpunkten för dessa insprutningar. Detta ledde till slutsatsen att insprutning av bränsle till mycket intensiva förbränningsområden delvis kan släcka förbränningen i delar av dessa regioner längs insprutningens riktning. Intensiv förbränning ersätts med mycket svagare och kallare förbränning. Medan minskningen av tidsfördröjningen mellan piloterna tenderar att jämna ut värmefrigörelsetakt och leda till lägre ljud, så kan släckningen orsaka en reduktion i värmefrigörelsetakt, vilket ger motsatt effekt. Detta indikerar att en noggrann balans krävs för att uppnå optimalt resultat.

Sammanfattningsvis har undersökningar i denna avhandling lett till bättre förståelse för hur förbränningsprocessen ska anpassas. Resultaten kan användas i syfte att uppnå en förbättrad balans mellan bränsleekonomi, utsläpp och förbränningsbuller, vilket inte var möjligt med tidigare hårdvaror. Dessutom har en ny analysmetod skapats, dels för att beskriva förändringarna i förbränningsbuller men även för att vägleda kalibreringsprocessen med möjligheten att skräddarsy förbränningsljudets egenskaper både i volym- och frekvensinnehåll.



# Acronyms

$f_0$  fundamental frequency

**CAD** crank angle degrees

**DFT** discrete Fourier transform

**ECU** engine control unit

**EGR** exhaust gas recirculation

**FIE** fuel injection equipment

**HRR** heat release rate

**LD** light-duty

**LTC** low temperature combustion

**MBT** maximum brake torque

**MFB** mass fraction burned

**MLR** multiple linear regression

**NL** natural luminosity

**P1, P2,...** pilot injection 1, 2,...

**PAH** poly-cyclic aromatic hydrocarbons

**PCA** principal component analysis

**PLSR** partial least squares regression

**POF** partially oxidized fuel

**PPRR** peak pressure rise rate

**TDC** top dead center. Can be preceded by “a” or “b” for after or before.

**UHC** unburnt hydrocarbon

**V1, V2,...** valley 1, 2,... in the HRR profile

# Chapter 1

## Introduction

### 1.1 Background

Personal vehicles (ranging from small cars to light trucks) are one of the prime movers of societies around the globe. They have become so widespread because they allow people the freedom to travel where and when they please with levels of convenience and comfort which cannot be matched by other modes of transportation. One alternative to personal vehicles is public transportation. However, even in the most connected large cities, cars are still prevalent. Due to their benefits, their popularity has led to approximately 1 billion passenger cars across the globe [1]. That number has been growing and is expected to continue to do so in the future. While recent sales in some markets have started to fall, the total number of passenger cars in the world continues to increase [1, 2, 3].

These vehicles also have drawbacks. The combustion engines powering them emit greenhouse gases and pollutants, such as  $\text{NO}_x$  and soot, which in high quantities are hazardous to health [4, 5]. Due to these drawbacks, the last several decades have seen worldwide legislation impose stricter and stricter requirements on vehicle emissions [6]. The aim of this has been to reduce the impact on global warming caused by greenhouse gas emissions and to reduce health risks caused by air pollution.

One proposed solution to reduce local emissions is to instead have battery electric vehicles. Much of the world, however, does not have completely renewable, pollutant free electricity generation [7]. This moves the local emissions from one area to another. The growth of electric vehicles has also been very slow.

As of 2017, less than 0.5% of the vehicles in the world were electrically driven and sales only increased by 1 million units annually since 2015 [8]. Considering a large increase in that number, there are then concerns on the environmental and human impact of mining the vast amounts of precious metals that would be required for producing hundreds of millions of battery packs for these electric vehicles. Many of the raw materials used in battery production are densely packed into limited regions of the globe [9]. This puts rapidly increasing and high stresses on not only the land usage but also infrastructures of less developed countries where these raw materials are often found. Unethical treatment of local miners, often children, has also been occurring in some of these countries [10]. Specifically, the world's reserves of cobalt and nickel, elements used in the most common vehicle battery cells, are not sufficient to meet the projections of electric vehicle production two decades out [11]. Since the daily commute is much less than the total range of most electric vehicles, it may be a better use of raw materials to produce plug-in hybrid vehicles instead. These vehicles have smaller battery packs aimed at being sufficient for daily commuting distances. A wider spread of the battery resources over more vehicles could increase the total distance traveled on electric energy. These vehicles would still have combustion engines to achieve an acceptable long distance range. Electric vehicles have a very low share and slow growth, significant concerns behind the mining of battery materials, are a questionable worldwide solution to the emissions and greenhouse gas problems, and hybrid vehicles may be a better solution for the coming decades. Because of these reasons, continued research and development of combustion engines is still very relevant.

## 1.2 Motivation

One difficulty in the combustion engine development process is that engine attribute requirements often compete and compromises need to be made. One such situation is related to balances between fuel efficiency, NO<sub>x</sub>, soot, and combustion noise emissions in diesel engines (which power about 40% of passenger cars in Europe) [12]. These attributes are the result of the combustion process. Combustion noise is the sound that originates from the cylinder pressure and is emitted from the structure of the engine. It is important not only for the occupants of the vehicle, but it is speculated that pass-by noise requirements could come into future vehicle legislation. Improving the fuel efficiency, thus lowering the CO<sub>2</sub> emissions, often results in higher NO<sub>x</sub> and combustion noise emissions. Sound deadening materials could be added to the engine and the aftertreatment could be designed to accept an increased engine out emissions

level. However, these are not standalone cost-effective solutions for light-duty engines. To mitigate this and related dilemmas, advancements have been made in fuel injection hardware [13, 14, 15]. These advancements allow for fuel injection strategies which were previously not possible and create new opportunities in the combustion process.

The underlying motivation for the research presented in this thesis is in understanding how the combustion process can be altered with these new possibilities and how this can allow for greater headroom in balancing critical engine attributes.

### 1.3 Scope and Approach

The investigations within this thesis were limited to studying first: How differing injection strategies affected key performance attributes in a characteristic, practical load case, and second: Identifying the key differences in the combustion progression which were responsible for those changes in performance attributes. A statistical investigation on large pre-existing experimental data sets was performed in an attempt to correlate certain calibration features to emissions, efficiency, and noise levels. That pre-study had limited success and more pointed experiments were designed. All of the work herein was built upon experimental investigations. Conventional engine tests were used to deliver a multitude of performance attributes and to rapidly target interesting investigations within the new capabilities. As a refinement to those conventional studies, laser-based combustion diagnostics combined with high speed imaging have been performed to identify the changes in the combustion progression. Engine out emissions of  $\text{NO}_x$  and soot have been measured to better understand the impact certain injection strategies create in this regard. Those effects may then be weighed against the potential efficiency and noise changes also resulting from the different strategies.

The experiments have been performed in two different types of single-cylinder engines. One conventional, and one with optical access. The key engine geometries and components of both engines are either identical to or functionally similar to those of their multi-cylinder variant, a Volvo Cars Gen I/II VED engine [16, 17]. The single cylinder engines will be described in greater detail later on.





## Chapter 2

# Diesel Combustion

Diesel combustion is classically characterized as proceeding in the following manner: Fuel is injected at high pressure into air which has undergone rapid compression thus increasing the temperature well above the autoignition temperature of the fuel. There is some short mixing time before the newly formed mixture autoignites as a single event, creating sharp spikes in released heat and, therefore, pressure and temperature. After this point, the in-cylinder conditions are sufficiently high such that the combustion continues as a lifted, mixing-controlled diffusion flame for the remainder of the injection [18, 19].

The clarification about it being mixing controlled is important. Diffusion combustion itself is characterized by a gradient of fuel and oxygen within the reaction zone which is driven by molecular diffusion, a relatively slow process. Combustion in a diesel fuel jet, however, is not as passive a process as plain diffusion combustion. There is indeed a gradient of equivalence ratios, and diffusion does take place, but the main source of that gradient is the result of air entrainment into the expanding fuel jet. Naber and Seibers conducted a thorough optical investigation of fuel jets to create a conceptual model and scaling law for the average cross-sectional equivalence ratio along a quasi-steady fuel jet [20]. Since the air entrainment rate is limited and dependent upon the fuel jet's properties, the combustion process in quasi-steady jets is primarily controlled by mixing rates on this level.

## 2.1 Emissions From Diesel Engines

Regulated emissions from diesel engines include particulate matter, oxides of nitrogen (NO and NO<sub>2</sub>), carbon monoxide, and unburned hydrocarbons. A diesel engine is almost always operated globally fuel-lean of stoichiometry and fuel rarely gets trapped in crevice volumes. This results in very low carbon monoxide and unburned hydrocarbon emissions [18]. The exception to this can be during cold starts and until the engine has reached proper operating temperature. For the scope of this thesis, only warm engine, globally lean mixture operating points are chosen, so only particulate and NO<sub>x</sub> emissions will be considered.

### 2.1.1 Particulates

Particulate matter in a light-duty diesel engine is largely composed of soot—agglomerated carbon structures. Therefore, particulate matter emissions will be simply referred to as soot emissions hereafter. Soot is formed in fuel rich mixtures, but sufficiently high temperatures are also required. Otherwise, it is possible to avoid soot formation even in rich mixtures by operating in a low temperature combustion mode [21, 22]. When soot is formed, however, the pyrolysis of fuel leads to the formation of poly-cyclic aromatic hydrocarbons (PAH), acetylene being one of the dominant species. A process called nucleation transforms the gas-phase hydrocarbons into solid particles. These nuclei coagulate while other hydrocarbons continue to condense onto them. These coagulates form larger structures through agglomeration [23]. The soot emissions from light-duty diesel engines have a broad range of particle sizes, but the primary constituent is the agglomerates. Engine out levels are not solely dependent on soot formation, however. There is balance between early formation and later oxidation of the particles [24, 25].

### 2.1.2 Oxides of Nitrogen

Nitric oxide, NO, and nitrogen dioxide, NO<sub>2</sub> will be grouped together and referred to as NO<sub>x</sub> emissions hereafter. NO is the dominating species of the two, comprising up to 90 % of the NO<sub>x</sub> emissions [18]. These pollutants can be formed through several mechanisms, but the thermal NO<sub>x</sub> mechanism is the one which dominates the formation in light-duty diesel engines. NO<sub>x</sub> is formed at high temperatures via the extended Zeldovich mechanism [18]. NO<sub>x</sub> production increases at higher temperatures and since the thermal mechanism is not

directly dependent on the combustion of the fuel (only indirectly via the increase in pressure and temperature), longer residence times at sufficiently high temperatures affect the global formation rate throughout the combustion chamber. As Heywood points out, mixture fractions which burn early will become heated even further as the global pressure and temperature rise during the rest of the combustion process [18]. This will increase the  $\text{NO}_x$  formation especially in those early combusted regions. Since pilot injections are the focus of this study, the separation times between the pilot injections will effect  $\text{NO}_x$  production by changing the residence time at elevated temperatures not only globally, but especially for the regions combusting first. Unfortunately, unlike soot, engine out levels of  $\text{NO}_x$  are primarily dependent on the formation process. As the mixture temperatures drop during the expansion stroke, the reaction freezes preventing the reduction of  $\text{NO}_x$  back into nitrogen and oxygen.

## 2.2 Quasi-Steady Conceptual Models

Dec was the first to create a well-rounded conceptual model of a combusting fuel jet from the start of injection through the quasi-steady phase [19]. This model is shown in Figure 2.1a. Traveling further downstream of the fuel rich mixture, the jet has a thin premixed flame region followed by an equally thin initial soot formation zone. Thereafter, the soot concentration stays at a low level for the majority of the jet until it rapidly transforms into a high concentration. Surrounding the entire jet, a thin layer where the mixture is near stoichiometry oxidizes the soot formed within. While based on the best experimental data at the time, the investigations did not probe for formaldehyde and PAH within the quasi-steady phase of the jet. Aware of this limitation, Dec proposed the fuel-rich premixed flame tenuously, pointing out the lack of visual data in that region under quasi-steady conditions.

More recent investigations have revealed that these products of rich combustion extend farther into the core of the jet, and are the precursors to soot formation. From these investigations, a more detailed conceptual model was put forth by Kosaka et. al in 2005 which is shown in Figure 2.1b [27, 26]. This model improves the understanding downstream of the rich fuel vapor region. The rich premixed flame and initial soot formation zones in Dec’s model are replaced by PAH formation leading to “young” soot formation of small diameter and high number density. As the soot travels further downstream, coagulation and agglomeration increase the size and decrease the number density of the soot particles. This model also shows increased detail of air entrainment along the jet and recirculation within the head vortex. They found that after the hot ignition

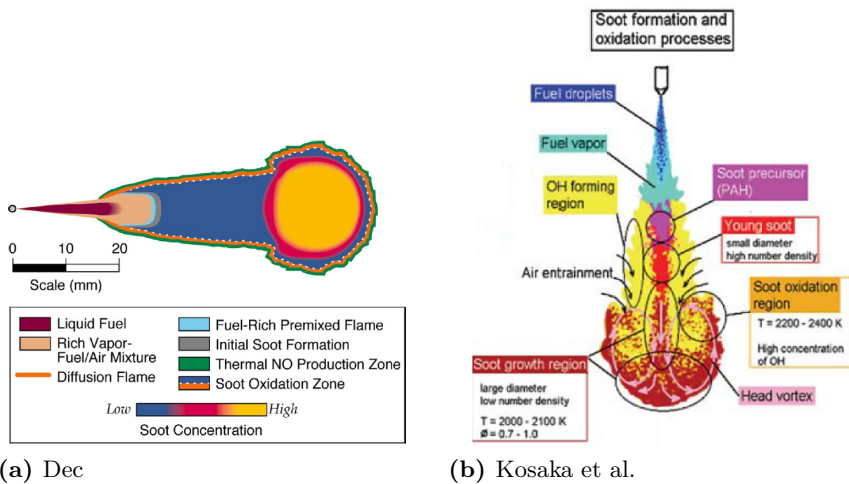


**Figure 2.1:** Comparison between the conceptual models of quasi-steady combustng fuel jets from Dec and Kosaka et al. Reproduced from [19] and [26], respectively.

takes place, the formaldehyde is quickly consumed and therefore not visible later on. This is why their model does not include a region of formaldehyde between the fuel vapor and PAH regions for a quasi-steady jet. They had detected this only in the ignition phase in a prior study in the year 2000 [27]. However, they did not account for a shortening of lift-off-length as temperature and pressure rise or due to re-entrainment of combustion radicals, so it may be possible the emission simply moved out of the investigation window.

Idicheria and Pickett confirmed the presence of both formaldehyde and PAH within the core of the jet in their study investigating high (1100 K) and low (850 K) temperature combustion in diluted and ambient oxygen concentrations [21]. From this improved understanding of the makeup of the core of a quasi-steady combustng fuel jet, they proposed their own conceptual model, depicted in Figure 2.2. The orange line labeled “diffusion flame” indicates the near-stoichiometric layer where OH radicals are plentiful, not to be interpreted as the only place the combustion can be characterized as a diffusion flame. The blue region represents high temperature premixed combustion on un-investigated species which transition from formaldehyde, a cool product of combustion, to PAH, a hotter product of very rich mixtures.

Unlike the findings of Kosaka et al., formaldehyde was present in all cases, residing just after the fuel vapor region. During low temperature combustion cases, PAH was not detected and soot was not formed. In both higher tem-

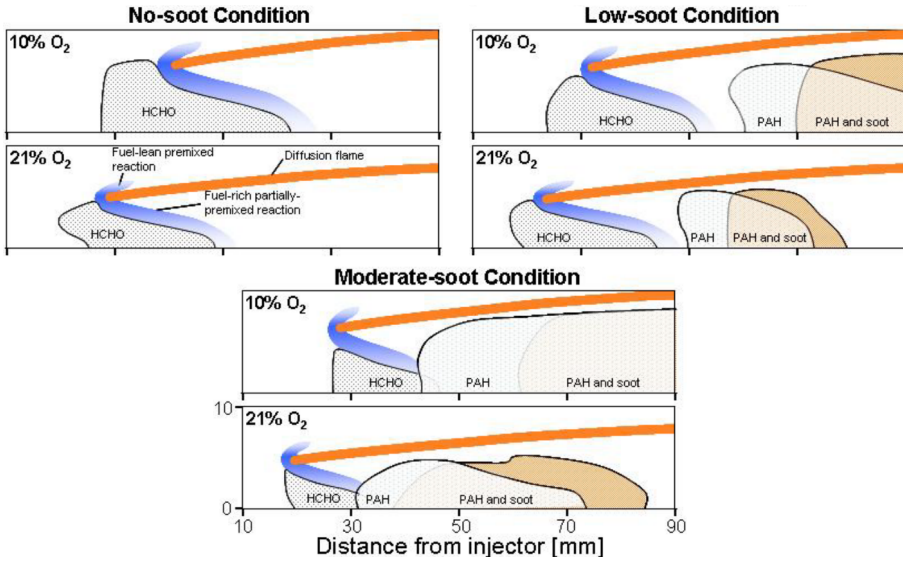


**Figure 2.2:** Conceptual model of a quasi-steady combustor fuel jet proposed by Idicheria and Pickett. Adapted from [21].

perature combustion cases, PAH was formed and always accompanied by soot just downstream. The relationship between the formaldehyde and PAH regions was a distinct separation at mid-temperatures and a blended interface at high temperatures. Higher oxygen concentration converted formaldehyde into PAH further upstream, which also caused the same upstream shift in soot formation. In summary, as mixture reactivity increases (in terms of oxygen concentration and temperature) from a non-sooting case, PAH appears, then increases in proportion which leads to increased soot production. The formaldehyde appears further upstream, but so does the high temperature stoichiometric layer, eventually encapsulating the formaldehyde.

Judging by the reduced formaldehyde region as mixture reactivity increases, one could argue that this region disappears all together at even higher temperatures, meaning the Dec model is only missing the PAH region. The experiments leading to that model, however, were not performed at higher ambient temperatures than in the Idicheria and Pickett investigation. A similar distribution of species likely occurred in the Dec investigation, but lack of LIF probing during the quasi-steady phase caused it to remain undetected. As mentioned before, the reason that Kosaka et al. did not detect formaldehyde in the quasi-steady phase of the jet could have been their limited investigation window. The most upstream location investigated was still 30 mm away of the injector. It is also important to note that the Kosaka and Idicheria models were developed from

investigations in constant volume spray chambers. The pressure and temperature history do not progress as they would in an engine. As a result, the absolute positioning of combustion features may change when replicated in an engine. However, the relative location of these chemical species should generally be applicable. These different conceptual models represent important strides in understanding the combustion of a quasi-steady fuel jet under diesel-like boundary conditions. They are also good examples of scientific progress; subsequent studies built upon earlier findings intent on closing the identified knowledge gaps of the prior investigations.

## 2.3 Fuel Injection Systems

The picture so far has been developed by studying single sustained injections. There are several reasons for this. This quasi-steady state is frequent in medium and heavy duty engines which often operate at medium to high loads. While less frequent in light-duty engines, higher loads are still important to study for transient speed purposes. But another reason for studying sustained injections was the limited functionality of fuel injection equipment (FIE) available at the time these phenomena were researched, or at least how the research had to catch up to the advancements of technology. Approximately a century had passed between Diesel's first engine and Dec's conceptual model, but it was around that time when FIE was advancing rapidly. These new systems would allow the injection of fuel to be started and stopped multiple times within the same cycle, clearly a more complex sequence of events. Research had to explain the more simple case before tackling the new freedoms of the latest hardware. Therefore, a brief history, covering just the last several decades, will be provided to highlight the changes in how the fuel has been physically introduced into the cylinder. This history is important since the novel investigations in this thesis would not have been possible without the latest FIE technology.

### 2.3.1 Nozzles

One feature which remains fairly consistent in its general layout is the nozzle of the injector. A representative drawing is shown in Figure 2.3. The blue regions are occupied by fuel, with the lower portion experiencing only the cylinder pressure when the needle is closed. While some very early systems had a single large nozzle hole, the standard for several decades now is an array of holes angled slightly downwards creating an included angle called the umbrella angle. The

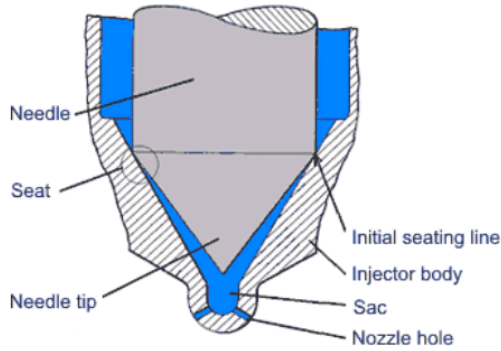


**Figure 2.3:** General representation of an injector nozzle. Its features have remained largely unchanged over the decades. Reproduced from [29].

umbrella angle and piston bowl shape need to be designed together since the interaction between the two has a large effect on in-cylinder flow motion and soot oxidation. The details of this interaction will not be discussed here, but the prior works [17, 22, 28] are good resources for interested readers.

In the early mechanical systems, the needle was positively closed by a stiff spring. Increased fuel pressure induced by flow delivered from the pump would eventually overcome the spring pressure. The needle would be lifted, allowing fuel to flow out the nozzle. In electrically controlled systems a relatively weak spring is used and the fuel pressure itself is used as the primary force to control needle movement. Depending on how the flow is controlled across different cross-sectional areas of the needle, it will either rise or fall. One exception to this is a system called direct-acting piezo-electric control where the expansion or contraction of a piezo-electric crystal directly controls needle movement.

The length, shape, and diameter of the nozzle holes as well as the sac volume are where the primary changes have occurred over system evolutions. In general, nozzle hole diameter has decreased over the years thanks to improved machining techniques (such as laser drilling). The purpose is to improve fuel jet characteristics at low injection pressure. This reduction in diameter is enabled by a higher maximum system pressure still allowing for the necessary peak fuel flow rates, e.g. at peak power.

The sac volume should be very small to minimize unburned hydrocarbon emissions. As the needle closes, there is inevitably an asymmetry between the flow in each nozzle hole. This can be from manufacturing tolerances in the hole diameters, radial needle movement during closure, or also just the stochastic nature of high Reynolds number flows. Due to this asymmetry, some of the fuel



jets will have higher momentum than others. This causes a scavenging effect after needle closure, evacuating the sac volume at low flow velocities. This flow has poor breakup and forms relatively large droplets of fuel which lead to a significant proportion of the unburned hydrocarbon emissions. Recall, however, combustion efficiency is very high in diesel engines, so absolute values are not necessarily high.

## **2.3.2 High Pressure Fuel Delivery**

The most significant changes to fuel injection systems have all been related to how and when the fuel is pressurized, how this high pressure fuel is delivered to the injectors, and how those injectors handle this delivered pressure. There are generally three categories: In-line and distributor pumps; solenoid unit injectors; and common-rail systems. These are ordered from lowest to highest in terms of capability, control flexibility, cost, and system complexity (considering not only the mechanical, but also the electrical and software requirements of the systems).

### **2.3.2.1 In-line and Distributor Systems**

In-line and distributor systems are mechanically driven off of a dedicated camshaft. They have single injections whose characteristics are tied to mechanical relationships of the engine. Needle actuation is a result of fuel pressure exceeding the needle spring force. Fuel flow rate and injection pressure are not adjustable and a function of engine speed. The pressure increases at higher engine speeds due to the flow restriction of the nozzle holes. Maximum injection duration is fixed by the pumping cam's duration. Due to the transient pumping behavior and many individual components between the cam and nozzle, mechanical compliances will affect fuel delivery precision as pressure increases.

### **2.3.2.2 Solenoid Unit Injector Systems**

Unit injector systems are roughly similar to in-line pump systems in that a shared camshaft actuates individual pumping elements. These are now within the injectors themselves, however. The addition of the solenoid valve is critical since it adds additional control over the injection process. Compared to the prior system, multiple injections are possible via control of the solenoid valve. The timing of each injection can be independently controlled for each cylinder,

but still with the limitations of the camshaft lift duration. The solenoid valve drives added complexity. ECU hardware and software are now necessary. The calibration design space also increases significantly.

### 2.3.2.3 Common-rail Systems

Common-rail systems are very distinct from those above. There is a single pumping unit which does not need to be related to any engine timing nor have the same number of pumping strokes as there are cylinders. This pump has a single high pressure line leading to a larger shared (common) fuel rail. This fuel rail has individual high pressure lines leading to each injector, which is similar in function to the unit injector's flow control. Both solenoid and piezo-electric actuation of the flow control valves are common. This system has several benefits over the older systems. Fuel flow rate and injection pressure are adjustable (with the prior being a function of the latter). Fuel can now be injected at any point in the cycle and the injection duration is unlimited. Component compliance is no longer an issue since the high pressure system maintains a constant, adjustable level. As before, the calibration design space increases even further as a result of the increased freedom.

In summary, the evolution of diesel fuel injection systems has removed the dependency on fuel injection properties from mechanical processes. It has allowed for; multiple injection events per combustion event; more control over the flow rate and pressure; improved control over the phasing and available window for injection; and increased precision of the injected quantities.

## 2.4 Pilot Injections

In the discussion of diesel combustion up to this point, only single, quasi-steady injections have been considered. As a reminder, the initial ignition delay after the start of injection allows for some degree of premixing which ignites all at once. This high rate of heat release and the pressure spikes associated with it create significant combustion noise levels. They also lead to early formation of high temperature combusted regions, which are heated further as combustion progresses. The long residence time at high temperatures promotes  $\text{NO}_x$  formation in these regions.

The mitigation of those negative attributes is what drove the evolution in FIE hardware to allow for multiple injections. The nomenclature of these separate

injections are as follows: The main injection contains the bulk portion of the fuel. This can be preceded and followed by smaller pilot and post injections, respectively. Individually, these pilot and post injections are small compared to the main injection. At low loads, together they can add up to significant portions of the total fuel. At mid-to-high loads, the main injection is still much larger than the combined pilot and post injection quantities.

Pilot injections have, for several decades back, been used to mitigate combustion noise [30], emissions [31], and (while not a concern in this study but still worth mentioning) improve cold start performance [32]. Noise and  $\text{NO}_x$  are reduced by limiting the amount of premixed combustion. The pilot injection preceding the main injection has its own autoignition event, but it is much smaller due to the limited size of the injection. Its contribution to pressure and temperature rise shortens the ignition delay of the following main injection, reducing the amount of premixed combustion caused by it.

Modern light-duty engines only use single pilot strategies at high loads [14]. At more common speed-load points, multiple-pilot injection strategies are implemented. This allows for improved control over the progression of the combustion, which affects combustion noise and emissions formation.

### 2.4.1 Effects on Noise, Soot, and $\text{NO}_x$

Several groups since the early 2000's have investigated how to improve the diesel combustion process through the implementation of multiple-injection strategies, often considering more than one pilot injection. The pilot masses were typically much smaller than the main injections, but there have also been variations on this. Some groups have investigated split injections where the fuel mass in each injection is equal. One group even studied spatially separated injections by using different injectors. The studies from the early 2000s tended to investigate injection strategies with very large dwells (the time between the end of one injection and the beginning of the other), sometimes even values over 40 CAD bTDC (crank angle degrees before top dead center) were found as the most beneficial. Nearly a decade later, research on pilot injections had reduced the beneficial dwells down to around 20 CAD. Another 5 or so years later, beneficial values were on the order of 5 CAD. Today, injection strategies have the most desired dwell values referenced in hundreds of microseconds ( $\mu\text{s}$ ). For reference, at 1280 rpm, a common engine speed investigated in this thesis, 1 CAD passes in 130  $\mu\text{s}$ .

In a study from 2002, Tanaka et al. found that combustion noise was mini-

mized for pilot dwells of 30 to 40 CAD. At shorter dwells, combustion noise increased, and even became louder than with a single injection when large pilot injections of 5 to 7 mm<sup>3</sup> were used. While the closest pilot injection was 10 CAD, the trend even for the smallest pilots on the order of 1 mm<sup>3</sup> was still towards increasing combustion noise at shorter dwells. Regarding emissions, the most beneficial points were found at the longest dwells. Otherwise, running a single main injection was actually beneficial [33]. That same year, Badami et al. found that a double-pilot injection strategy with dwells ranging from 35 CAD to approximately 5 CAD (considering the hydraulic lag in their system) had penalties of up to 100% in both soot and NO<sub>x</sub> but benefits in combustion noise and efficiency. Fuel consumption was reduced by 10% and noise by 4 dB. The behavior was notably flat across the dwell sweep. They did also note that pressure waves in the injection system caused by earlier injections affected later delivered masses significantly [34]. This deviation should be taken into consideration in the interpretation of their results. The response with respect to dwell is often not flat in other studies, so this may have been the result of irregular injected masses.

There were several studies performed in 2008 and 2009, mainly investigating the effects on emissions. Husberg et al. discovered that by going from a single to triple-pilot injection strategy, combustion noise was reduced, but they did not provide any values. Soot levels were too low to be detected by their measurement system, but NO<sub>x</sub> was reduced by 30%. Dwells in their investigation were on the order of several degrees between the pilots themselves, but were offset from the main by over 20 CAD [35]. It should also be noted that this was performed in a heavy-duty engine which have larger geometries and more quiescent turbulence. In contrast, injections in light-duty engines have more interaction with the piston bowl wall and a swirling flow motion, which can lead to differences in combustion. Lee et al. discovered that a double-pilot strategy produced a 73% reduction in NO<sub>x</sub> emissions, 84% reduction in smoke emissions, and improvements in efficiency. Due to the way they present the results, it is difficult to say how much efficiency improved, but potentially by as much as 5%. These results were in comparison to a single pilot strategy. The dwells investigated were a reasonable 10 CAD to a very distant 80 CAD, but most of the benefits were noted below 40 CAD [36]. Mendez and Thirouard found that the maximum heat release rate (HRR) value correlated with combustion noise levels in their 2008 study. From this understanding, they split the injection into as many as four equal pieces to limit the main HRR. They were able to decrease combustion noise by between 3.5 and 11 dB depending on the load. The largest gains were achieved by implementing a single pilot injection with diminishing returns for each additional pilot injection thereafter. Increasing soot emissions

were noted for additional pilot injections. Dwells in their study ranged from 20 to 2 CAD. They also noted difficulties in controlling the quantities in subsequent injections due to the pressure waves in the fuel system [37].

Spatial separation of injections was also studied. In the same study as before, Mendez et al. were able to spatially separate injections through the unique shape of the piston bowl and long dwell times. The momentum of a prior injection would carry it away from the injector before the next fuel injection. Their results regarding noise, soot, and  $\text{NO}_x$  showed no benefit for neither the single nor double injection strategies at mid load. At high load, however, noise was reduced by 11 dB while  $\text{NO}_x$  remained constant and soot increased only moderately.  $\text{NO}_x$  levels were low for all cases since low temperature combustion was achieved via high dilution ratios. The other investigation on spatial separations was performed by Binde et al. by adding an injector just for pilot injections. For similar dwells, the spatially separated pilot did not produce the same pre-conditioning effect on the mixture that the conventional injection method did. Peak pressure rise rate (PPRR) increased significantly for dwells less than 10 CAD for the spatially separated pilot. The conventional injection method had a relatively flat behavior at these dwell levels [38].

In the most modern investigations outside those performed as part of this thesis, several publications appeared around 2014-2016. Investigations into very short separations, even less than 1 CAD, are investigated. The main fuel injection equipment manufacturers published how closely-coupled triple-pilot injection strategies with dwells of less than 200  $\mu\text{s}$  could provide benefits in combustion noise at similar or even improved soot- $\text{NO}_x$  levels. This is in comparison to previous state of the art double-pilot injection strategies on earlier systems with dwells about twice as long as what the latest hardware could achieve [14, 13, 15, 39]. In 2015, Busch et al. investigated dwells separating a single pilot from a main injection in the range of 1200 to 80  $\mu\text{s}$ . This translates to just over 10 CAD to less than 1 CAD. A local minimum in noise was achieved at 140  $\mu\text{s}$ , reducing combustion noise by about 3 dB compared to the values at shorter and longer dwells. This was caused by a reduction of sound pressure level in a frequency band which was significant in defining the pressure trace behavior during the combustion of the pilot injection.

In summary, over the last two decades, the beneficial dwell values for multiple-pilot injection strategies went from very far, on the level of 40 CAD, to approximately half that after a decade of development. The latest state of the art findings are for dwells on the order of 1 CAD. One conclusion has often been the same over the years: There was always the possibility to have dwells which were both too short and too long. That optimum point continued shifting towards

shorter values as the combustion system and fuel injection hardware developed. The exact trade-offs between combustion noise, soot, and  $\text{NO}_x$  emissions were rarely consistent, however, and more often contradictory. Some of this is due to some studies targeting low temperature combustion modes, or radical concepts such as spatial separation of fuel via vastly different hardware solutions. The state of research at the start of this project was that promises from the manufacturers were attractive, but there was a lack of academic research in the area. Closely-coupled multiple-pilot injections strategies had rarely to never been investigated by those not developing, and trying to sell, the systems capable of such injection strategies. It was clear that further research needed to be performed to investigate not only the trade-offs and possibilities of these new injection strategies, but also identify the underlying mechanisms responsible for the results. In understanding those, more beneficial strategies can be developed and directions in how the hardware capabilities should develop in the future can be identified.



# Chapter 3

## Research Methods

### 3.1 Data Mining

In the early stages of this project, parallel work was performed to investigate a calibration design space for closely-coupled multiple-pilot injection strategies. That work was performed at Volvo Cars by Volvo Cars engineers. The intent was neither for those investigations to be the basis of the work in this thesis, nor for this thesis work to address practical calibration tasks. The author did not design these experiments nor participate in them. These data were already pre-processed and only considered as a bonus set of data which might help highlight important characteristics and therefore guide the investigations in this work.

These investigations totaled over 1500 operating points featuring more than 10 input variables. To handle the breadth and depth of this data, statistical analysis software is used to search for correlations, create response models, and predict outcomes from unique inputs.

#### 3.1.1 Response Modeling

The software *Unscrambler X* by CAMO Software is used to perform PLSR and MLR analyses on the data sets. PLSR stands for partial least squares regression and is similar to principal component analysis (PCA), but better suited for systems where inputs and responses can be separated. MLR stands for multiple linear regression and is well a suited method when several inputs generate a single response.



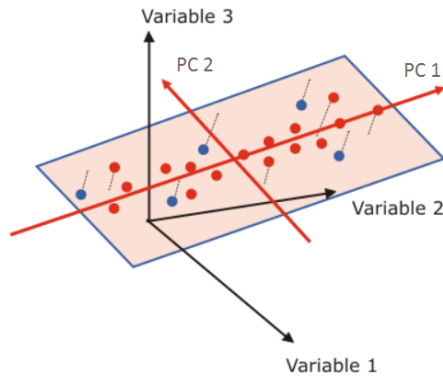


**Figure 3.1:** Graphical representation of principal components used to describe variation in data. Two PCs are shown. A third PC would be perpendicular to the plane the first two components create. This figure is adapted from the Unscrambler X user manual.

A PCA describes the variation in the data set along several dimensions, called principal components (PC). Each higher level principal component describes the largest remaining variation in the data and is perpendicular to all lower dimensions. This quickly becomes near impossible to picture if more than three principal components or variables should be considered at once. Up to this point, though, a graphical representation is helpful in understanding the concept.

Two principal components based on a three dimensional data set are shown in Figure 3.1. The first two PCs are shown. PC 1 describes the largest variation in the data from the global mean, located where the two PCs cross. PC 2 describes the second largest variation in the data which cannot be described by PC 1. A third component would describe the variation relative to the plane formed by PCs 1 and 2.

PLSR is best suited for data sets where independent inputs (X) produce multiple responses (Y) and correlation of their interaction is desired. The covariance between X and Y is maximized so that the latent variables in X can be used to predict the latent variables in Y. This analysis method is well suited for the engine data studied. The input variables are the injection strategy parameters, which are fully independent of the outputs. Those of concern are combustion duration, emissions, combustion noise, and peak pressure rise rate.

Response modeling is also investigated for just a single Y response. In this situation a MLR is well suited for the task. The output is a linear combination of the X variables with associated coefficients which describe the response in the

form  $Y = b_0 + b_1 \times X_1 + b_2 \times X_2 + \dots + b_n \times X_n + f$ . Combination and squared terms can also be included.

### 3.1.2 Prediction

After creating a regression model, Unscrambler X can use the model it created from one data set to predict the responses for another new data set. The number of PCs used in the prediction can be selected to avoid the accidental prediction (and therefore obfuscation) of statistical noise modeled in higher PCs.

Predicting responses from other known data sets can help determine if the model generated from one set of input variables is valid across different ranges of those inputs. If so, it may then be possible to search for phenomenological explanations based on the primary input variables identified in the regression. If the model is robust across other data sets, the additional benefit is its ability to predict system responses from prospective input variables, or identify optimal parameters for a desired system response.

## 3.2 Engine Experimentation

The experimentation performed by the author (this excludes only the data used in the initial data mining) was carried out in two different single cylinder engines. One engine is a single cylinder variant of the multicylinder production engine, a VEA Gen I/II diesel engine from Volvo Cars [16, 17]. The other engine is a Bowditch-style optical variant of the production engine [40]. A cross-section of the optical portion of this engine is shown in Figure 3.2. These engines will be referred to as either the conventional or optical engines, respectively. The conventional engine resides at Volvo Cars in Gothenburg, Sweden and the optical variant resides at Lund University in Lund, Sweden.

Both of these engines have the same combustion system, e.g. port, valve, injector, and piston geometries as the production engine. Some of these key dimensions are presented in Table 3.1. The intake manifold from the multicylinder engine is mounted on a bespoke single cylinder head. This is to maintain the swirl flap which sits in one of the two intake runners per cylinder, which are already split in the manifold. The extra ports in the manifold are capped off with a blocking plate.

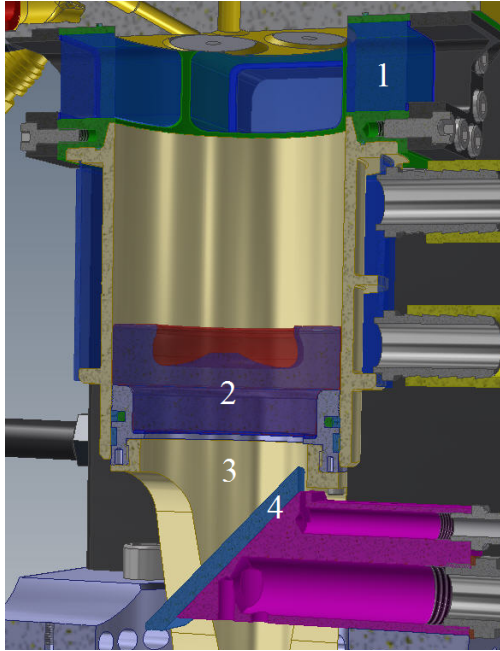


**Figure 3.2:** Cross-section of the portion of the engine allowing for optical access into the combustion chamber. Key features are 1: Windows in the cylinder liner. 2: Transparent portion of the piston. 3: Piston extension. 4: Mirror to access the view from below the piston. Both 1 and 2 are made of fused silica quartz.

**Table 3.1:** List of the engine's key dimensions.

Displaced volume	492 cc
Bore	82 mm
Stroke	93.2 mm
Connecting rod length	147 mm
Compression ratio	15.8:1
Number of valves	4
Nozzle hole diameter	125 $\mu$ m
Number of nozzle holes	8
Injector spray umbrella angle	155°
Max injection pressure	2500 bar

The single cylinder engines do not have scaled down complete gas-exchange systems similar to those on the production engines. Instead, air handling systems installed in each test cell recreate the intake and exhaust boundary conditions measured on the multi-cylinder engines. The conventional engine employs cooled high pressure exhaust gas recirculation (EGR) to dilute the intake charge. For

the optical engine, the exhaust of a lean-burning diesel-fired furnace is mixed with fresh intake air in the air handling system before it is sent to the engine. The systems in both test cells dry the fresh ambient air. When EGR is implemented in the optical test cell, that too is dried before being sent to the engine. Therefore, the fraction of water normally present in the EGR flow is replaced by  $\text{CO}_2$ .

### 3.2.1 Engine Control

The two different test cells have completely different engine control and data acquisition systems. While the differences in acquisition don't pose a significant problem, the lack of a common engine control system does present several difficulties. The main issue is the control of the injector behavior in complex injection strategies such as those studied in this work.

The fuel injection rate can be significantly affected by pressure pulsations in the common rail system. The injection of fuel creates a pressure drop within the injector and the fuel line connecting it to the common rail. When this negative pressure wave reaches this volume change a positive wave will be reflected back towards the injector. This behavior is analogous to what occurs during the intake stroke in an intake runner attached to a manifold [18]. While the flow through an orifice is dependent on the pressure drop across it, the direct effect of an unsteady pressure differential has only a minor implication on the injected fuel quantity. The fluctuation in the pressure is very small compared to the total pressure drop over the nozzle hole. The primary way these pressure fluctuations affect the flow is through injector needle movement. As mentioned in section 2.3.1, the needle movement is controlled by the fuel pressure in the injector. The pressure drop over these control surfaces will change the behavior of the needle. A delay in opening or closing events has a significant effect on the injected quantity. This can also create a domino effect of error cascading through the remaining injection sequence.

To compensate for this, the behavior of the fuel injector is modeled in the production ECU. Combined with fast-sampled fuel pressure feedback, empirical models make changes to the actuating current sent to the injector to ensure the desired injected quantity and dwell times are maintained. This ECU controls the conventional engine and these models ensure that as one injection parameter is changed, the others are not affected.

The optical engine is controlled in a very different manner. Instead of the production ECU, LabView software is entirely responsible for the engine control.

Drivven brand injector drivers with significantly longer electrical wires are used. Both of these hardware variations lead to variations in the delivered electrical current. The LabView software also lacks the proprietary models which would otherwise resolve any deviations resulting from this hardware setup.

Unfortunately, these differences were great enough that the electric current settings from the conventional test cell did not create the same injector behavior in the optical test cell. This was first seen in the heat release rate (HRR) and also confirmed by comparing the fuel pressure traces between the two engines. Initial correction attempts were made by studying the behavior of the fuel pressure, but these were unsuccessful. The behavior proved too complex for the time resolution of the data in the optical test cell. Instead, the behavior of the HRR was studied. The injection parameters were adjusted until the individual HRR traces in the optical engine fell to within  $\pm 3\sigma$  of the ensemble averaged HRR traces from the conventional engine. These high  $\sigma$  limits are not large in absolute values since combustion was very stable in the conventional engine. The coefficient of variation for indicated mean effective pressure was less than 0.5% and the standard deviation of the point of 50% heat released (CA50) was on the order of the crank angle resolution, 0.1 CAD.

### 3.2.2 Considerations of Optical Engines

There are several characteristics about Bowditch-style optical engines which require differences in both geometry and operation to conventional engines. These primarily deal with mechanical interference, optical access, and heat management concerns.

Due to the added length and mass of the reciprocating assembly, deflection from inertial forces will be increased. This requires the static squish height to be increased so that the piston assembly has ample clearance during gas exchange TDC. Additionally, the piston rings are moved lower down the piston in order to obtain an unobstructed view of the entire piston bowl height from the side. These two allowances increase the crevice volume significantly, lowering the compression ratio to about 13.5:1. To compensate for the lower compression ratio, the intake pressure and temperature are increased so that the air density and temperature at TDC match what is achieved in the conventional engine.

The concerns related to heat management are due to the material properties of fused silica quartz. The thermal conductivity is approximately two orders of magnitude lower than for aluminum, the material used for the conventional piston. The implication of this is continuous firing operation, meaning to com-

bust fuel every cycle, would lead to very high wall temperatures for the piston bowl and windows in the liner. From a mechanical perspective, this could build up significant thermal stresses in the material which could lead to catastrophic failure. From a combustion perspective, however, appropriate wall temperatures become a concern first. Large deviations in the wall temperatures affect how the combustion proceeds, and the comparability of this progression between the two engines becomes questionable.

Skip-firing is used as a countermeasure to the heat buildup in the combustion chamber walls. When skip-firing the engine, one cycle experiences combustion while some remaining number of cycles in the repeating sequence are just motored by the dynamometer. Several skip-firing ratios were tested and at the engine load studied, a ratio of one combustion cycle out of every ten was selected. This ratio quickly stabilizes the HRR within two to three combustion cycles and there is no appreciable trend thereafter.

Due to skip-firing, the EGR content taken from the exhaust would not be consistent. This is why the external furnace is used to generate the simulated EGR mixture. Skip firing also clears out combustion residuals which are normally trapped in the cylinder at the end of the exhaust stroke. The inlet O<sub>2</sub> concentration must be reduced in order to match the in-cylinder O<sub>2</sub> concentration in the continuously fired conventional engine. This has been achieved by first back calculating the wet emissions from the dry measured emissions of the conventional engine. The dry mole fractions,  $x_i^*$ , can be related to the wet fractions,  $x_i$ , by

$$x_i = x_i^*(1 - x_{\text{H}_2\text{O}}) \quad (3.1)$$

where the mole fraction of H<sub>2</sub>O is found through

$$x_{\text{H}_2\text{O}} = \frac{b}{2a} \frac{x_{\text{CO}}^* + x_{\text{CO}_2}^*}{\left(1 + \frac{x_{\text{CO}}}{x_{\text{CO}_2}K}\right) + \frac{b}{2a} (x_{\text{CO}}^* + x_{\text{CO}_2}^*)} \quad (3.2)$$

the derivation for which can be found in [41].  $a$  and  $b$  are the number of C and H atoms in the fuel and  $K$  is a ratio (typically equal to 3.5) of CO and H<sub>2</sub>O to CO<sub>2</sub> and H<sub>2</sub> mole fractions.

From there, a simple weighted average provides the O<sub>2</sub> mole fraction at the end of the inlet stroke. It is calculated from the mole fractions of O<sub>2</sub> in the intake and exhaust weighted by their associated volumes and densities before and after the intake stroke. This assumes no exhaust scavenging and perfect filling, but since there is minimal valve overlap in this engine, this is expected to produce

reasonable values nonetheless. The trapped oxygen concentration is then

$$x_{O_2,cyl} = x_{O_2,exh} \frac{1}{r_c} \frac{\rho_{exh}}{\rho_{int}} + x_{O_2,int}^* \frac{r_c - 1}{r_c} \quad (3.3)$$

where the values  $\rho$  and  $r_c$  are the density and compression ratio terms.

This is then used as the target intake value for the optical engine, which has no combustion residuals preceding each fired cycle. For the boundary conditions and load studied here, the inlet  $O_2$  concentration needed to be reduced by approximately 1 percentage point to recreate the conditions in the conventional engine. This improved the matching between the HRR behaviors of the two engines.

Another consideration of optical engine experimentation is related to the desired optical diagnostic technique and how that impacts fuel choice. Diesel fuel is composed of many different hydrocarbon molecules which can fluoresce during laser excitation. If the combustion is to be probed for the presence of formaldehyde, a cool combustion intermediate, or PAH, a precursor to soot, laser induced fluorescence is a useful diagnostic to do so [21, 26, 42, 43, 44]. However, the wavelength commonly used to excite those species, 355 nm, will also excite components in the diesel fuel, obfuscating the results.

Therefore, it is important to have a single component fuel which does not fluoresce from excitation at this wavelength. Having a similar cetane number as diesel, 99.9% pure n-heptane fuel is an appropriate replacement [45]. This fuel, however, has a lower density than diesel. This must be compensated for by adjusting the in-cylinder conditions to maintain the same density ratio between the air and fuel as achieved in the cases when diesel fuel is used. It is important to maintain the density ratio since it strongly impacts the air entrainment, and therefore cross-sectional equivalence ratio, along the jet [20]. Since the experiments with n-heptane are intended to match the investigations using diesel fuel, it is important to maintain a similar air entrainment behavior.

### 3.3 Heat Release Analysis

Fast sampled cylinder pressure is the starting point from which the HRR is calculated. In the conventional engine, the resolution of the pressure trace is 0.1 CAD and 0.03 bar. These figures are 0.2 CAD and  $< 0.005$  bar for the optical engine. The resolution in pressure comes from the respective bit depths in each test cell and do not reflect sensor accuracy. The resolutions are only mentioned

to provide assurance that the values of certain metrics derived from the pressure trace are not biased by coarse resolutions.

First, the pressure trace is filtered using a digital zero phase-shift low-pass Butterworth filter with a 3 dB cutoff frequency of 12 kHz and 80 dB of attenuation occurring at 15 kHz. This falls well below the Nyquist criterion frequencies for both CAD resolutions and avoids attenuation at or below 11220 Hz; the upper end of the range for which combustion noise is calculated.

### 3.3.1 Calculation of the Heat Release Rate

The heat release rate analysis in this work treats the combustion chamber as a single zone and samples the pressure from a single location. Only the net apparent heat release rate is considered here. This means the values provided represent the difference between the heat addition from chemical energy and the heat loss from heat transfer across the system boundary. Mass loss due to blow-by is also ignored. For example, if there is less chemical energy being released than there is heat lost to the walls of the combustion chamber, the net heat release rate will be negative. Cylinder pressure and volume are required for the calculation of this apparent net heat release rate. A thorough derivation can be found in [18], and the final relationship is

$$\frac{dQ_n}{dt} = \frac{\gamma}{\gamma - 1} p \frac{dV}{dt} + \frac{1}{\gamma - 1} V \frac{dp}{dt} \quad (3.4)$$

Considering the pressure term,  $p$ , the absolute value must be pegged to a known value. This is because the DC level of a piezoelectric pressure transducer drifts over time. It is very good at detecting changes in pressure, but lacks a constant reference. In the optical engine, a slow response absolute pressure sensor is mounted in the intake manifold. This value is used in the initial pegging of the pressure trace. However, due to flow losses in the port and across the valve and the pulsatile flow behavior during the intake stroke, the pressure in the cylinder at valve closure is likely not the same as in the manifold. To account for not only this bias, but also the more complex level of cycle-to-cycle fluctuations, each pressure trace is pegged once more using polytropic relationships. Assuming an imperfect pegging, the entire pressure trace will have a constant offset at all locations. By choosing a point early in the compression stroke and calculating what the pressure should be at a later point using the ideal gas law, the error can be determined. The polytropic relationship

$$P_1 V_1^\gamma = P_2 V_2^\gamma \quad (3.5)$$



is rearranged and a constant error term is added:

$$\frac{P_2 + P_{err}}{P_1 + P_{err}} = \left( \frac{V_1}{V_2} \right)^\gamma \quad (3.6)$$

Setting the right hand side to  $Y$  and rearranging gives

$$P_{err} = \frac{Y P_1 - P_2}{1 - Y} \quad (3.7)$$

To avoid errors from high frequency pressure fluctuations,  $P_{err}$  is calculated at 9 adjacent starting points and the average value is taken. The  $\gamma$  value is estimated from the slope of the  $\log p - \log V$  diagram early in the compression phase. The pegging affects this slightly, so an iterative process is used to settle on an appropriate assumed  $\gamma$  value.

Considering  $V$ , the volume term, there is an appreciable deformation of the reciprocating components due to the high cylinder pressures. In order to improve the accuracy of the HRR, this deformation is accounted for by modifying the ideal volume trace based on the instantaneous in-cylinder pressures. Aronsson et al. investigated the magnitude of this deformation through physical static testing. They determined the inverse spring constant of a very similar light-duty optical engine to be  $4 \times 10^{-6}$  m/bar [46]. They also used a more complete compensation by accounting for the tendency of the inertial forces to stretch the assembly, but the spring constant related to that was not provided. With both corrections in place, they showed that for a motored heavy-duty optical diesel engine, the HRR deviation from 0 just before and after TDC was reduced by approximately a factor of 5 at a TDC cylinder pressure of 86 bar. In this work, only the compressive deformation from the gas forces is accounted for since the tensile spring rate is not known.

Considering  $\gamma$ , the ratio of specific heats, a 3-period approach is implemented in the calculation. The compression and expansion periods have separate and constant values as determined by the slopes of the  $\log p - \log V$  diagram in their respective phases. By using these values, the effects of some portion of real losses (heat loss and blow-by) are accounted for. Compared to calculating  $\gamma$  based on an assumed in-cylinder temperature (a more idealized method) this method provides HRR values which lie closer to zero at times of no actual heat release. The  $\gamma$  values for the combustion phase are defined by a linear interpolation between the compression and expansion values from the start of injection to the end of combustion. This linear gradient is more accurate than a 2-period approach, which has a sharp transition at TDC, while still being easy to implement. A non-linear transition more representative of the actual

combustion progression would be more accurate, but would also be an iterative process. This is both more difficult to implement and more computationally intensive.

Absolute values of efficiency and heat loss are not of paramount importance in this work. Since comparative analyses were prioritized, the assumptions and simplifications taken in the calculation of the HRR provide a good balance between accuracy and simplicity.

### 3.3.2 Ratio of Reduced Heat Release

Through both a review of the literature and direct work with the metric, it can be concluded that PPRR is not good predictor of combustion noise for multiple-injection strategies. It is often positively correlated to combustion noise, but with poor reliability which varies between studies [47, 38, 35, 48]. Lacking a good predictor of combustion noise, the author created one based on the shape of the HRR. The combustion noise is the result of the pressure history in the cylinder, which is driven by the net HRR. Therefore, it should be possible to describe combustion noise by studying the HRR.

A new metric called the ratio of reduced heat release (RRHR) has been developed to study the behavior of the HRR. It can be used to both predict and explain combustion noise levels. A peak detection algorithm, specifically the MatLab function “findpeaks,” is used to find the location and values of the local peaks in the HRR which can be associated to the combustion of individual fuel injections. The gaps between the peaks are then bridged, capping off the valleys in the HRR. Finally, a ratio is calculated for the areas between the HRR trace and the bridges, and the total area below the bridges down to the x-axis. Examples of what this looks like for both double and triple-pilot injection strategies are shown in Figures 3.3a and 3.3b. The RRHR is the quotient of the orange areas and the sum of the orange and blue areas between each pair of HRR peaks. This represents how much of the total area between the peaks was not used for heat release. It can also be seen as a measure of the potential for the HRR to cause undulations in the pressure trace. This, of course, assumes that the HRR calculated from the pressure trace is representative of the true net HRR progression. As the RRHR approaches a value of 1, the peaks become infinitely thin with no heat release between them. As the RRHR approaches 0, the HRR has a linear progression with no definable local peaks. Incidentally, the RRHR values cannot be calculated for a perfectly linear HRR since there are no local peaks to detect.

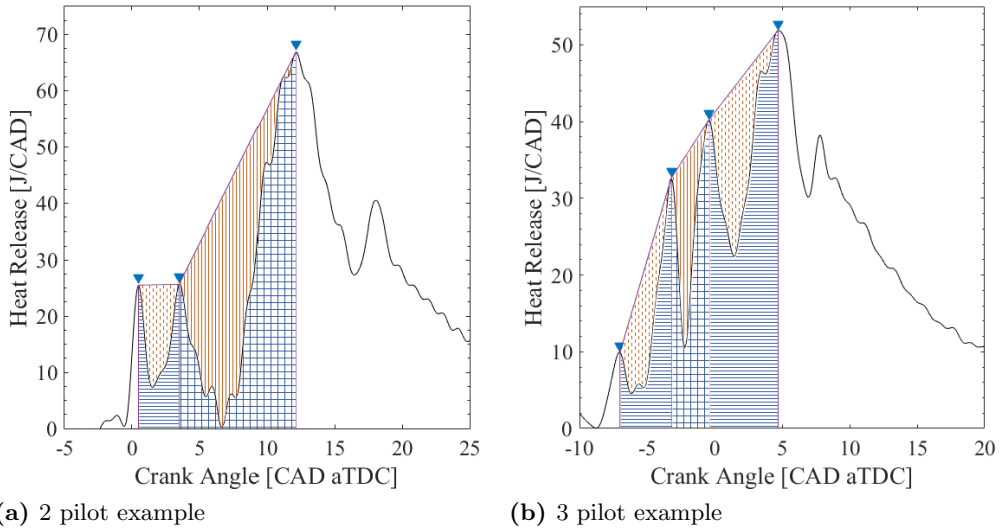


**Figure 3.3:** Graphical representation of how the ratio of reduced heat release is calculated. It is the quotient of the individual areas marked with an orange hash and the total area under each bridge (between adjacent peaks). (a) shows an example with a double-pilot injection and (b) with a triple-pilot injection.

Since the RRHR is a ratio, it is not a universal predictor of combustion noise levels. One can imagine that scaling a given HRR up or down to change load would produce the same RRHR values but cause higher or lower combustion noise levels. This metric's strengths are in providing a comparison to other operating conditions at constant load-speed points. It also is able to indicate how a HRR should be changed in order to minimize combustion noise. Research in this thesis has shown that minimizing RRHR values, thus linearizing the HRR, minimizes combustion noise. This will be discussed later in the presentation of the results.

Working with several RRHR values for a single operating condition is cumbersome, however. Especially considering that the relative size of the valleys should have bearing on this metric. For example, the valleys in Figure 3.3a have approximately the same RRHR values, but clearly different potentials to affect the behavior of the pressure trace. This metric has been tested over a broad span of injection strategies and boundary conditions (however only at a single load-speed point) and it has been determined that calculating a single weighted average RRHR value is a good predictor of combustion noise. The individual RRHR values are weighted by the size of their valley's area to the total valley area. These individual values indicate the relative contribution each valley in

the HRR has towards the combustion noise level.

From a practical implementation perspective, the HRR should be filtered by another low-pass Butterworth filter. Cutoff frequencies between 3500 Hz and 6500 Hz have been tested and 4500 Hz creates HRR profiles which provide the best correlation between weighted average RRHR values and combustion noise. At lower frequencies, important frequency content in the range which contributes to combustion noise starts to be filtered out. At higher frequencies, the effects of cylinder ringing from single point pressure measurement create undulations in the HRR which affect the local peak and minimum values, irregularly skewing the depth of the valleys. The RRHR values can be calculated for each cycle and then averaged, but this requires significant error checking to ensure the peak detection algorithm selected the appropriate peaks. It has been shown that the RRHR values calculated from the ensemble averaged HRR fall within 1 standard deviation of the mean, calculated on the cycle-by-cycle basis [49]. This greatly reduces the error checking process.

## 3.4 Noise Analysis

### 3.4.1 Sound Pressure Level

Combustion noise is the sound that originates from the cylinder pressure and is emitted from the structure of the engine. It is calculated very similarly to the method outlined by Shahlari et al., which is based on AVL's Noise calculation [47]. The only differences are for the calculation of additional noise metrics and slight adjustments to the upper and lower frequency bounds. These adjustments are not significant, however, and values calculated for any of these methods will lead to nearly identical values. In this calculation, the discrete Fourier transform of an entire cycle of cylinder pressure is taken, then both structural and A-weighted attenuation curves are applied. The structural attenuation is based off of much older engines from the 1980s [50]. While not representative of the actual structural attenuation of the light-duty engine studied here, it is a generic attenuation curve that is likely used widely in this field. This will provide combustion noise levels which peers will find relatable.

After the selected attenuations are applied, the sound pressure level (SPL) can be calculated for binned frequency bands and as one total SPL. The magnitude spectrum is also useful for understanding at a more detailed frequency resolution which frequencies are strong contributors.

### 3.4.2 One-third Octave Bands

Each octave is a doubling of frequency content. This resolution quickly becomes very coarse, however, so improved resolution is achieved by considering one-third octave bands. The lowermost and uppermost limits of the frequency spectrum for which combustion noise is calculated are 89.1 and 11220 Hz. The lower, center, and upper frequencies of each of the one-third bands are presented in Table 3.2.

**Table 3.2:** Values in Hz for the lower, center, and upper frequencies of each one-third octave band studied.

Upper limit	112	141	178	224	282	355	447	562	708	891	1122
<b>Center</b>	<b>100</b>	<b>125</b>	<b>160</b>	<b>200</b>	<b>250</b>	<b>315</b>	<b>400</b>	<b>500</b>	<b>630</b>	<b>800</b>	<b>1000</b>
Lower limit	89.1	112	141	178	224	282	355	447	562	708	891

Upper limit	1413	1778	2239	2818	3548	4467	5623	7079	8913	11220
<b>Center</b>	<b>1250</b>	<b>1600</b>	<b>2000</b>	<b>2500</b>	<b>3150</b>	<b>4000</b>	<b>5000</b>	<b>6300</b>	<b>8000</b>	<b>10000</b>
Lower limit	1122	1413	1778	2239	2818	3548	4467	5623	7079	8913

### 3.4.3 Magnitude Spectrum

By considering the one-third octave bands, the bounds of the strongest frequency content can be identified. This frequency resolution can still be quite coarse, however, and the decibel scale graphically compresses appreciable differences. The magnitude spectrum is then investigated since it has higher resolution in the frequency domain and features a linear y-axis. The magnitude spectrum is the absolute value of the one-sided discrete Fourier transform normalized by the number of points used in the calculation of it.

### 3.4.4 Pressure Rise Rate

Peak pressure rise rate is not a direct noise metric, but it historically is an indicator of combustion noise. Their comparison will test the ability of the former to predict the latter.

After its initial filtering, the derivative of the cylinder pressure is calculated for each cycle. A moving average filter with a length of 1 CAD is then applied. This corresponds to 10 and 5 averaging points for the data from the conventional and optical engines, respectively. The peak value for each cycle is taken from within

the crank angle range between the start of injection and end of heat release. The peak values are averaged to provide the main PPRR for the operating point. This method produces values which closely match those provided by commercial engine analysis software.

## 3.5 Optical Analysis

The optical analyses performed in this work are qualitative in nature. The investigated operating conditions are above the LTC temperature range and soot is formed during the combustion process. This soot builds up on the piston and windows of the optical engine, gradually attenuating more light with each subsequent combustion cycle. This fouling of the combustion chamber walls is difficult to quantify and is one reason quantitative optical data is difficult to achieve under such conditions. Even with the allowances qualitative investigations provide in this regard, only about 20 fired cycles can be captured before the combustion features become too faint to discern. After each set of cycles, the engine is stopped so that the combustion chamber can be cleaned for the next round of data acquisition.

### 3.5.1 Line-of-Sight Imaging

All images in this work are captured from light exiting through the bottom of the piston. When capturing the natural luminosity (NL) of the combustion, as well as potential elastic scattering of light from voluminous regions such as the fuel spray, the precise vertical location of distinct features cannot be known. The light intensity is also an integration through the depth of the volume. Conversely, features may also block light emitted from other sources. This can happen, for example, when dense soot clouds wrap around the bottom of the piston bowl, blocking the light above it from reaching the camera.

### 3.5.2 Planar Laser Induced Fluorescence

Laser induced fluorescence is the excitation of a chemical species to a higher energy state by pumping it with a specific wavelength of light. When the species relaxes from that excited state, it emits photons at either the same or different wavelength than the excitation source [51]. Planar laser-induced fluorescence (PLIF) denotes the specific technique of forming the laser light into a flat plane

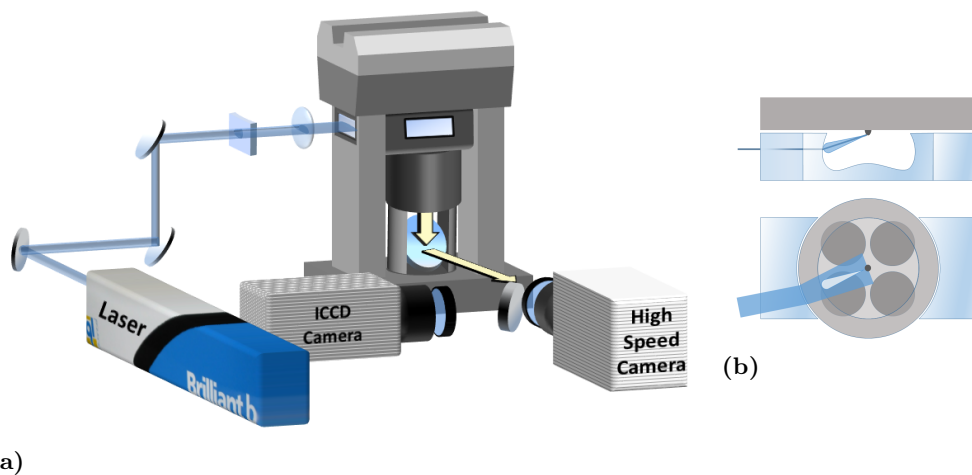


**Figure 3.4:** (a) Schematic of the optical setup for capturing both PLIF images and high speed video of NL. (b) Illustration of the laser sheet bisecting a fuel jet.

with optical lenses. A thin plane makes it possible to achieve a high resolution of the 3-dimensional location of the species in a larger volume. Line-of-sight effects are now minimal, but care is still taken to limit the investigation time to avoid attenuation of the signal from the wraparound of soot clouds later in the cycle.

PLIF images are obtained by exciting formaldehyde and other intermediate combustion species present in partially oxidized fuel (POF) at elevated temperatures. The fundamental wavelength of a 10 Hz Quantel Brilliant B Nd:YAG laser is frequency tripled to produce a 355 nm emission.

A schematic of the optical setup is shown in Figure 3.4. The laser sheet is aimed along a jet axis in order to bisect the spray and combusting plume. Chemiluminescence and blackbody radiation from the voluminous combustion are reduced with optical filters placed before the cameras. The signal to noise ratio is further improved by decreasing the exposure time of the camera and increasing the laser power to maintain good exposure of the excitation. Images of the fluorescent emission are captured on an intensified CCD (ICCD) camera. One drawback of this camera and the laser is they do not have a high enough repetition rate for same-cycle imaging. Due to this, the progression of the investigated features with respect to CAD do not clearly follow one another. Averaging is necessary to obtain qualitative changes over time. The natural luminosity of the combustion is captured on the high speed video (HSV) camera. The frame rate of this camera is able to resolve the combustion process within each cycle. The proper

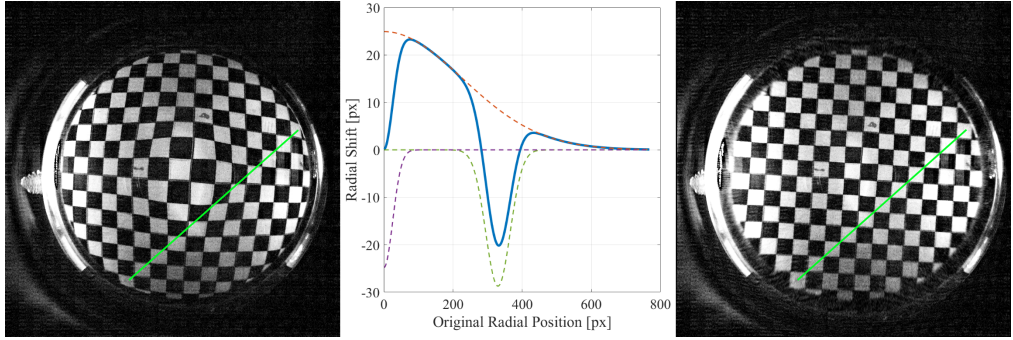


**Figure 3.5:** Left: A raw image of a straight grid pattern, distorted by the shape of the piston bowl. Middle: Individual and composite (solid blue line) Gaussian curves define the radial pixel shift (y-axis) vs. original radial position (x-axis). Right: Image after the distortion correction is applied, returning the grid to its original uniformity. The overlaid straight green lines highlight the original distortion final uniformity.

frame from the high speed footage is matched with the frame from the ICCD camera so that the images may be overlaid. For investigations without PLIF, the Nd:YAG laser is replaced with a continuous wave laser diode. This creates a diverging beam which fills much of the combustion chamber, providing elastic scattering off of the liquid portion of the fuel spray. In those investigations, the ICCD camera is not used.

### 3.5.3 Image Distortion Correction

The curvature of the piston bowl geometry creates significant distortion of the image as viewed from below the piston by the camera. To correct for this distortion, images of a known, uniform grid pattern are taken for each camera setup. Compositing Gaussian curves define a radial pixel correction which is swept around the axis of the piston bowl. An example of the raw distorted image, individual and composited Gaussian curves, and final uniform image is displayed in Figure 3.5. The overlaid green lines highlight the original distortion before and final uniformity after the correction.

One limitation with this method is that the distortion correction is only most valid at the plane of the grid image. This is because the distortion also changes along the height of the combustion chamber. For the cases relying on line-of-sight investigation, even complete knowledge of the distortion throughout the volume would not allow for correct placement of the combustion features since it





**Figure 3.6:** Sample images used in the determination of combustion propagation speed. Combustion regions are shown in white. The images are sequential from left to right with a timestep of 32.26  $\mu\text{s}$ .

is not possible to know their height. Understanding this, correcting for distortion at a single plane is the chosen compromise. For the cases where a planar region is investigated, the grid pattern is placed as close to the investigation plane as possible, minimizing the potential distortion error.

### 3.5.4 Combustion Area Growth

The flame speed is investigated for early stages of combustion. The intent is to identify what combustion mode is likely dominating during the initial stages of development; deflagration or sequential autoignition.

After the distortion correction, masking is applied to the images to remove the fuel jets of the subsequent injections. Reflections are removed via image subtraction based on images taken without combustion. The images are binarized since the combustion intensity detail is not important at this point, only that the boundary is defined by a threshold. The change in area and perimeter of these regions is tracked as time progresses. An example of the resulting images is provided in Figure 3.6. An average growth rate can then be calculated for the mean propagation speed of the flame perpendicular to its perimeter as

$$v = \frac{\Delta A}{s \times \Delta t} \quad (3.8)$$

where  $v$  is the velocity perpendicular to the perimeter,  $\Delta A$  is the change in total combustion area after the time step,  $\Delta t$ , and  $s$  is the total perimeter length of all regions at the interrogation time. This equation is identical to the one used for the same purpose in prior work [52].

Since this is based on line-of-sight imaging, this only provides the transversal growth rate. The vertical growth rate (along the cylinder axis) cannot be known but it is not expected to be significantly different. The first injection duration is short and has too little momentum to interact with the bowl wall before ignition. Since the individual jets are symmetric about their respective axes, the fuel-air mixture should not favor the transverse or vertical directions.

### **3.5.5 Combustion Feature Tracking**

Similar to particle image velocimetry analysis methods, combustion features can be identified and tracked over time either by using direct cross-correlation, or the discrete fast-Fourier transform methods [53, 54].

A 5 pixel wide high-pass filter is applied to the images so that only the brightest features remain. The motion of these small flamelets is tracked over time to create velocity vectors. Combustion features are not stable by nature, so they are used to obtain an approximate, qualitative understanding of the flow fields that is easy to illustrate pictorially.



# Chapter 4

## Results

### 4.1 Data Mining

Multicylinder tests were performed at three different load-speed points to investigate the calibration space of closely-coupled triple-pilot injection strategies. As mentioned earlier, these test were neither designed nor performed by the author. The intent was to statistically investigate available cycle averaged data to identify the critical input variables responsible for key engine performance characteristics such as PPRR, noise, emissions, and combustion durations.

The models created from the PLSR had mixed success. Prediction of burned mass fractions was very good with high coefficients of determination,  $R^2 > 90\%$ . Emissions predictions of both  $\text{NO}_x$  and soot were also good, with  $R^2 \approx 85\%$ . PPRR predictions performed at a slightly lower, with  $R^2 \approx 70\%$ . Combustion noise, unfortunately, had a poor result at  $R^2 \approx 40\%$ . A MLR was run, this time modeling only the response in combustion noise. The prediction performed better than for the PLSR, but still only achieved  $R^2 \approx 67\%$ .

After investigating the data manually, and confirming with the scores and factors from the PLSR, dominant variables were changed with too wide a span compared to the change in pilot injection parameters. For example, the CA50 was swept over 10 CAD. This single variable created very large changes in all the responses. This explains why the models were successful at predicting burned mass fractions and emissions. The impact that the injection strategy parameters had were much less significant than much more dominant variables. The value above for noise was also using 4 principal components in the PLSR. The first 2-3 were very poor at describing noise and an additional 3 only increased the  $R^2$  by

8 percentage points. Therefore, the regression analysis treated the change in combustion noise due to injection parameters as statistical noise.

Within this data set, it was actually possible to predict combustion noise with a high accuracy,  $R^2 > 90\%$ . This was achieved through MLR modeling of pre-processed noise components, similar to the one-third octave analysis described earlier but with much larger bands. This high accuracy was not due to the sound signatures being very similar either, as strategies with the same total sound pressure level could have very different relative strengths in the frequency content breakdown.

This model is not useful from a phenomenological perspective, however. It cannot predict the noise signature or level based on the injection variables. Neither can it describe why, physically, the combustion noise has a certain frequency content or sound pressure level. Creating such an understanding was the goal, and the first experiment was designed to investigate a hypothesis of what may be the underlying phenomena.

## 4.2 Investigation into Noise Minimization

Some key findings, results, and conclusions from Paper I are summarized in this section. This work investigates the potential to lower combustion noise and improve efficiency by implementing closely-coupled triple-pilot injection strategies. It also tests the hypothesis that the variation of the global heat release rate as combustion progresses is the primary responsible factor controlling the measurable combustion noise. In order to do this, three different multiple-pilot injection strategies are compared at the same speed-load point with identical boundary conditions.

### 4.2.1 Injection Strategies

One injection strategy consists of two pilot injections which are followed by single main and post injections. Each pilot injection is followed by a moderate dwell on the order of several CAD. This injection strategy is representative of a Euro 6c production calibration and is used as the reference in this study. Due to combustion noise and NOx targets, the combustion phasing (CA50 location) is retarded from maximum brake torque (MBT) timing. One triple-pilot strategy, “B,” is optimized primarily for minimizing combustion noise first, maximizing efficiency second, and minimizing soot (via closely coupling the post injection)

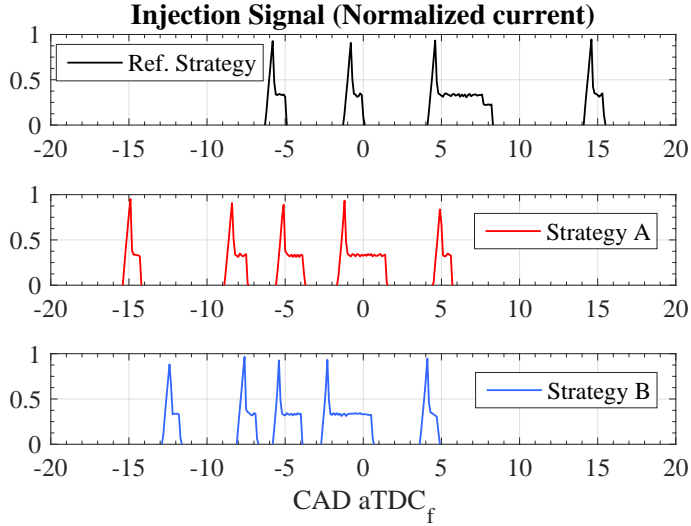


**Figure 4.1:** Normalized injection signal for each strategy studied in Paper I.

third. The  $\text{NO}_x$  limit is removed to investigate the potential efficiency improvements with triple-pilot injection strategies. Strategy “A” tests the hypothesis by increasing the dwells after each pilot injection. This accentuates the peaks and valleys in the HRR which should increase combustion noise compared to strategy “B.” The post injection settings were identical for both triple-pilot strategies. A graphical representation of the injection scheduling is shown in Figure 4.1. Compared to the reference case, the short dwells in strategies A and B are readily apparent.

#### 4.2.2 Efficiency and Emissions

Results for the combustion progression, efficiency, and emissions levels are summarized in Table 4.1. The combustion duration is quite consistent between each case. This means the significant improvements in indicated specific fuel consumption (ISFC) come primarily from the advanced phasing of strategies A and B. They could be phased to MBT timing since the combustion noise level of the reference case was not exceeded.

As expected from a classic soot- $\text{NO}_x$  trade-off due to combustion phasing [18],  $\text{NO}_x$  increases and soot decreases for the advanced triple-pilot strategies. Some of this reduction could have also resulted from the closely-coupled post. Between those two strategies there is evidence suggesting that as the dwell times are

reduced, this will tend to increase the soot emissions.

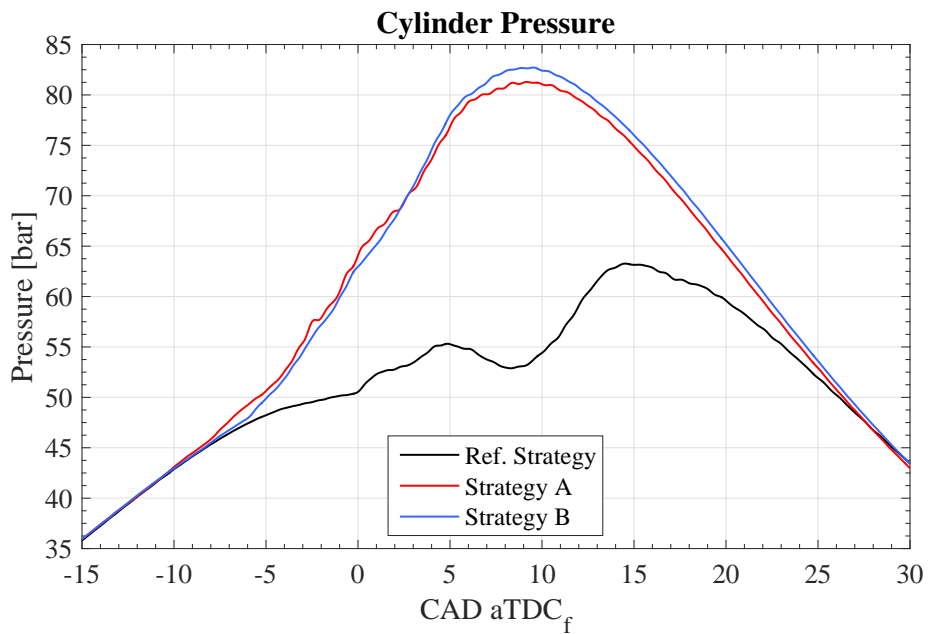
**Table 4.1:** Cycle averaged results for each injection strategy.

	Reference	Strategy A	Strategy B
ISFC [-]	-	-3.7%	-3.6%
CA50 [CAD aTDC]	14.5	6.2	5.9
MFB 10-90 [CAD]	22.9	22.9	22.0
NOx [g/kWh]	0.6	1.1	1.1
Smoke [-]	-	-33%	-16%
Noise [dBA]	80.9	79.5	77.1
PPRR [bar/CAD]	2.7	3.6	3.8

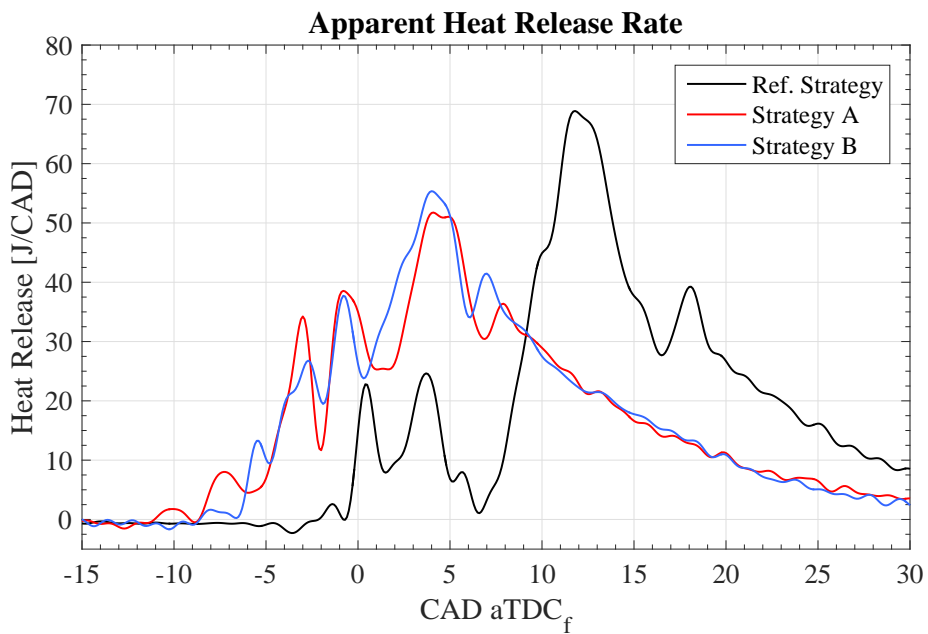
### 4.2.3 Pressure

A characteristic pressure trace from a single cycle is shown for each strategy in Figure 4.2a. Considering first the reference strategy, a non-monotonic behavior exists on the scale of several CAD. The pressure drops between 5 and 9 CAD aTDC. This occurs due to an increasing cylinder volume and normal losses such as heat transfer and blow-by during a period of little-to-no heat release. Moving on to the triple-pilot strategies, the most notable differences are the earlier pressure rise and higher peak pressures. This is expected from an advanced combustion phasing. The unique finding is that the undulations in the pressure traces are significantly reduced. Both traces increase monotonically to their peak values. Strategy A has some undulation just before and after TDC from the heat addition from the pilot injections. However, the undulation amplitude is much lower than that seen just after TDC in the reference case. For strategy B, this trend is carried further and the individual contributions to pressure rise from the combustion of each pilot injection are difficult to discern.

Cycle averaged results based on cylinder pressure are also collected in Table 4.1. Despite increases in PPRR and peak cylinder pressure (shown in Figure 4.2a), combustion noise was significantly lower both for strategies A and B. Between them, the case with the shortest dwells, B, has the lowest noise level. The reduction in noise for these cases is significant considering that every 3 dB is a doubling of sound power. These findings do not agree with the conventional wisdom that combustion noise and PPRR are positively correlated.



(a)



(b)

**Figure 4.2:** Characteristic single cycle results for cylinder pressure and HRR. No averaging is applied to maintain the fine detail in each.



#### 4.2.4 Heat Release

The reasoning behind the drop in combustion noise through the smoothing out of the pressure traces is explained by studying the HRR traces, which are presented in Figure 4.2b. Each injection strategy features local peaks in the HRR which result from the combustion of each individual injection. In the reference strategy, the magnitude of the HRR undulates severely. The value dips to less than half the adjacent peak values associated with the combustion of pilots 1 and 2 (appearing at 1 and 4 CAD aTDC). Due to the long dwell before the main injection, the HRR drops to nearly zero before rapidly climbing up to the highest value seen for all strategies.

In contrast, the behavior of both triple-pilot strategies is very different. Each subsequent local peak leading to the main is higher than the last, as are the local minima. While strategy A still has substantial dips in the HRR, the width of the valleys is significantly reduced. Strategy B, the quietest strategy, has reduced the size of the valleys in both depth and width compared to strategy A.

While the plain RRHR values were presented in Paper I, further study of additional data has shown that considering the weighted values provides a better understanding. The additional insight the weighted values provide is what valleys are currently the largest contributors to combustion noise. These values are presented in Figure 4.3. As seen for the reference strategy, the second valley (V2) is the overwhelming contributor to the weighted average RRHR. For strategy A, the largest potential to reduce combustion noise lies in V1 whereas for strategy B, this is instead V3. By considering the combustion noise level for each strategy, it is clear that if combustion noise is to be minimized, the weighted RRHR value in each valley of the HRR should be minimized. This leads to a more linear HRR and smoother pressure rise. This metric is useful not only for quantifying the magnitude of the valleys, but also as a tool for indicating how the HRR should be modified in order to reduce combustion noise.

Another significant finding is that the fundamental frequencies of the valleys,  $f_0$ , match the frequency content of the pressure trace which strongly contributes to combustion noise. These fundamental frequencies are calculated from the separation of the HRR peaks in the time domain. It is only an estimation since the valleys are not perfect sinusoids. This can also be calculated for non-adjacent peaks. While it is obvious that the total spectrum of the HRR should match that of the pressure trace, this does not also make the first statement of this paragraph equally obvious. The reason the total spectra should match is because the HRR is the derivative of the pressure trace. This, however, does not also

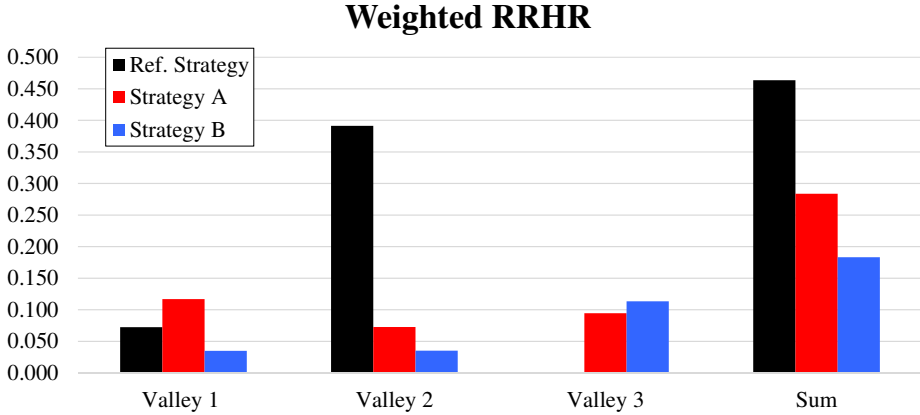


**Figure 4.3:** Weighted RRHR values for each valley in the HRR of each strategy.

guarantee that the  $f_0$  of the valleys should match with the pressure frequencies which strongly contribute to combustion noise. Even in a more general sense, there is no fundamental guarantee that any single notable frequency in the HRR should do so. One example is cylinder ringing. In the plots shown here, this has been filtered out of the HRR, and for good reason: While the cylinder ringing would otherwise show up strongly on the HRRs, the contribution to combustion noise from that frequency is negligible. Furthermore, it is also similar for each strategy studied. For confirmation of this, the readers are referred to Figure 7 in Paper I and its discussion in the body of that text.

The magnitude spectra and  $f_0$ 's of the valleys are displayed in Figure 4.4. The  $f_0$ 's of non-adjacent peaks are also included and are marked as the peaks they span. Within each strategy, and often between the strategies, the relative values of weighted RRHR correlate well with the relative magnitudes of the combustion noise at those  $f_0$ 's. Combinations of non-adjacent peaks are also significant in some cases i.e. the P1-P3 combination. The remainder of the combinations for the triple-pilot strategies are not found to be significant contributors to combustion noise levels. This is further evidence that not all frequencies in the HRR are significant.

As an example, without the consideration of the  $f_0$ , the magnitude of the values around 2500 Hz for the reference strategy would be perplexing. The adjacent local peaks are cascading harmonics of the strong fundamental frequency centered near 800 Hz. The third harmonic of the V2  $f_0$  should have occurred near 2511 Hz and had a much lower magnitude than the second harmonic near 1600 Hz, but it does not. The  $f_0$  of V1 explains that its magnitude has increased the

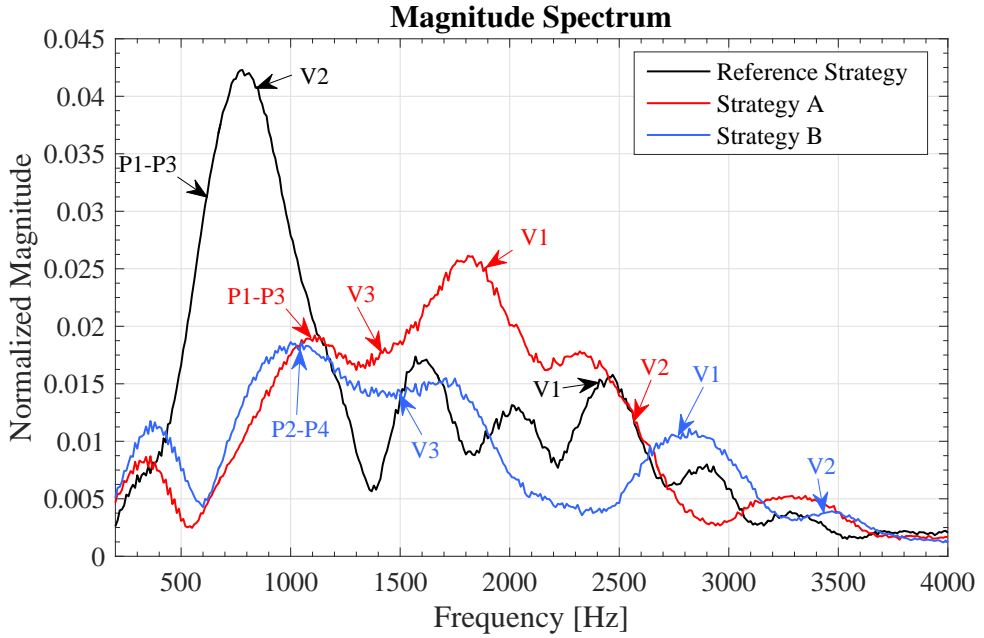


**Figure 4.4:** Ensemble averaged magnitude spectra of the pressure traces within the range of significantly contributing frequencies to the combustion noise level. The peak-to-peak frequencies of occurrence are labeled for each injection strategy and color coded. P# represents the peak number (labeled from early to late CAD). When the peaks are adjacent, V# is used instead to reference the valley so that an easy correlation to the weighted RRHR values can be made.

local values and shifted the local center frequency lower due to its contribution at 2400 Hz.

#### 4.2.5 Conclusions

By implementing closely-coupled triple-pilot injections, the combustion noise is reduced significantly which allows the combustion phasing to be advanced to MBT timing, reducing fuel consumption. Physically, the combustion noise decreased because the ratios of reduced heat release were decreased. This reduced the magnitude of the undulations in the pressure trace as a result of a more linear global HRR. Comparing the magnitude spectra with the fundamental frequencies of the valleys showed that the spacing of these peaks describes the character of the combustion noise. The magnitude of the weighted RRHR values agrees well with the relative strength at these frequencies in the magnitude spectra. Depending on an engine architecture's unique structural attenuation,

it may be possible to not only minimize noise by minimizing the RRHR, but also by tuning the frequency content into spectral regions of stronger structural attenuation.

### 4.3 Optical Investigation of the Combustion Progression

Some key findings, results, and conclusions from Paper II are summarized in this section. The HRR profiles achieved with closely-coupled pilot injections are significantly different to those of the reference case. Based on the short dwell levels and HRR behavior, it is likely that a different interaction between the prevailing combustion regions from earlier injections and subsequent fuel injections occurs. Shorter dwells reduce the time for the prior combustion regions to disperse throughout the combustion chamber. Additionally, the combustion will be less developed by the next fuel injection.

Earlier optical studies in engines which featured relevant injection strategies did not resolve the early stages of combustion. Thus, the interaction between it and the subsequent pilot fuel injection could not be commented on [35, 55]. Optical studies in constant volume spray chambers were more successful in capturing the interface between prevailing combustion and subsequent fuel injections [56, 57]. In those studies, however, the injections were not closely-coupled. The combustion progression in spray chambers is also not fully representative of what occurs in an engine. Spray chambers lack the pressure and temperature progression and wall effects which occur in light-duty engines. The motivation of this study is to identify the differences in combustion phenomena when changing from moderately spaced pilot injections to closely-coupled injections in an engine.

#### 4.3.1 Initial Combustion Development

Since this study investigates diesel combustion, it is obvious that the first ignition event will occur from autoignition. The onset of combustion is well after the end of injection so the fuel burns in some sort of premixed mode. However, based on the behavior of the HRR, it is not clear if the combustion growth thereafter is via pre-mixed flame propagation or sequential autoignition as in HCCI combustion.

According to a prior work by Hultqvist *et al.*, if deflagration occurs, the mean

propagation speeds should be on the order of 15 m/s. If sequential autoignition occurs, 80 m/s is more appropriate [52]. The peak propagation speed is determined for each cycle. The median of those values for each injection strategy are presented in Table 4.2. Based on these results, the conclusion is that after a multitude of autoignition sites occur throughout the mixture, these kernels propagate via deflagration. The values are higher than suggested from Hultqvist and coworkers, and this could be due to several factors. The speed can be biased upwards by significant areas crossing the intensity threshold between frames, rapidly adding to the area growth rate. Another reasoning is that the prior high velocity injection locally increases the turbulent flame speed above what is characteristic for the SI engine used in their study.

**Table 4.2:** Median values of the peak flame front propagation speed during the combustion of P1.

	Reference	Strategy A	Strategy B
Speed [m/s]	23.3	14.5	20.0

### 4.3.2 Contact Ignition

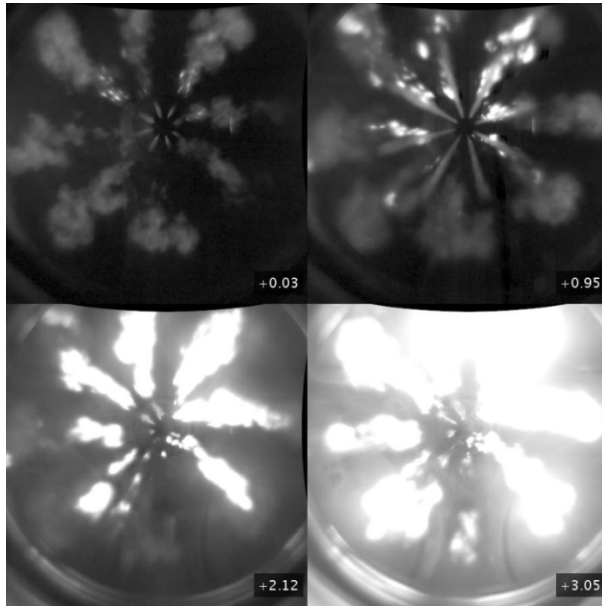
After the development of those very first combustion regions, the interface between them and the subsequent fuel injections is studied. For all three of the injection strategies, the primary mechanism responsible for the onset of combustion is contact ignition. When the incoming fuel physically interacts with portions of the prevailing combustion regions, that fuel is ignited after a very short delay. When that interaction does not occur, the injected fuel experiences a much longer ignition delay (on the order of several CAD) as well as a much slower progression of combustion. This is depicted in Figure 4.5. The contact ignition behavior is compared between the reference and B strategies since those have the most extreme differences in dwells.

The top left image of Figure 4.5a shows the combustion regions from pilot 1 (P1). The very beginning of the P2 injection can be seen exiting the injector in the middle of the frame. In the next frame, top right, the fully developed injection of P2 is seen interacting with the prevailing combustion regions. However, this does not occur for the fuel jet in the clockwise five-thirty position (at least not for the liquid portion of it). Due to the stochastic behavior of combustion and the clockwise bulk swirl motion, this fuel jet failed to contact a combustion region in this cycle and this has significant consequences for its ignition. Shown in the lower left frame, some portion of all the other fuel jets has ignited. By

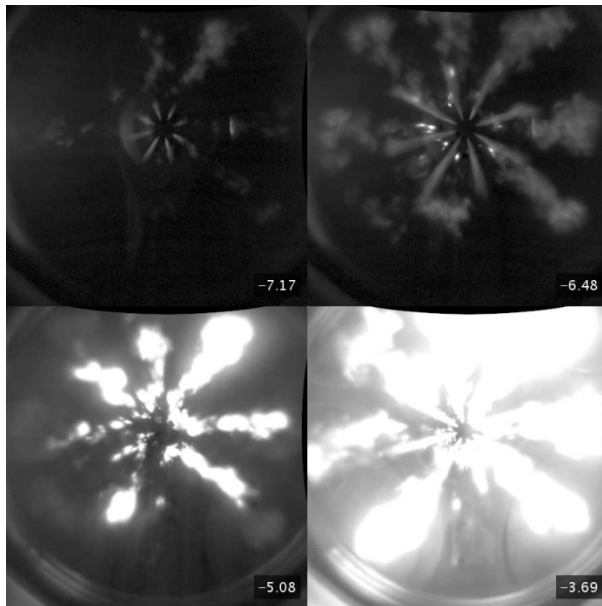
the time faint combustion of the five-thirty jet can be detected in the lower right frame, the combustion of the other jets is already well developed.

The bright regions near the injector in the last two frames are from the elastic scattering of light from fuel droplets. These droplets are created at the tail end of injection when breakup is poor, and during injector dribbling from the sac volume emptying. These droplets are believed to be the source of the intense regions of combustion closer to the nozzle. Some droplets evaporate before the bright combustion is seen and some regions may be elastic scattering of liquid fuel, so it cannot be definitively stated at this time. No matter their source, the intense spots of combustion play a strong role in contact ignition since they tend to generate more intense combustion of the following impinging injection. This can be seen, for example, by comparing the one o'clock and eight o'clock fuel jets of Figure 4.5a.

The short dwell spacings implemented in Strategy B are very appreciable in comparison to the reference strategy. Refer to Figure 4.5b. The first frame is again the very beginning of P2 injection. While the dwell after P1 is not much shorter than that in the reference strategy, the advanced phasing has increased the ignition delay of P1 such that the start of P1 combustion is simultaneous with the start of P2 injection. The combustion is much less developed by the time the P2 injection is fully developed and this leads to less consistent strengths in the contact ignition of it. Again, the jet in the five-thirty position failed to interact with a combustion region and has a significantly extended combustion delay. The second and third injections are so closely coupled that the lower right frame shows the fully developed flow of P3 occurs even before ignition of the P2 fuel in the five-thirty position can be detected. It should be noted that the five-thirty and eight o'clock fuel jets did not always have poor ignition, it is just a coincidence of the cycles chosen here. On the vast majority of cycles in all strategies, however, one of the jets between the five-thirty and eleven-thirty positions failed to achieve a solid contact interface.



(a) Reference Strategy



(b) Strategy B

**Figure 4.5:** After the combustion of P1, the subsequent fuel injections interact with the prevailing combustion regions. In cases where the interface is missed, the fuel has a significantly longer ignition delay and slower growth. CAD aTDC are displayed in the lower left of each frame.

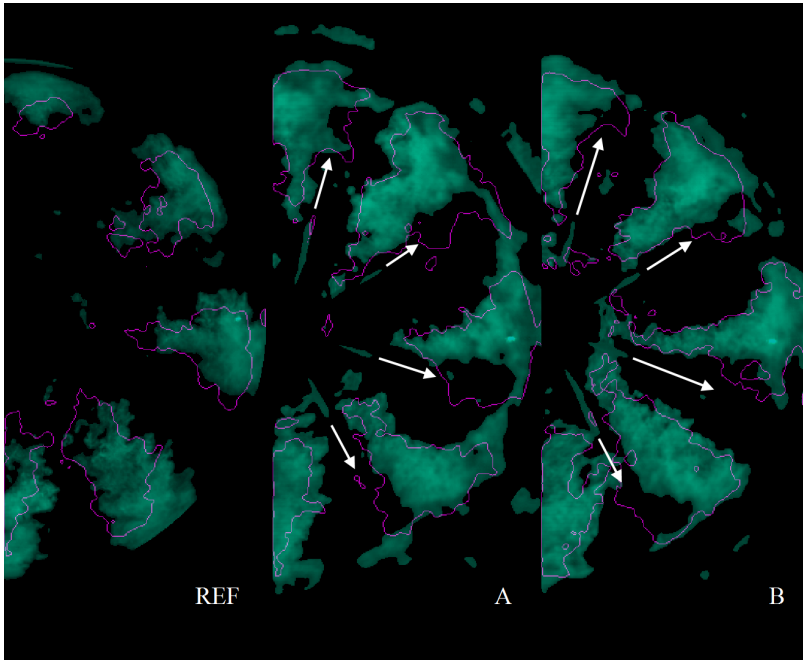


**Figure 4.6:** Combustion regions at the beginning and end of the drop in HRR preceding the main injection. The purple outline shows the extent of the region in the beginning and the green regions show what remains after. White arrows continue the trajectories of the faint liquid portions of the fuel jets, which align with the extinguished portions of the combustion.

### 4.3.3 Extinguishing of Prevailing Combustion

While a strong contact ignition phenomenon is present (at least in the early stages of combustion) a strong extinguishing phenomenon is also present. This occurs for every fuel injection after P1, but it is most notable later on in the sequence when large combustion regions are established and the fuel injection durations increase.

When a fuel jet impacts regions of strong combustion, an extinguishing of those regions occurs along the fuel jet's axis. The drop in HRR just after the peak combustion of the last pilot injection is studied to identify this extinguishing phenomenon. Figure 4.6 shows the combustion regions present at the beginning and end of this HRR drop for each case. In strategies A and B, this decline in HRR is associated with an injection, but not for the reference strategy. As shown in the figure, the purple outlined regions in the reference strategy are very similar to those shaded green. These are the before and after images, respectively. The



regions have slightly drifted down-swirl in the counter-clockwise direction, but no significant difference in their shape occurs. For strategies A and B, significant portions of the combustion along the jet axes are extinguished. There is more extinguishing present in A than in B. The reason for this is the shorter dwells of strategy B. Shorter dwells mean the subsequent injections are entering into less developed regions of combustion, so the extent of the extinguishing phenomenon is reduced.

This shows that the dips in the HRR can be due to the exhaustion of the fuel source, as in the reference strategy, but also by the extinguishing of prevailing combustion during otherwise intense heat release. Less extinguishing occurs in strategy B, and recalling from Figure 4.2b, the dip in HRR is also reduced compared with strategy A. This could not have been determined without optical investigation into the combustion process. The details of this extinguishing phenomenon are not yet clear, however, and will be investigated in further detail in Section 4.4.

#### **4.3.4 Re-entrainment of Combustion Radicals**

Another phenomenon which is observed is the re-entrainment of combustion radicals into subsequent fuel jets. This is most noticeable for sustained jets, especially the main injection. This provides very clear evidence for how far the effects of air entrainment into the fuel jets extend throughout the combustion chamber. Small flamelets drifting towards the bowl wall are seen to reverse direction, being drawn in radially towards the nozzle at the center of the cylinder and into the jet axes.

The implications of this are not studied, but this consistent phenomenon may create important interactions affecting ignition and emissions formations within a quasi-steady jet and the soot clouds downstream of it.

#### **4.3.5 Conclusions**

The first injection combusts primarily via deflagration initiated by a multitude of autoignition sites. Contact between those combustion regions and the subsequent injections stabilize the ignition of the newly injected fuel. Despite this contact ignition, extinguishing of the prevailing combustion also occurs. Extinguishing should be minimized in order to help create a more linear HRR. In order to minimize the extinguishing phenomenon, smaller fuel injections should

be injected into less well developed regions of combustion. This is achieved by closely-coupling the injections.

## 4.4 Investigations on the Extinguishing Phenomenon

Some key findings, results, and conclusions from Paper III are summarized in this section. This work investigates the extinguishing phenomenon identified in the prior investigation. The quasi-steady combustion models in Section 2.2 are good indicators of what chemical species are likely to exist in this extinguishing interface. Closely-coupled injections are significantly different from quasi-steady sprays, but they will be more comparable during the longer duration P3 and main injections. This is also where the extinguishing phenomenon is the greatest. This work uses planar laser-induced fluorescence (PLIF) to probe the extinguishing zone along the fuel jet axis for partially oxidized fuel (POF). The POF signal collected will be the result of both formaldehyde and PAH fluorescence, but the two will not be distinguishable directly. It is possible, however, to consider the natural luminosity (NL) signal to motivate which species is more likely at a certain stage of combustion.

Prior works where multiple-injection strategies are investigated in an engine with formaldehyde LIF have not targeted diesel-like combustion. Different LTC modes have been investigated in prior works [44, 58, 59, 60, 42, 43], including homogeneous charge compression ignition, partially premixed compression ignition, and low temperature diesel combustion. Those combustion modes are not similar to diesel combustion because they have a high degree of homogeneity caused by very early injections far from TDC, and/or occur at much lower temperatures.

### 4.4.1 Temporal and Spatial POF Behavior

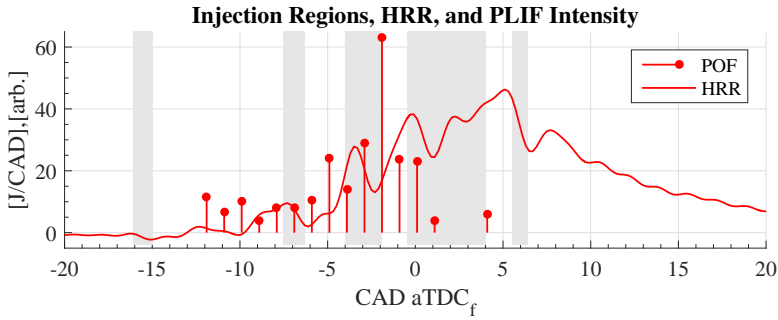
The mean POF signal intensity is investigated throughout the combustion process to determine the relative production and destruction of POF via combustion and the extinguishing phenomenon. Refer to Figure 4.7 for the following explanation of the evolution of the POF location, distribution, and intensity with respect to the HRR and fuel injection events.

The mild heat release from approximately -13 to -10 CAD aTDC is due to the first stage ignition of P1 fuel, which was injected between -16 and -15 CAD aTDC. The mean spatial POF frames show a long and broad distribution of POF

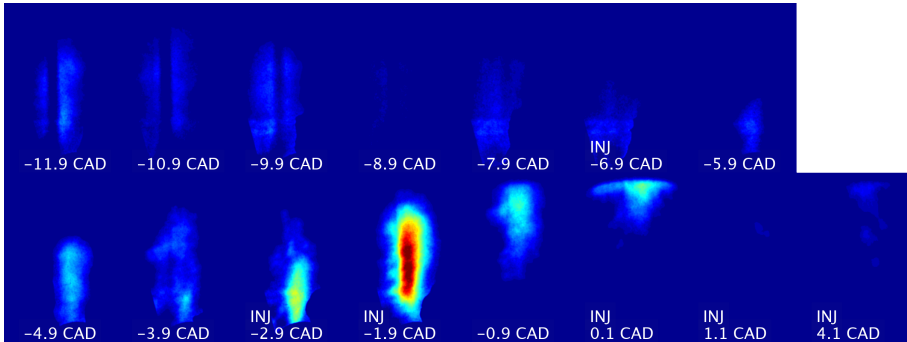
without any intense peaks. This is from ample time after injection for the fuel to disperse into the bowl. A lack of NL signal at this time (not shown) suggests that the POF signal is due to formaldehyde, a product of cool combustion. The dark band present on the images of Figure 4.7b is due to an artifact on the window attenuating the laser sheet. It has no connection to combustion features. Up until just after the injection of P2, the mean temporal POF intensity remains fairly stable at low levels. Considering the mean spatial images, the coverage continues to shrink up until -4.9 CAD aTDC. This is due to the consumption of formaldehyde during the main combustion of P1 during this time.

There is a sudden rise in the mean temporal POF value at -4.9 CAD aTDC. The mean spatial image shows that this area resides near the nozzle (towards the bottom of the frame) and the overlay images shows the absence of NL in this region, suggesting the signal comes from formaldehyde again, likely the first stage ignition of P2 fuel judging by the modest increase in the HRR. This is followed by a sudden decrease in mean temporal POF intensity at -3.9 CAD aTDC. The spatial POF image shows the region is more disperse and less intense. The overlay image shows a sudden appearance of NL intensity which is coincident with the POF signal. Therefore, further oxidation of the POF is occurring. The sharp increase in HRR at this point corroborates this conclusion. The prior work by Idicheria and Pickett also provides evidence this POF is oxidizing further. In their work developing their conceptual model, discussed in section 2.2, they identified the coexistence of POF and soot in the mid to far regions downstream in the jet. At these locations, the combustion is more mature and further along in the oxidation process. The P3 injection is just beginning at this CAD, but it is not developed enough to interact with the combustion yet.

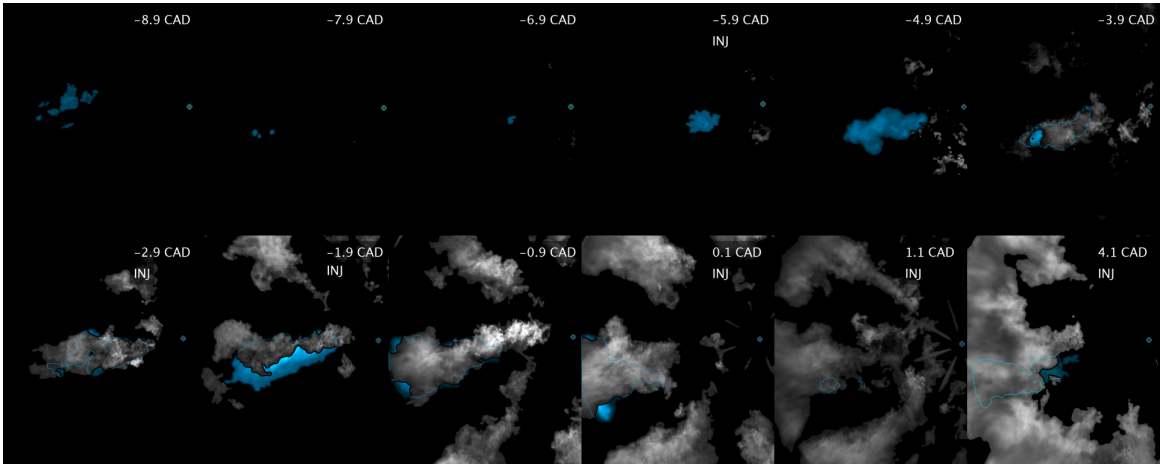
The overlay image doesn't show much of a change at -2.9 CAD aTDC, but the spatial POF image elucidates more detail. There is an intense region of POF at the bottom of the frame, near the injector. This intense region is surrounded by a much more faint, disperse POF region which resembles the one at the prior CAD, just at a more consumed state. The spatial POF signal is comprised of older, hotter species undergoing further oxidation, and new species which have just been ignited off of the hotter region. The placement and timing of this intense region reinforces the contact ignition phenomenon highlighted in the prior investigation.



(a) Mean temporal POF evolution and HRR. Injection durations shown by gray bars.



(b) Mean spatial POF evolution.



(c) Instantaneous NL overlaid onto POF. Different cycle each frame.

**Figure 4.7:** (a) displays the ensemble average HRR with hydraulic injection durations indicated by gray bars. The mean temporal POF signal is displayed as stems. (b) shows the average spatial distribution and intensity of POF only. (c) shows individual and cycle representative combined NL and POF images. The blue regions are false color images of the POF signal. "INJ" denotes an injection is occurring.

At the next investigation point, -1.9 CAD aTDC, the mean temporal POF intensity has a sharp increase just at the end of the P3 injection. The spatial POF frame shows an extremely intense core which extends deep into the combustion chamber. The overlay image at this CAD shows that significant portions of the NL signal have been extinguished by the injection, just as identified in the prior investigation. The immediate decline in mean temporal POF intensity thereafter is associated with another sharp rise in HRR, diminishing POF spatially, and coincident placement of the NL signal. As before, the POF is being oxidized into hotter combustion products.

At 0.1 CAD aTDC, the injection has had less than 1 CAD to develop, and with the NL and POF signals located towards the piston bowl wall, a lack of interaction can explain the stagnation of the mean temporal POF signal. Thereafter, during the fully developed main injection, almost no POF can be detected. This is despite regions of the NL signal clearly being extinguished along the jet axis at 1.1 and 4.1 CAD in the overlay images. Instead of intense POF signal, there is simply lack of signal from either. The same is noted in strategy B. This is not what occurs for the reference strategy, where extinguished regions of the NL signal are filled with POF. The earlier phasing of both the triple-pilot strategies may explain this. During the main injection, the global temperatures and pressures are much higher than for the reference case. It may be possible that at these temperatures, the residence time of the cooler species of POF are much shorter lived. When some POF is noticeable at 4.1 CAD, it is far from the injector and likely a very late state of POF. The exposure time of the camera and fluence of the laser may both have been too low to detect young, cool POF at these conditions.

#### 4.4.2 Conclusions

The contact and extinguishing phenomena are confirmed in this deeper dive study. PLIF probing for POF along the jet axis has shown that when the extinguishing takes place, this does not result in a total destruction of combustion. Instead, hot combustion products are replaced with cooler ones. This has been determined through the combined consideration of the HRR, NL, and POF intensity behaviors over time and their relation to the fuel injection events.

**Table 4.3:** Measured hydraulic dwell separations for each level, labeled -3 to +1 from the shortest to longest dwells. The EGR sweep maintains the “0” level values. Individual pilot masses are maintained with acceptable accuracy.

<b>Hydraulic Dwells</b>	-3	-2	-1	0	+1
dwell after P1 [ $\mu\text{s}$ ]	258	419	551	692	794
d.a. P2 [ $\mu\text{s}$ ]	61	112	175	239	320
d.a. P3 [ $\mu\text{s}$ ]	fused	9	89	207	262

## 4.5 Minimizing Combustion Noise

Some key findings, results, and conclusions from Paper IV are summarized in this section. Paper I led to the understanding that the HRR should progress linearly to minimize combustion noise. Papers II and III showed that the interaction between the prevailing combustion and subsequent fuel injection affect the HRR through extinguishing of hot combustion products. Larger injections colliding with well developed regions of combustion lead to more extinguishing and more pronounced undulation in HRR.

Paper IV investigates how the main control variables, such as dwell, EGR, injection pressure, and injection duration affect engine efficiency, emissions, noise levels and frequency content.

### 4.5.1 Dwells and Mixture Dilution

The injection parameters for a sweep of all dwell values changed together are presented in Table 4.3. The pilot masses are the same for all strategies, with masses of 1.8, 2.3, and 6.7 mg for P1-P3, respectively. The values at the “0” level are maintained for the sweep of EGR where inlet  $\text{CO}_2$  concentration is swept from 2.15 to 3.75 %. The main injection duration and timing are altered for each operating point to maintain constant CA50 phasing and engine load. The engine load is the same as in Paper I, 9 bar gross indicated mean effective pressure.

Results for selected engine performance characteristics are shown in Table 4.4. Considering the all dwells sweep, combustion noise decreases with dwell, but up to a point; noise increases at the -3 level, returning to nearly the baseline’s value. Similarly, the dilution level for a given injection sequence can be increased too far. Combustion noise tends to decrease with increasing  $\text{CO}_2$  concentration up until 3.28%. Beyond this, noise exceeds the baseline level and nearly matches

**Table 4.4:** Results from the sweep where all dwell times are adjusted simultaneously as well as the EGR sweep. -3 is the shortest dwell level and +1 is the longest. The “0” and 2.81% CO<sub>2</sub> levels are replicates of the same operating conditions. Percentage point changes of gross indicated efficiency are in relation to the baseline.

<b>All Dwells Sweep</b>	-3	-2	-1	0	+1
Comb. noise [dBA]	81.2	79.2	80.7	81.9	83.0
PPRR [bar/CAD]	5.5	4.0	4.3	4.3	4.3
CA10-CA90 [CAD]	17.5	20.6	21.8	22.0	22.1
Efficiency [p.p.]	0.1%	0.0%	0.0%	-	0.0%
<b>EGR Sweep</b>	2.15	2.49	2.81	3.28	3.75% CO <sub>2</sub>
Comb. noise [dBA]	83.1	82.3	81.9	81.4	83.0
PPRR [bar/CAD]	4.0	4.1	4.2	4.7	5.4
CA10-CA90 [CAD]	21.3	21.8	22.2	22.6	23.2
Efficiency [p.p.]	0.1%	0.2%	-	-0.2%	-0.1%

the value at the minimum dilution level. PPRR does not reflect the variation in combustion noise for either sweep. The efficiency does not vary significantly from the baseline’s value but generally follows the change in CA10-CA90 combustion duration.

Figures 4.8a through 4.8f explain the change in noise for both of these sweeps. Both HRR plots show that at the respective levels where the decreasing noise trend is broken, the HRR behaves very differently. Individual combustion events for each pilot injection can no longer be discerned at the -3 level, and are barely recognizable in the 3.75% CO<sub>2</sub> level. Significant portions of the mass in the early pilots burn together in condensed, more aggressive heat release events. In the EGR sweep, this combined combustion appears to be anchored on the P3 injection, likely stabilized by the contact ignition phenomenon identified in Paper II. After the ignition of P3, the combustion of this fuel injection either directly consumes the remaining unburnt fuel in the chamber or increases the global temperature and pressure enough to trigger the combustion of the unburnt mass fractions.

The blending of the combustion events is due to different mechanisms. In the dwell sweep, the separations between the pilot injections were much shorter than the combustion durations of the initial pilot injections, causing bulk portions of those combustion durations to overlap. A similar overlap occurred in the EGR sweep, but due to an increase of the ignition delay for the early pilots which is caused by the higher dilution ratio.

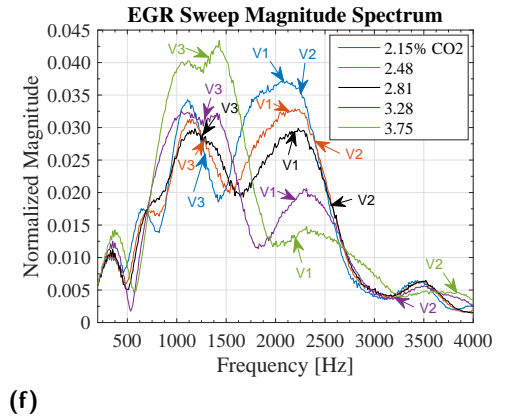
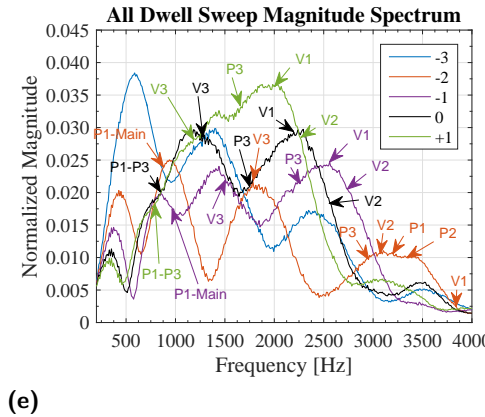
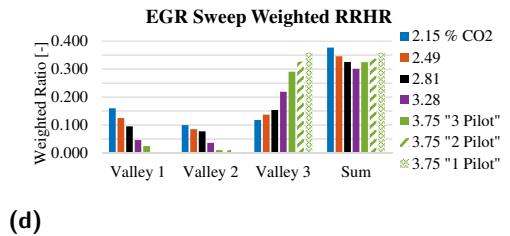
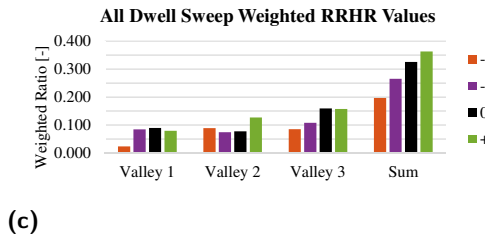
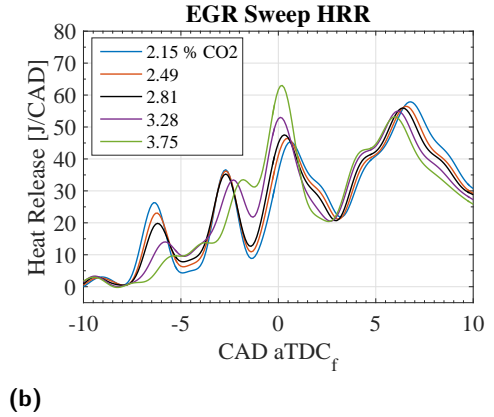
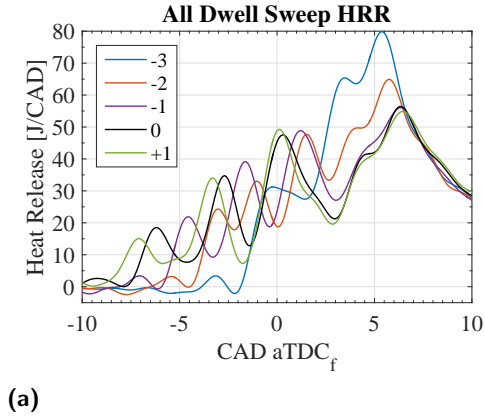


**Figure 4.8:** HRR, RRHR, and magnitude spectrum plots from the investigations where either all dwell values (left) or EGR (right) are swept at otherwise constant conditions.

Both of these operating points show a limitation in the RRHR metric. Each injection should have its own distinct peak in the HRR to be able to associate the behavior in noise to the combustion behavior of each injection. This is the



reason the -3 level does not appear in the weighted RRHR graph of Figure 4.8c. Since it is vaguely possible to do so at the 3.75% level, attempts are made by treating it like a 3, 2, or 1 pilot strategy. Treating it as a single pilot strategy gives the best correlation to the behavior in noise, but the weighted average RRHR value is still lower than it should be.

Apart from those difficult cases, the weighted RRHR values are able to explain the change in combustion noise. For the swept dwell investigation, shorter dwells decrease the width and depth of the valleys, which is reflected in the weighted RRHR values. Considering the magnitude spectrum, the local magnitude at the same frequencies as the  $f_0$ 's of the valleys follows the relative magnitude of the weighted RRHR values. For instance, the weighted RRHR values in V3 are similar at the 0 and +1 levels and decrease at the -1 and -2 levels. Considering the magnitude spectrum, the combustion noise magnitude at the V3  $f_0$  also reflects this relative positioning.

Considering the inverse of the valleys (the peaks) in the HRR, their fundamental frequencies can also be determined by the spacing of the local minima. In some cases, this perspective of the HRR can describe some of the strong frequency content in the combustion noise. These are marked by P1, P2, P3 (not to be confused with P1-P3 which is the  $f_0$  of non-adjacent peaks). As the -2 level shows, however, P1, P2, and P3 are clumped together and do not give a good representation of the frequency spectrum, whereas the valleys do. The conclusion is that while the  $f_0$  of the peaks can be useful at times, the  $f_0$  of the valleys gives the best correlation between the HRR and combustion noise.

For the EGR sweep, the increased dilution ratio smooths out the HRR by limiting the peak combustion rate of the first two pilot injections. This increases the combustion duration for the pilot fuel, maintaining higher combustion rates in the valleys as well. This is an effective way to limit combustion noise. The combined interpretation of the weighted RRHR and magnitude spectrum plots confirms that the combustion noise between 1750 and 2750 Hz was caused by valleys 1 and 2 in the HRR. Reducing the size of these valleys increases the relative size of the third. When done moderately, this does not overcome the benefits earlier in the HRR. The largest drawback of increasing the inlet  $\text{CO}_2$  concentration is increased soot emissions.

## 4.5.2 Injection Pressure

A detailed analysis on the effects of injection pressure will be left to the scope of Paper IV. The main findings will be shortly summarized here.

Injection pressures between 700 and 1100 bar were not found to have a significant impact on combustion noise, but can modify the frequency content of the combustion noise. As injection pressure is changed and pilot masses are kept constant, the duration of each injection decreases. This has a similar effect to reducing the dwell as the  $f_0$  tends to increase for the early valleys; the local peaks are closer together. This can reduce the width of the valleys which decreases the weighted RRHR values. This is also reflected in the magnitude spectrum. Decreases in the 1st and 2nd valleys were canceled out by increasing the area of V3, however. In this particular investigation, P3 mass was not held as consistently as desired and this makes the interpretation difficult. This is discussed more in Paper IV, but the size of V3 should still be representative of the results with correct injection quantities.

The most significant factor injection pressure influences is soot emissions. Higher injection pressure decreases soot dramatically. This, combined with the fact that higher injection pressure does not significantly increase combustion noise, is beneficial since it has been shown that high dilution ratios are useful for decreasing both combustion noise and  $\text{NO}_x$  emissions.

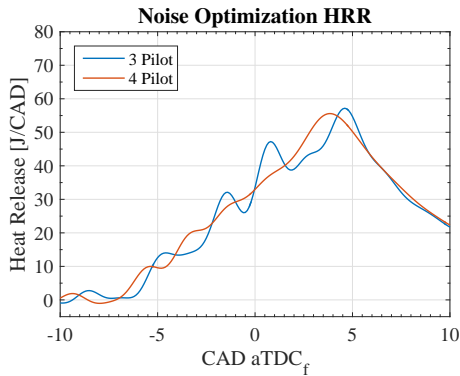
### 4.5.3 Noise Optimization

By implementing the best attributes from each of the investigations above (including the learnings from the optical experiments), a triple and quadruple-pilot strategy are both optimized for minimum combustion noise. The inlet  $\text{CO}_2$  concentration is 3.65% and injection pressure 700 bar. The injection masses and dwells are summarized in Table 4.5.

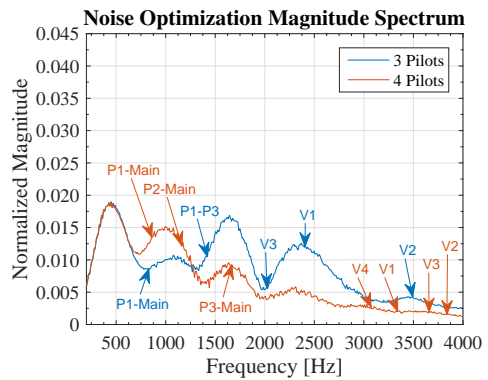
**Table 4.5:** Values of each noise optimized injection strategy. Injection pressure is 700 bar and inlet  $\text{CO}_2$  is 3.65%. \*The masses of these pilots are found by dividing the fused injection at the inflection point between the final pilot and main injection.

<b>3 Pilots</b>	P1	P2	P3	
Dwell after [ $\mu\text{s}$ ]	607	175	fused	
Mass [mg]	1.7	2.5	7.2*	
<b>4 Pilots</b>	P1	P2	P3	P4
Dwell after [ $\mu\text{s}$ ]	481	183	69	fused
Mass [mg]	1.3	1.4	3.1	6.8*

The resulting HRR and magnitude spectra from those operating conditions are shown in Figure 4.9. The weighted RRHR values are all very small so the plot is



(a)



(b)

**Figure 4.9:** HRR and magnitude spectrum for the noise optimized triple and quadruple pilot injection strategies.

not reproduced here, but can be found in Paper IV. The HRR for the quadruple pilot strategy is very nearly linear. Its weighted average RRHR value is just 0.083. An unprecedented behavior for both of these injection strategies is that the frequency content on the order of the combustion duration itself, just below 500 Hz, has the single strongest amplitude in the magnitude spectrum. The combustion noise levels for these strategies are 76.7 and 75.3 dBA for the triple and quadruple-pilot strategies, respectively. Despite this significant reduction in noise, the PRRR values remain at similar levels to the other, much louder operating points.

Unfortunately, due to technical difficulties, the soot levels of the noise optimized cases cannot be directly compared to the others. Between those two, however, soot emissions doubles for the quadruple-pilot strategy, which is its largest drawback.

It should be noted that the nearly linear progression of the HRR for both of these strategies is achieved through injection rate shaping, where the injection flow rate changes but never stops. In this case it takes the form of two separate injections fused to each other, creating an inflection in flow between adjacent maxima. This same phenomena occurred in the -3 dwell case earlier, but the surrounding settings led the overall result to be worse than the baseline. In understanding the effects of dwell, dilution, and injection pressure through the entire sequence, injection rate shaping can be implemented to reduce the HRR undulation near the global peak values.

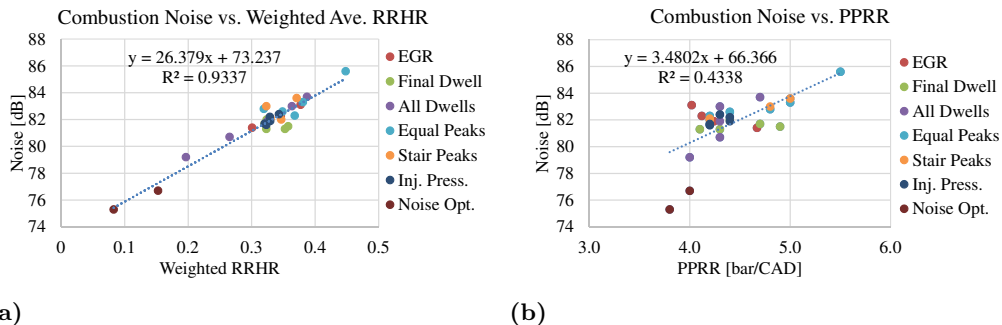


**Figure 4.10:** Regression models of both weighted average RRHR and PPRR predicting combustion noise.

#### 4.5.4 RRHR as a Predictor of Noise

It has been shown case-by-case that the individual weighted RRHR values describe the relative strengths in the magnitude spectra of the combustion noise via the behavior of the HRR. The single weighted average RRHR has also been shown to correlate well with total noise levels, but the results have been dispersed. Figure 4.10 shows regression models of a multitude of operating points studied in Paper IV. On the left is weighted average RRHR predicting combustion noise, and on the right, PPRR predicting the same. These regressions confirm the statements throughout the studies: PPRR is not a good indicator of combustion noise for closely-coupled multiple-injection strategies, but RRHR is, due to its phenomenological basis. This metric is therefore a useful tool for; identifying which valleys in the HRR should be targeted to reduce combustion noise; indicating how the HRR should be modified to achieve that reduction; providing a comparison between different operating conditions at the same speed-load point; indicating a minimum achievable noise level at that point; and predicting combustion noise.



# Chapter 5

## Conclusions

Closely-coupled multiple-pilot injection strategies have been experimentally investigated in conventional and optical engines. They have been contrasted to a conventional, production-like multiple-pilot strategy with moderate dwells after each pilot injection, several times longer than the closely-coupled dwells.

Compared to a conventional injection strategy which is representative for a modern light-duty diesel engine, close-coupling of the pilot injections greatly reduced the combustion noise. This allowed the combustion to be phased to maximum brake torque timing while still remaining almost 4 dB quieter than the conventional case. This phasing was done to quantify what efficiency improvement could be attained.  $\text{NO}_x$  emissions increased while soot emissions decreased largely as a result of this phasing, but the gross indicated efficiency rose by nearly 4%. Understanding the magnitude of these trade-offs can better motivate compromises which may be necessary to create a well rounded injection strategy meeting all engine performance targets.

Physically, the combustion noise was reduced by a more linear heat release rate (HRR) which reduced the undulations in the pressure trace. This is characterized by the weighted ratios of reduced heat release (RRHR). This metric has been developed by the author to analyze the HRR profile to both explain and predict the combustion noise level and relative frequency content therein. When predicting total combustion noise at a constant load-speed point, weighted average RRHR performed very well with a coefficient of determination of 0.934. In comparison, PPRR (a metric commonly used to indicate changes in combustion noise) only performed at 0.434 for the same cases.

Since the RRHR metric has a phenomenological foundation, it can also be used

as a calibration tool to indicate how a HRR should be modified to minimize combustion noise. The intuitive aim of reducing the size of the valleys in the HRR obviates massive multiple factor DoEs which would otherwise be needed to investigate a full injection strategy parameterization. It can also explain why boundary conditions can affect combustion noise while the injection parameters remain unchanged. Boundary conditions which affect the buildup of the heat release rate will affect combustion noise, and this change can be captured and explained by the weighted RRHR values. The fundamental frequency of the valleys explains what frequency content in the pressure trace is caused by specific valleys in the HRR. The individual weighted RRHR values indicate which valleys contribute the most to combustion noise so that appropriate changes to either the boundary or injection parameters can be made to reduce the size of those valleys. This metric does have limitations, however. It is not yet a universal predictor of combustion noise across all load-speed points, but potential improvements are discussed in the Future Outlook chapter. It also cannot describe or predict combustion noise when significant portions of separate injections combust as a group.

The combustion process was investigated optically to identify key differences between the conventional and closely-coupled strategies. Contact ignition of subsequent fuel injections on prevailing combustion regions was observed in all cases. Another key discovery in this thesis work was that the injections were also the cause of extinguishing of said prevailing combustion regions. Through further investigation, this extinguishing phenomenon was found to replace hot combustion products with cooler ones, such as formaldehyde and PAH. By considering the behavior of the HRR during this extinguishing, it has been shown that it is partially responsible for the undulation in the HRR. Spatial knowledge provided by the optical investigation identified how the dwell timing could affect both the ignition and extinguishing phenomena. At shorter dwells, the subsequent injections occurred at less developed stages combustion. This reduced the strength of both the contact ignition and extinguishing phenomena, which led to a more linear HRR buildup. With this improved understanding and the comparison of HRR profiles from optical and conventional engine experiments, it may be possible to identify combustion interactions based on obvious HRR behaviors. An example of this is when otherwise severely delayed combustion of early pilots has a HRR feature anchored in time with a later injection. This is likely a case of contact ignition stabilizing the combustion of the later injection. As another example, a reduction in the depth of a valley as dwell is decreased is likely due to less extinguishing of the prevailing combustion. Consideration is still required, however, since the other primary reason for the dips in HRR are the simple exhaustion of the prior fuel source.

The effects of dwell, mixture dilution, injection pressure, and even injection rate shaping were then investigated. This further reinforced prior discoveries while also adding an understanding of how these boundary conditions affect combustion noise and the HRR directly. High dilution ratios and decreased dwell times were the primary factors which allowed combustion noise to be reduced. They both effectively created a more linear progression the HRR, which decreased combustion noise despite higher peak pressures and occasionally peak pressure rise rates. Injection pressure did not have a significant impact on combustion noise, but tended towards higher values at higher pressures. It did have a significant ability to reduce soot emissions, however. These combined factors are beneficial since high EGR ratios should be used to lower both  $\text{NO}_x$  and combustion noise. Using the combined learnings from this and prior investigations, triple and quadruple-pilot injection strategies were created at appropriate boundary conditions to minimize combustion noise as far as possible with the specific hardware setup. A more linear buildup of the HRR was achieved through injection rate shaping between the final pilot and main injections.





## Chapter 6

# Future Outlook

The following are several recommendations to improve the understanding of the combustion characteristics of closely-coupled multiple-pilot diesel injection strategies.

As noted in Paper II, the entrainment of combustion products into sustained jets is a consistent phenomenon, but highly dependent on the injection strategy. It is most notable during sustained injections, but if the prevailing combustion regions lie close to the nozzle there is the possibility for shorter injection durations to entrain significant amounts. With multiple, short duration injections, combustion products will be closer to the nozzle since these smaller injections have less momentum. Short dwells allow for less time for combustion to drift away from the injector as well. An interesting investigation would be to identify if this has an effect on ignition or emissions. Entraining intense combustion products in the liquid phase of the jet could help stabilize ignition, similar to the contact interface identified in Paper II. From an emissions perspective, large soot particles may be physically wetted by the fuel before they re-enter the combustion zone and this may affect soot formation.

Regarding the injections themselves, the combustion behavior from injection rate shaping should be optically investigated in conjunction with closely-coupled, but hydraulically separate, injections. An investigation into the extinguishing phenomenon should be able to shed light upon how the net HRR can be made nearly linear as was done in the quadruple-pilot noise optimization.

The RRHR metric is very young and needs more broad vetting and, if necessary, adjusting to become a more widespread tool for heat release analysis. Two perspectives in particular were not investigated in this work. One is speed, the

other is combustion phasing. For a given injection strategy, as engine speed is increased, the rate of volume change follows suit. Since the injection hardware and combustion are time-based phenomena, the HRR profile will not behave in precisely the same way at higher engine speeds. For example, a valley in the HRR ahead of TDC may become more shallow due to more rapid compression increasing reaction rates, but the local peaks may also increase, maintaining the size of the valley. After TDC, one example has already been highlighted in the reference strategy of Paper I. When periods of little to no heat release occur during more rapid volume expansion, the pressure trace develops an inflection, a clear contributor to combustion noise. This is also coupled to the phasing question. It is presumed that the weighted RRHR values will still be good predictors at different phasings, as was shown in Paper I, but that was a limited investigation. In comparison of weighted RRHR vs combustion noise, a regression for the data in Paper I still shows a linear trend with a good fit, but the slope is shallower than for the one created from the Paper IV investigations, where the engine speed was 7% higher. Based on the behavior of the slope at this small engine speed difference, there is reason to believe large increases in engine speed will lead to steeper slopes for this regression. If the slope of this linear trend is indeed tied to engine speed, it is an important factor to include. This would extend this metric's comparability across the speed range at a constant load point. On the topic of load, it may also be possible to normalize the metric once more based upon load to create a fully universal predictor of combustion noise throughout the load-speed map.

Some further suggestions more outside the investigations of this thesis are recommended:

From a perspective which could sit apart from combustion phenomena, PIV studies of air entrainment along the jet axis during unsteady injections would also be an interesting investigation. Such a study could lead to an improved conceptual model similar to the one put forth by Kosaka et al. where recirculation zones are depicted, but not well motivated in their text [26].

On the topic of combustion region location and spray momenta, an analysis from a heat loss perspective can also shed light into the efficiency potential of these strategies. With less combustion in contact with the bowl wall, and less convective transfer from the reduced wall interactions, the heat transfer may be reduced.

# Chapter 7

## References

- [1] International Organization of Motor Vehicle Manufacturers, “PC World Vehicles in Use.” [http://www.oica.net/wp-content/uploads/PC\\_Vehicles-in-use.pdf](http://www.oica.net/wp-content/uploads/PC_Vehicles-in-use.pdf), 2015. Online; Accessed on 2019-03-06.
- [2] International Organization of Motor Vehicle Manufacturers, “Provisional New PC Registrations or Sales.” <http://www.oica.net/wp-content/uploads/Sales-Passenger-cars-2017.pdf>, 2017. Online; Accessed on 2019-03-06.
- [3] Y. Sun and N. Shirouzu, “China auto sales post biggest drop in 7 years as growth engine stalls.” <https://www.reuters.com/article/us-china-autos-sales/china-auto-sales-post-biggest-drop-in-7-years-as-growth-engine-stalls-idUSKCN1MM0KV>, October 12 2018. Online; Accessed on 2019-03-06.
- [4] World Health Organization, *Evolution of WHO air quality guidelines*. Copenhagen: WHO Regional Office for Europe, 2017.
- [5] S. C. Anenberg, J. Miller, R. Minjares, L. Du, D. K. Henze, F. Lacey, C. S. Malley, L. Emberson, V. Franco, Z. Klimont, and C. Heyes, “Impacts and mitigation of excess diesel-related NO<sub>x</sub> emissions in 11 major vehicle markets,” *Nature*, vol. 545, p. 467, may 2017.
- [6] Delphi, “Worldwide emissions standards, passenger cars and light duty vehicles.” Booklet, G.D. of Luxembourg, 2019.
- [7] REN21, *Renewables 2018: Global Status Report*. Paris: REN21 Secretariat, 2018.

- [8] International Energy Agency, “Global ev outlook 2018.” <https://www.iea.org/gevo2018/>, 2018. Online; Accessed on 2019-03-06.
- [9] Commission Staff, “Report on Raw Materials for Battery Applications - Commission Staff Working Document,” tech. rep., European Commission, Brussels, 2018. SWD(2018) 245/2 final.
- [10] V. Walt and S. Meyer, “Blood, sweat, and batteries.” <http://fortune.com/longform/blood-sweat-and-batteries/>, August 23 2018. Online; Accessed on 2019-03-06.
- [11] K. Turcheniuk, D. Bondarev, V. Singhal, and G. Yushin, “Ten years left to redesign lithium-ion batteries,” *Nature*, vol. 559, pp. 467–470, jul 2018.
- [12] European Automobile Manufacturers Association, “Passenger car fleet by fuel type.” <https://www.acea.be/statistics/tag/category/passenger-car-fleet-by-fuel-type>, 2017. Online; Accessed on 2019-03-06.
- [13] J. Hagen, O. E. Herrmann, J. Weber, and D. Queck, “Diesel Combustion Potentials by Further Injector Improvement,” *MTZ*, pp. 16–21, 2016.
- [14] D. Schöppe, F. Atzler, O. Kastner, and F. Kapphan, “High Performance Diesel Direct Driven Piezo Common Rail Injection System,” in *23rd Aachen Colloquium Automobile and Engine Technology 2014*, (Aachen), pp. 773–790, 2014.
- [15] D. Zeh, J. Hammer, C. Uhr, M. Rückle, A. Rettich, B. Grota, W. Stöcklein, J. Gerhardt, D. Naber, and M. Raff, “Bosch Diesel Injection Technology — Response for Every Vehicle Class Production,” *23rd Aachen Colloquium Automobile and Engine Technology 2014*, pp. 757–772, 2014.
- [16] N. Möller, M. Fleiss, S. Rengmyr, and J. Somhorst, “VEA – the new engine architecture from Volvo,” *MTZ*, sep 2013.
- [17] H. Persson, A. Babajimopoulos, A. Helmantel, F. Holst, and E. Stenmark, “Development of the Combustion System for Volvo Cars Euro6d VEA Diesel Engine,” *SAE Technical Paper*, no. 2017-01-0713, 2017.
- [18] J. B. Heywood, *Internal Combustion Engine Fundamentals*. New York: McGraw-Hill, 1988.
- [19] J. E. Dec, “A Conceptual Model of DI Diesel Combustion Based on Laser-Sheet Imaging,” *SAE Technical Paper*, no. 970873, 1997.

- [20] J. D. Naber and D. L. Siebers, “Effects of Gas Density and Vaporization on Penetration and Dispersion of Diesel Sprays,” *SAE Technical Paper*, no. 960034, 1996.
- [21] C. A. Idicheria and L. M. Pickett, “Formaldehyde Visualization Near Lift-off Location in a Diesel Jet,” *SAE Technical Paper*, 2006.
- [22] Ö. Andersson and P. C. Miles, *Diesel and Diesel LTC Combustion*, pp. 1–36. Wiley, 2014.
- [23] D. R. Tree and K. I. Svensson, “Soot processes in compression ignition engines,” *Progress in Energy and Combustion Science*, vol. 33, no. 3, pp. 272–309, 2007.
- [24] Y. Gallo, P.-E. Bengtsson, H. Bladh, T. Lind, J. Simonsson, and Ö. Andersson, “A Study of In-Cylinder Soot Oxidation by Laser Extinction Measurements During an EGR-Sweep in an Optical Diesel Engine,” *SAE Technical Paper Series*, vol. 1, no. 2015-01-0800, 2015.
- [25] Y. Gallo, Z. Li, M. Richter, and Ö. Andersson, “Parameters Influencing Soot Oxidation Rates in an Optical Diesel Engine,” *SAE International Journal of Engines*, vol. 9, no. 4, pp. 2044–2055, 2016.
- [26] H. Kosaka, T. Aizawa, and T. Kamimoto, “Two-dimensional imaging of ignition and soot formation processes in a diesel flame,” *International Journal of Engine Research*, vol. 6, no. 1, pp. 21–42, 2005.
- [27] H. Kosaka, V. H. Drewes, L. Catalfamo, A. A. Aradi, N. Iida, and T. Kamimoto, “Two-Dimensional Imaging of Formaldehyde Formed During the Ignition Process of a Diesel Fuel Spray,” *SAE Technical Paper*, 2000.
- [28] Ö. Andersson, J. Somhorst, R. Lindgren, R. Blom, and M. Ljungqvist, “Development of the Euro 5 Combustion System for Volvo Cars’ 2.4.I Diesel Engine,” *SAE Technical Paper*, no. 2009-01-1450, 2009.
- [29] H. Jääskeläinen, “Diesel fuel injector nozzles.” [https://www.dieselnet.com/tech/engine\\_fi\\_nozzle.php](https://www.dieselnet.com/tech/engine_fi_nozzle.php), 2017. Online; accessed 2019-02-20.
- [30] M. Russell, C. Young, and S. Nicol, “Modulation of Injection Rate to Improve Direct Injection Diesel Engine Noise,” *SAE Technical Paper*, no. 900349, 1990.
- [31] M. Dürnholz, H. Endres, and P. Frisse, “Preinjection A Measure to Optimize the Emission Behavior of DI-Diesel Engine,” *SAE Technical Paper*, no. 940674, 1994.

- [32] I. Osuka, M. Nishimura, Y. Tanaka, and M. Miyaki, "Benefits of New Fuel Injection System Technology on Cold Startability of Diesel Engines - Improvement of Cold Startability and White Smoke Reduction by Means of Multi Injection with Common Rail Fuel System (ECD-U2)," *SAE Technical Paper*, no. 940586, 1994.
- [33] T. Tanaka, A. Ando, and K. Ishizaka, "Study on pilot injection of DI diesel engine using common-rail injection system," *JSAE Review*, no. 3, pp. 297–302, 2002.
- [34] M. Badami, F. Mallamo, F. Millo, and E. Rossi, "Influence of Multiple Injection Strategies on Emissions , Combustion Noise and BSFC of a DI Common Rail Diesel Engine," *SAE Technical Paper*, no. 2002-01-0503, 2002.
- [35] T. Husberg, I. Denbratt, and A. Karlsson, "Analysis of Advanced Multiple Injection Strategies in a Heavy-Duty Diesel Engine using Optical Measurements and CFD-Simulations," *SAE Technical Paper*, 2008.
- [36] J. Lee, J. Jeon, J. Park, and C. Bae, "Effect of Multiple Injection Strategies on Emission and Combustion Characteristics in a Single Cylinder Direct-Injection Optical Engine," *SAE Technical Paper*, 2009.
- [37] S. Mendez and B. Thirouard, "Using Multiple Injection Strategies in Diesel Combustion: Potential to Improve Emissions, Noise and Fuel Economy Trade-Off in Low CR Engines," *SAE Int. J. Fuels Lubr.*, pp. 662–674, 2008.
- [38] A. Binde, S. Busch, A. Velji, and U. Wagner, "Soot and NOx Reduction by Spatially Separated Pilot Injection," *SAE Technical Paper*, no. 2012-01-1159, pp. 1242–1259, 2012.
- [39] J. Weber, N. Sashima, O. Herrmann, and J. Hagen, "Reduction of Diesel Engine Emissions Performance – Further Steps Towards a Fast and Flexible Fuel Injection," *Springer*, pp. 25–40, 2017.
- [40] F. Bowditch, "A new tool for combustion research: A quartz piston engine," *SAE Technical Paper*, no. 610002, 1961.
- [41] B. Johansson, *Förbränningsmotorer*. Lund University, 2006.
- [42] L. Hildingsson, H. Persson, B. Johansson, R. Collin, J. Nygren, M. Richter, M. Aldén, R. Hasegawa, and H. Yanagihara, "Optical Diagnostics of HCCI and Low-Temperature Diesel Using Simultaneous 2-D PLIF of OH and Formaldehyde," *SAE Technical Paper*, no. 2004-01-2949, 2004.

- [43] L. Hildingsson, H. Persson, B. Johansson, R. Collin, J. Nygren, M. Richter, M. Aldén, R. Hasegawa, and H. Yanagihara, “Optical Diagnostics of HCCI and UNIBUS Using 2-D PLIF of OH and Formaldehyde,” No. 2005-01-0175, 2005.
- [44] R. Collin, J. Nygren, M. Richter, M. Aldén, L. Hildingsson, and B. Johansson, “The Effect of Fuel Volatility on HCCI Using Simultaneous Formaldehyde and OH PLIF,” *SAE Technical Paper*, no. 2004-01-2948, 2004.
- [45] F. Tao, R. D. Reitz, and D. E. Foster, “Revisit of Diesel Reference Fuel ( n-Heptane ) Mechanism Applied to Multidimensional Diesel Ignition and Combustion Simulations,” *17th International Multidimensional Engine Modeling User’s Group Meeting*, vol. 15, pp. 1–8, 2007.
- [46] U. Aronsson, H. Solaka, G. Lequien, Ö. Andersson, and B. Johansson, “Analysis of Errors in Heat Release Calculations Due to Distortion of the In-Cylinder Volume Trace from Mechanical Deformation in Optical Diesel Engines,” *SAE Int. J. Engines*, vol. 5, no. 2012-01-1604, pp. 1561–1570, 2012.
- [47] A. J. Shahlari, C. Hocking, E. Kurtz, and J. Ghandhi, “Comparison of Compression Ignition Engine Noise Metrics in Low-Temperature Combustion Regimes,” *SAE Int. J. Engines*, pp. 541–552, 2013.
- [48] R. Diwakar and V. Domenech-Llopis, “Physics of Combustion Noise Reduction with Multiple Injections in a DI Diesel Engine - A Computational Study,” *SAE Technical Paper*, vol. 01, no. 2017-01-0566, 2017.
- [49] M. Denny, F. Holst, A. Helmantel, H. Persson, P. Tunestål, and Ö. Andersson, “Impact of closely-coupled triple-pilot and conventional double-pilot injection strategies in a LD diesel engine,” *Fuel*, vol. 246, no. February, pp. 141–148, 2019.
- [50] M. F. Russell and R. Haworth, “Combustion Noise from High Speed Direct Injection Diesel Engines,” *SAE Transactions*, vol. 94, pp. 810–831, 1985.
- [51] A. C. Eckbreth, *Laser Diagnostics for Temperature and Species in Unsteady Combustion*. Amsterdam: Gordon and Breach Science Publishers, second ed., 1988.
- [52] A. Hultqvist, M. Christensen, B. Johansson, M. Richter, J. Nygren, J. Hult, and M. Aldén, “The HCCI Combustion Process in a Single Cycle - Speed Fuel Tracer LIF and Chemiluminescence Imaging,” *SAE Technical Paper*, no. 2002-01-0424, 2002.



- [53] J. H. Sun, D. A. Yates, and D. E. Winterbone, "Evaluation of the Intensity of Turbulent Velocities by Using a Cross-Correlation Technique for Pattern Tracking," *SAE Technical Paper*, no. 960267, 1996.
- [54] H. W. R. Dembinski and H. E. Angstrom, "Optical Study of Swirl during Combustion in a CI Engine with Different Injection Pressures and Swirl Ratios Compared with Calculations," *SAE Technical Paper*, no. 2012-07-0682.
- [55] C. Beatrice, P. Belardini, C. Bertoli, M. G. Lisbona, and G. M. Rossi Sebastiano, "Combustion Process Management in Common Rail DI Diesel Engines by Multiple Injection," *SAE Technical Paper*, no. 2001-24-0007, 2001.
- [56] T. Brands, T. Huelser, P. Hottenbach, H.-J. Koss, and G. Grunefeld, "Optical Investigation of Combusting Split-Injection Diesel Sprays Under Quiescent Conditions," *SAE Int. J. Engines*, no. 2013-24-0034, pp. 1626–1641, 2013.
- [57] C. Park and S. Busch, "The influence of pilot injection on high-temperature ignition processes and early flame structure in a high-speed direct injection diesel engine," *International Journal of Engine Research*, 2017.
- [58] H. Zhao, Z. Peng, and T. Ma, "Investigation of the HCCI/CAI Combustion Process by 2-D PLIF Imaging of Formaldehyde," *SAE Technical Paper*, no. 2004-01-1901, 2004.
- [59] G. Särner, M. Richter, M. Aldén, L. Hildingsson, A. Hultqvist, and B. Johansson, "Simultaneous PLIF Measurements for Visualization of Formaldehyde- and Fuel- Distributions in a DI HCCI Engine," *SAE Technical Paper*, no. 2005-01-3869, 2005.
- [60] R. Florea, K. Zha, X. Yu, M. Jansons, D. Taraza, and N. Henein, "Ethanol/N-Heptane Dual-Fuel Partially Premixed Combustion Analysis through Formaldehyde PLIF," *SAE International Journal of Engines*, vol. 5, apr 2012.

# Scientific publications

## Author contributions

### **Paper I: Impact of Closely-Coupled Triple-Pilot and Conventional Double-Pilot Injection Strategies in a LD Diesel Engine**

**M. Denny**, F. Holst, A. Helmantel, H. Persson, P. Tunestål, Ö. Andersson  
*Fuel*, vol. 246, February, pp. 141-148, 2019

I performed the experiment, post-processed and analyzed the data, and was responsible for writing the paper.

### **Paper II: Optical Investigation on the Combustion Process Differences between Double-Pilot and Closely-Coupled Triple-Pilot Injection Strategies in a LD Diesel Engine**

**M. Denny**, A. Matamis, Z. Wang, H. Persson, P. Tunestål, M. Richter, Ö. Andersson  
SAE Technical Paper, 2019-01-0022, 2019

I performed the experiment along with Alexios Matamis and Zhenkan Wang. I was responsible for the experiment objectives and engine operation, Alexios and Zhenkan were responsible for the optical setup. I post-processed and analyzed the engine data. Alexios and I post-processed and analyzed the optical data. I was the lead author of the paper.

### **Paper III: Interaction between Fuel Jets and Prevailing Combustion during Closely-Coupled Injections in an Optical LD Diesel Engine**

**M. Denny**, A. Matamis, H. Persson, M. Richter, Ö. Andersson  
SAE Technical Paper, 2019-01-0551, 2019. To be published April 2nd, 2019.

I performed the experiment along with Alexios Matamis. I was responsible for the experiment objectives and engine operation, Alexios was responsible for the optical setup. I post-processed and analyzed the engine data. Alexios did the majority of the optical post-processing. We both analyzed the optical data. I was the lead author of the paper.

### **Paper IV: Manipulating Heat Release Features to Minimize Combustion Noise**

**M. Denny**, L. van den Ende, H. Persson, Ö. Andersson  
Submitted to *Fuel* on March 28th, 2019.

I performed the experiment with Luc van den Ende. I was responsible for the experiment objectives. I post-processed and analyzed the data and was responsible for the paper.

Currently under electronic hosting embargo.

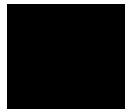
**Paper I**





Currently under electronic hosting embargo.

**Paper II**





Currently under electronic hosting embargo.

**Paper III**







Submitted to *Fuel* on March 28th, 2019.

**Paper IV**





# Manipulating Heat Release Features to Minimize Combustion Noise

Michael Denny<sup>1,\*</sup>, Luc van den Ende<sup>1</sup>, Håkan Persson<sup>1</sup>, Övind Andersson<sup>2</sup>

Volvo Car Corporation, PPS Advanced & Concept, Dept. 97622, VAK HD2S, SE-405 31 Gothenburg, Sweden

---

## Keywords:

Closely-Coupled Pilot, Closely-Spaced Pilot, Combustion Noise, Multiple Pilot Injection Strategy, Diesel Injection

---

Changes in combustion noise, efficiency, and emissions are investigated as responses to boundary conditions and injection scheduling parameters of closely-coupled multiple-pilot strategies. The effects of pilot injection separation times, mixture dilution, and injection pressure are investigated. In order to minimize combustion noise, the heat release rate (HRR) should be as linear in its buildup as possible. Through low injection pressure, high dilution ratio, and close-coupling of the pilot injections, combustion noise can be minimized. It is possible to have too much mixture dilution or dwells which are too short, however. This causes excessive blending of combustion events which tends to increase combustion noise. Noise minimization through HRR shaping has also been achieved through injection rate shaping. Based on the learnings from each investigation, triple and quadruple pilot injection strategies are created for lowest possible combustion noise. The investigations also reveal the relative extent to which emissions, noise, and efficiency are affected by each control parameter so that compromises in each response can be understood.

## 1. Introduction

Passenger car manufacturers must simultaneously meet emissions legislation targets and customer expectations. Over the years, legislative regulations have grown more strict and that trend is expected to continue [1]. These regulations themselves increase the technical demand upon the engine and its emissions aftertreatment system. The technical demand is increased further when also considering customer expectations.

Light duty (LD) diesel engines suffer from sub-optimal compromises when balancing these attributes. For high efficiency, the combustion should be phased to maximum brake torque (MBT) timing. This is often not possible, as such an early combustion phasing will lead to high engine out  $\text{NO}_x$  and combustion noise. The latter is an important attribute to the customer and occupants of the vehicle. It is also possible that pass-by noise regulations may be included in future regulations. Diluting the mixture or retarding combustion phasing slides the

trade-off in the other direction. Soot emissions increase and/or efficiency suffers while benefits in  $\text{NO}_x$  and combustion noise are achieved. If optimal efficiency is desired, additional sound deadening could be added to the structure of the engine and the aftertreatment system could be dimensioned to handle higher engine-out  $\text{NO}_x$  emissions. These are not cost effective standalone solutions for LD diesel engines, however.

Since these engine attributes result from the combustion process, a more elegant solution would be to modify its progression to minimize the compromises related with achieving the targeted engine characteristics. Several fuel injection equipment manufacturers have made advancements in the injector hardware capabilities in recent years [2, 3, 4]. Broadly, the minimum separation time between fuel injections, referred to as dwell, has been drastically decreased compared to earlier systems. This increases the opportunities in new injection strategies which can be directly leveraged to modify the combustion process.

Busch et al. investigated a range of dwells from relatively long (1200  $\mu\text{s}$ ) to very short (80  $\mu\text{s}$ ) values. They found that for a single pilot injection followed by a main, short dwells are beneficial (reducing noise by about 3 dB) but there is the possibility to reduce the dwell too far; combustion noise had a minimum value at 140  $\mu\text{s}$  [5]. In their investigation, this was equivalent to 1.26 crank angle degrees (CAD). Finding such short dwells as beneficial was in contradiction to the trend shown in a prior work by Tanaka et al. They had shown increases in combustion noise as the pilot injection is placed closer than 30 CAD to the main injection [6]. Over a broad range, 30 to 10 CAD bTDC, some of the largest pilot injections even increased combustion noise over that of a single main injection. The closest injection was 10 CAD bTDC, but the trends were still towards increasing noise at that dwell. The longest dwell Busch et al. investigated was just over 10 CAD but they showed a very flat behavior in combustion noise down to 200  $\mu\text{s}$  (1.8 CAD).

Regarding multiple injections, Mendez and Thirouard were able to reduce combustion noise by between 3.5 and 11 dB by breaking up the fuel mass into as many as four quantities [7]. They did this in order to reduce the peak heat release rate (HRR), which they found correlated with combustion noise. However, the dwells they implemented were still quite long; on the order of several CAD. This was a result of running in the

---

\*Corresponding Author

<sup>1</sup>Volvo Car Corporation

<sup>2</sup>Lund University

low temperature combustion regime, where ignition delays are much longer.

A recent study by Denny et al. combined the individual learnings from above by implementing multiple-pilot injection strategies with short dwells. Compared to a production-like double pilot strategy with moderate dwells of several CAD, combustion noise was reduced by nearly 4 dB [8]. This was achieved with a triple pilot strategy featuring dwells on the order of 1 CAD, or 140  $\mu$ s. The dwell after the first pilot, however, was up to several CAD. It was determined that the magnitude of the undulation in the HRR was directly responsible for the combustion noise level and frequency content. Therefore, it was more important to obtain a more linear HRR than target a specific low dwell value. With noise no longer preventing earlier phasing, combustion was advanced up to MBT timing, improving efficiency by nearly 4%. As anticipated from such a phasing,  $\text{NO}_x$  increased by 0.5 g/kWh and soot decreased by up to 33%. Subsequent optical investigations into the combustion process were performed. These showed that subsequent injections into regions of prevailing combustion lead to extinguishing of hot combustion products and their replacement with cooler ones [9, 10]. This balance of strong heat release and the extinguishing of it is partially responsible for the magnitude of the undulation in the HRR. Therefore, while closely-coupled strategies can make the heat release rate more linear, longer injection durations may limit the ability to smooth out the HRR through this extinguishing effect.

On the topic of emissions, the findings are again inconsistent and lacking in the regime of closely-coupled injections. Shorter dwells with two or more injections have shown to both increase [11] or decrease [6, 12] CO and unburned hydrocarbon emissions. Likewise, there is not a clear trend in soot- $\text{NO}_x$  trade-offs [6, 7, 8, 11, 12]. While some of the difficulty comes from inconsistent combustion phasings, even at iso  $\text{NO}_x$  or soot conditions, the trend is not unanimous.

In order to better understand these promising closely-coupled multiple-injection strategies, this work investigates a broader range of injection strategies and boundary conditions. The response of efficiency, emissions, and combustion noise will be understood in the context of injection strategy parameters, injection pressure, and EGR. All of those factors have direct control over the behavior of the HRR, which has been shown to be responsible for the overall combustion noise level and frequency content.

## 2. Experiment

A single cylinder variant of the second generation VEA diesel engine from Volvo Cars is used, the specifications of which can be found in Table 1 [13]. All test cases are run 1280 rpm and 9 bar IMEP gross, a valid part load operation point. A summary of the constant operating and boundary conditions, including ranges when appropriate, are provided in Table 2.

### 2.1. Injection Strategies

The injection strategies are composed of three pilot injections followed by a single main injection. The exception is in

Table 1: List of the engine’s key dimensions.

Displaced volume	492 cc
Bore	82 mm
Stroke	93.2 mm
Connecting rod length	147 mm
Compression ratio	15.8:1
Number of valves	4
Nozzle hole diameter	125 $\mu$ m
Number of nozzle holes	8
Injector spray umbrella angle	155°
Max injection pressure	2500 bar

Table 2: List of operating and boundary conditions.

Engine Speed	1280 rpm
IMEP <sub>g</sub>	9 bar
Fuel rail pressure	700-1100 bar
Intake temperature	328 K
Intake pressure	1.37 bar (abs.)
Intake CO <sub>2</sub> conc.	2.15-3.75 %
Exhaust pressure	1.48 bar (abs.)
Swirl ratio	2.2
Fuel	EN590 Diesel

the noise optimization case where four pilots are implemented. Post injections have been excluded since they are not an investigated variable. A common injection strategy is carried over in all swept variable investigations (called sweeps hereafter) so that relative impacts from individual variables can be compared. It is not an optimized point, but is designed such that proper headroom for both lower and higher variable settings are possible in each sweep. It is intended, however, to still reflect the characteristics of the beneficial triple-pilot strategies found in the prior work by the author. Specifically, the HRR should feature distinct local peaks associated to the combustion of each pilot injection. Furthermore, that the local peaks and minima should sequentially increase in magnitude. This baseline strategy is plotted in black wherever shown and its parameters are listed in Table 3. The dwells given are hydraulic, meaning separations of actual fuel flow. Deviations from these conditions will be outlined in their respective results sections.

The point at which 50% of the heat has been released (CA50) is held constant for all strategies. The phasing and duration of the main injection is adjusted to maintain this anchoring and a constant load.

Heat release rate shaping has been investigated by changing the dwell after the pilots, mixture dilution via EGR, and injection

Table 3: Properties of the baseline injection strategy used in all investigated sweeps. Injection pressure is 900 bar and the inlet CO<sub>2</sub> is 2.8% unless otherwise stated.

	P1	P2	P3
Dwell after [ $\mu$ s]	695	240	205
Mass [mg]	1.8	2.3	6.7

tion pressure. Two different dwell sweeps are performed. One changes the dwell after all pilots and the other shifts the pilots as a group by changing only the final dwell. The motivations behind each sweep will be given at the beginning of each results section, for the reader to have a fresh reasoning in mind when considering the results.

### 3. Analysis Methods

#### 3.1. Pressure

Fast sampled cylinder pressure with a resolution of 0.03 bar and 0.1 CAD is filtered with a digital zero phase-shift lowpass Butterworth filter. The cutoff frequency is set at 12 kHz, well below the Nyquist criterion frequency but just above the frequency content used for calculating combustion noise.

The heat release rate (HRR) is again filtered with another lowpass Butterworth filter to remove the effects of cylinder ringing caused by the measurement of cylinder pressure at a single point. Cut-off frequencies of 3500, 4500, and 5500 Hz were compared against each other. 4500 Hz produced the best correlations for HRR characteristics used to predict combustion noise characteristics. The other cut-off frequencies only lost several hundredths in their coefficients of determination, so the results are not very sensitive to this filtering. However, cut-off frequencies below 3500 Hz should be avoided, since significant frequency content in combustion noise lies just below that level.

#### 3.2. Combustion Noise

The combustion noise is calculated for each cycle and the energetic average is taken over all cycles to provide the mean value for a given operating point. The discrete Fourier transform is first taken, then structural attenuation and A-weighting are applied. This produces absolute combustion noise levels which are not totally representative of the multi-cylinder version of this engine, but are expected to be relatable to peers in this field. The structural attenuation curve is the same that is applied in prior work [14] which is based off that used in commercial engine analysis software.

#### 3.3. Ratio of Reduced Heat Release

Prior work [8] included the creation of the Ratio of Reduced Heat Release (RRHR) as a necessary metric for understanding combustion noise. A summary is provided here with the help of Figure 1. A HRR profile from a triple-pilot+main injection strategy is depicted and the areas involved in calculating this metric are identified by orange and blue hashing. The HRR should have as many distinct peaks as there are injections. This leads to a clearer understanding of the relationship between the impact each pilot injection has on the combustion noise level and frequency content. Having identified the peaks, the size of the valleys between these peaks but below the bridges spanning them can then be quantified. The RRHR is then the quotient of the area of each valley (the individual orange areas) and the total area under each bridge down to the x-axis (the sum of the orange and blue areas). In its raw form, it is a measure of how ineffectively the area between adjacent local peaks is utilized

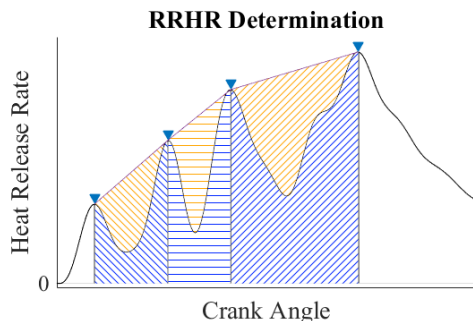


Figure 1: Graphical representation of the determination of the ratios of reduced heat release.

for heat release. A value of unity indicates infinitely thin peaks and a value of zero indicates a linear HRR trace. Incidentally, a limit of the metric is that values of zero cannot be calculated, as there are no longer any local peaks.

It is difficult to interpret multiple RRHR values (one for each valley) for a single HRR and then compare those several values to those at other operating points. In working more with this metric, it has been determined that a single weighted average is a good predictor of combustion noise. The individual weighted values are also useful in understanding which valleys in the HRR are more significant contributors to combustion noise than others. Previously, no distinction could be made between two different valleys of different absolute sizes but equal RRHR values.

The individual valleys are weighted by the size of their area (the individual orange areas) compared to the total valley area (the sum of all orange areas). Since the area of the valleys can be seen as the potential for the HRR to cause strong undulations in the pressure trace, and therefore combustion noise, this weighting system has a phenomenological foundation.

#### 3.4. Injection measurement

The injection strategies investigated in the engine tests are recreated and measured in an IAV injection analyzer. In this measurement device, the nozzle is surrounded by a liquid instead of air. The higher viscosity of this ambient substance will cause the injection results, most significantly mass, to vary slightly from what occurs in-engine. These tests are not used as an absolute indicator of individual injected masses, and are instead used to verify consistent delivered masses and to determine hydraulic separations of each injection.

### 4. Investigations

#### 4.1. Sweep of All Dwells

##### 4.1.1. Motivation

The dwells after all pilots are increased and decreased simultaneously. This is expected to affect the total noise level, frequency content therein, and both soot and  $\text{NO}_x$ . As the dwells

Table 4: Measured hydraulic dwell separations for each level, labeled -3 to +1 from the shortest to longest dwells. P1-3 indicate the pilot in the sequence.

All Dwells Sweep	-3	-2	-1	0	+1
dwell after P1 [ $\mu$ s]	258	419	551	692	794
d.a. P2 [ $\mu$ s]	61	112	175	239	320
d.a. P3 [ $\mu$ s]	fused	9	89	207	262

are increased, the width and depth of the valleys in the HRR should increase, which is expected to lead to an increase in combustion noise [8]. This should also shift the frequency content of the combustion noise lower by decreasing the fundamental frequency of the valleys ( $f_0$ ). This fundamental frequency is calculated from the separation of the HRR peaks in the time domain. It is only an estimation of the fundamental frequency since the valleys are not perfect sinusoids. This can also be calculated for non-adjacent peaks.

Soot emissions are expected to increase at shorter dwells since each subsequent injection is injected into more oxygen deprived, fuel rich regions.  $\text{NO}_x$  emissions are expected to rise at longer dwells since the early combusted fraction will have a longer residence time at higher temperatures, promoting  $\text{NO}_x$  formation via the thermal mechanism [15].

Changes in dwell were intended to increase on a percentage basis for each individual value. This was not fully achieved and caused an uneven spread in dwell values. Due to experimental limitations, another loop to remedy this effect could not be performed after the injector testing. The actual dwells achieved at each level in the sweep are summarized in Table 4. P1,2,3 denote the first, second, or third pilot in the sequence. The only notable deviations in pilot mass were an undershoot of 0.6 mg in P3 at the +1 level and an overshoot of 0.4 mg in P2 at the -1 level. No dwell can be given after P3 at the -3 level since there was a fusion of the injections; the injection rate had an inflection point, but did not reach zero fuel flow before the main injection.

#### 4.1.2. Results for Sweeping All Dwells

A summary of the results for each dwell level are presented in Table 5. Minimum noise did not occur at the level with the shortest dwells. Compared to the baseline (0) level, combustion noise decreases with shorter dwells up to a point. The dwell can be reduced too much, which causes noise to increase again at the shortest level, -3. Noise increases to the highest level at longer dwells. Results for gross indicated efficiency are given in percentage point changes from the baseline strategy. Efficiency is largely unaffected, except at the shortest dwell level which has a very small improvement. This is likely due to the combustion duration (CA10-CA90), which is notably shorter than for the other cases. From the -2 to +1 levels, while total dwell increases by 6.4 CAD (836  $\mu$ s), combustion duration increases by only 1.5 CAD. PPRR is highest for the -3 level where injection fusion occurred, but otherwise PPRR does not reflect the change in combustion noise for each level.

The behavior of the HRR for each dwell level is shown in Figure 2a. Considering the -3 level, it's clear that despite mea-

Table 5: Results from the sweep where all dwell times are adjusted simultaneously. -3 is the shortest dwell level and +1 is the longest.

All Dwells Sweep	-3	-2	-1	0	+1
Comb. noise [dBA]	81.2	79.2	80.7	81.9	83.0
PPRR [bar/CAD]	5.5	4.0	4.3	4.3	4.3
CA10-CA90 [CAD]	17.5	20.6	21.8	22.0	22.1
Efficiency [p.p.]	0.1%	0.0%	0.0%	-	0.0%

surable dwells after P1 and P2, separate combustion events cannot be identified for them. They appear to combust as a group, starting just before TDC. Likewise, the third pilot injection cannot be clearly identified. The local peak at 3 CAD aTDC may be from the combustion of P3, or it may be a pronounced feature of the main injection seen also at the longer dwell levels. This highlights that even without a fusion of the injections themselves, sufficiently short dwells can lead to the majority of individual pilot masses burning as groups, rather than separately. In order to create a more linear HRR, it is clear that some overlap of combustion must occur, else the HRR would fall back to 0 between them. However, excessive overlap of this combustion is not beneficial for minimum combustion noise either.

As dwell is increased at the higher levels, both the depth and width of the valleys increase, most notably in valleys 2 and 3 (V2, V3). Another notable behavior is the combustion of P1. The injected mass is the same in each strategy, yet the local peak value in the HRR is dependent on its phasing with respect to TDC. Earlier injections have a weaker peak HRR. This logically follows from the lower in-cylinder temperature and pressure at earlier CAD causing lower reaction rates. As shown in the prior work [9], the fuel from P1 ignites well after the end of injection, so the combustion is not mixing controlled. Deflagration initiated by multiple autoignition kernels dominates this phase of combustion. The implication of this effect on the HRR is that the depth of the valleys can be affected purely by the phasing of a specific injection.

The weighted RRHR values in Figure 2b do not include the -3 dwell level since individual valleys cannot be identified. At the -2 level, V2 and V3 have the largest contribution to the full weighted average RRHR in the "sum" category. At the -1 and 0 levels, V2 becomes the smallest contributor while V1 and V3 dominate. For all but the -2 level, V3 makes up the single largest portion of the weighted average.

For the quietest strategies, the strongest peaks in the magnitude spectrum displayed in Figure 2c are dominated by the  $f_0$ 's of the valleys, which are marked by  $\#$  on the plot. V1 in the -2 dwell level has a very low magnitude, and locally dominating values at V2 and V3. This is reflected in the weighted RRHR values for these valleys. The weighted RRHR values cannot predict the magnitude values, but do align with the important contributing frequency content. Considering the V1 and V2  $f_0$ , which are similar in frequency for the longer dwell strategies, the larger the sum of the weighted RRHR values for the first two valleys, the larger the magnitude in their frequency range.

For the quietest dwell levels, -2 and -1, the non-adjacent combination of the P1 and Main peaks is strong, but quickly be-

comes unimportant as dwell increases and is replaced by the P1 to P3 combination. This also becomes less significant as noise and dwell increase. These fundamental frequencies are marked on Figure 2c as P1-Main and P1-P3, respectively.

For the louder +1 dwell level, the frequency content which can't be explained by the  $f_0$  of the valleys can be explained by that of P3 itself (this would be spanning the minima of V2 and V3, the  $f_0$  of the peak as opposed to the valley). The importance of this other perspective on the HRR features is also investigated. For the other dwell levels, the P3  $f_0$ 's are weaker than the V3  $f_0$ . Considering the quietest case, -2, the  $f_0$ 's of P1,2,3 are clumped together and do not give a good representation of the spectrum, whereas the  $f_0$ 's of valleys do. The conclusion is that the  $f_0$ 's of the valleys are still the best way to correlate the HRR shape to the noise level (through the weighted average RRHR). And even when the frequency content described by a lone peak is significant, weighted RRHR are still capable of predicting noise well since, for a tall lonely peak, there will be adjacent deep valleys.

The magnitude spectrum of the -3 level is more characteristic of a strong fundamental frequency with cascading harmonics, similar to the double-pilot injection strategy in prior work [8] which featured a strong main HRR. The peaks in the magnitude spectrum below 500 Hz (above for the -3 level) are centered at frequencies which are on the order of the combustion duration. HRR profiles with more complex features are less similar to a simple sinusoid. This is reflected in the magnitude spectrum, where the frequency corresponding to the entire combustion duration decreases as HRR complexity increases.

Emissions results are presented in Figure 3. The same color coding used to identify the dwell levels in Figure 2 are used in Figure 3. As expected, higher soot values occur at the shortest dwells, creating up to half again as much as the baseline.  $\text{NO}_x$  increases with dwell, likely because the mixture experiences higher temperatures for more time at longer combustion durations and an earlier temperature rise.

## 4.2. Final Dwell Sweep

### 4.2.1. Motivation

In this sweep, only the value of the dwell after P3 is changed. This shifts the pilot injections as a group with respect to the main injection. This will help understand combustion noise, since so far we have seen that the last valley often contributes the most to the weighted average RRHR values, and therefore noise levels as well. It will also help understand emissions trade-offs. The prior sweep has shown that shorter dwells everywhere tends to increase soot emissions and decrease  $\text{NO}_x$ . Shifting the pilots as a group will help determine how much of this soot penalty is due to the main injection interacting with the strong combustion of the final and largest pilot injection. Prior works [9, 10] have shown the most significant extinguishing event via subsequent injection into prevailing combustion occurs during this valley. Confounding effects are an expected increased combustion duration and earlier temperature rise at longer dwell values. The effects from the latter on emissions have been seen in the prior sweep. However, these effects

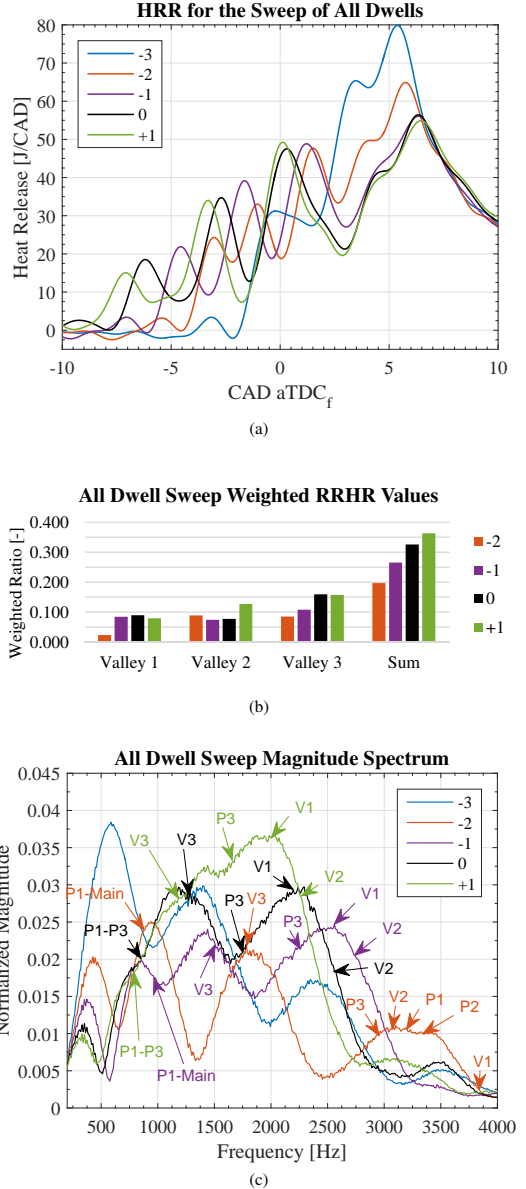


Figure 2: (a) Ensemble averaged HRR, (b) weighted RRHR values, and (c) magnitude spectrum for the sweep of all dwells. The shortest dwell level is -3 and the longest is +1. The black trace is the baseline strategy which also appears in the other sweeps, but is re-run for each sweep.



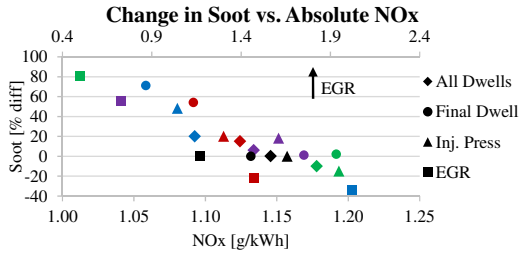


Figure 3: Emissions behavior for each sweep. The colors of each point within a sweep match those used in the various other plots presented.

Table 6: Measured hydraulic dwell separations for each level, labeled -2 to +2 from the shortest to longest dwells.

Final Dwell Sweep	-2	-1	0	+1	+2
dwell after P3 [ $\mu$ s]	fused	56	205	374	497

are unavoidable while also keeping other boundary conditions comparable.

The measured hydraulic dwell values after P3 are listed in Table 6. In this sweep there are no deviations in the other injection parameters worth noting.

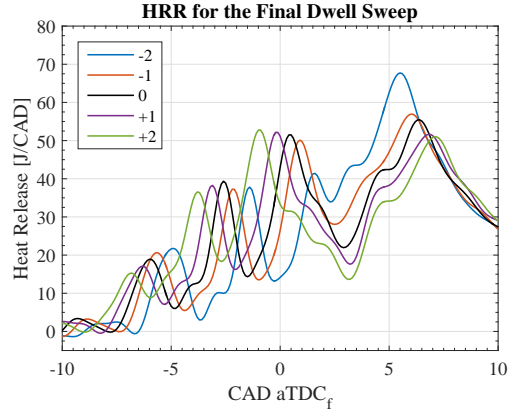
#### 4.2.2. Results for Sweeping the Final Dwell

A summary of the results for each dwell level are presented in Table 7. Despite a significant spread in dwell, there is little variation in combustion noise. Both shorter and longer dwells than the baseline reduce combustion noise to approximately the same degree. Despite a fusion of the P3 and main injections once more, the combustion noise has not significantly risen as in the sweep of all dwells. PPRR tends towards higher values at longer dwells, and therefore has little similarity to the trend in combustion noise. The CA10-CA90 combustion duration increases with dwell as expected, and this time more closely reflects the variation in dwell. Both shorter dwells lead to very slight gains in gross indicated efficiency while there is no penalty at longer dwells.

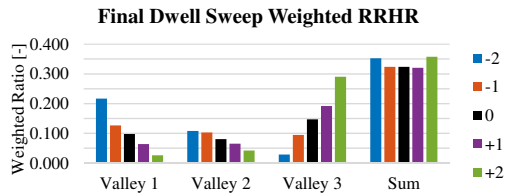
The HRR profiles are shown in Figure 4a. As in the sweep of all dwells, the peak HRR for the combustion of P1 is very much affected by its phasing. This must be entirely due to the in-cylinder conditions since there is no variation in P1 mass. Injections closer to TDC have a more aggressive combustion and their V1 valleys are also deeper. The phasing in itself has

Table 7: Results from the sweep where only the final dwell time is adjusted. -2 is the shortest dwell level and +2 is the longest.

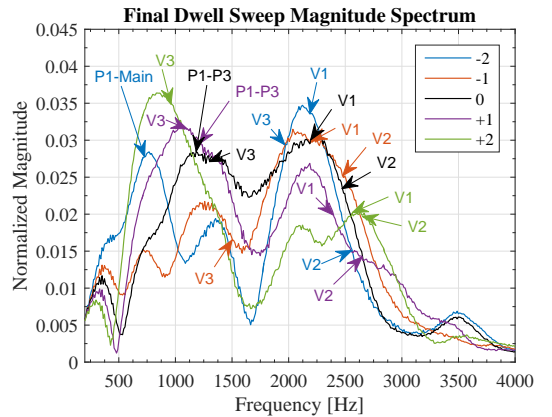
Final Dwell Sweep	-2	-1	0	+1	+2
Comb. noise [dBA]	81.3	81.3	82.0	81.7	81.5
PPRR [bar/CAD]	4.3	4.1	4.4	4.7	4.9
CA10-CA90 [CAD]	21.1	22.0	22.2	22.4	23.4
Efficiency [p.p.]	0.1%	0.1%	-	0.0%	0.0%



(a)



(b)



(c)

Figure 4: Ensemble averaged HRR, weighted RRHR values, and magnitude spectrum for the sweep of the final dwell. The shortest dwell level is -2 and the longest is +2. The black trace is the same point as those in the other sweeps, but re-run for each sweep.

an effect on the weighted RRHR values of the early pilots by determining how aggressively they combust. This is clearly reflected in Figure 4b where the weighted RRHR values are presented. The shortest dwells create a large V1 but small V3 and the longest dwells cause the opposite result. This trade-off is why the total combustion noise had little variation; the weighted average RRHR values have little variation. The values at the -2 and +2 dwells do not follow the combustion noise trend, but the deviation is not significant.

The main injection's peak HRR trend also follows that of the P1 peak trend. That is, higher HRR closer to TDC. However, as opposed to phasing being the cause, the likely reason for this trend is due to the amount of P3 fuel left unburnt at the start of the main injection. This causes more fuel to burn in a shorter time frame, increase the HRR.

Consider now the magnitude spectra for these different injection strategies, shown in Figure 4c. The magnitude values of the combustion noise at the same frequencies as the individual valley  $f_0$ 's directly correlate with their weighted RRHR values. There are a few exceptions to this statement, but they do not sit in contrary to one another; one metric helps explain the true nature of another. One specific case is V3 at the -2 level. According to the magnitude spectrum, one could be lead to believe that this valley contributes strongly along with V1 to the combustion noise level. By considering the V3 weighted RRHR value, however, we understand that this  $f_0$  is just coincidentally similar to V1's  $f_0$  which is primarily responsible for the magnitude in this frequency range.

At the -1 level, the magnitude where V3 sits is sensitive to the location of the HRR peaks; if the peaks were separated by an additional several tenths of a CAD, the  $f_0$  of V3 would lie much closer to 1250 Hz, the local peak in the magnitude spectrum. This is a reminder that the  $f_0$  is an approximation of a simple sine wave, but each valley has a relatively broad bandwidth making up its shape. The same can be said for V1 at the +1 dwell level.

The emissions response in Figure 3 shows a flat response in soot for dwells longer than the baseline. At shorter dwells, soot increases substantially up to an increase of over 70% at the -2 level. This suggests that for dwells longer than the baseline, the combustion region from P3 has drifted sufficiently far from the injector so that the fuel jet from the main injection has minimal interaction with it. The fuel jet would be less likely to interact with oxygen deprived, possibly even fuel rich zones which would further promote soot formation. The response at shorter dwells reinforces this reasoning since higher levels of interaction between the fuel jet and prevailing combustion region should lead to higher soot formation. During the fused injection there is no pause, so the mechanism is not the same as with a hydraulic separation. This injection mode was not present in the prior works with optical access so it cannot be commented on and is suggested as a future investigation. The increase in  $\text{NO}_x$  for longer dwells follows the trend in combustion duration and earlier onset of first heat release. Therefore it is concluded that longer time spent at higher temperatures promotes the creation of thermal  $\text{NO}_x$ .

### 4.3. Injection Pressure Sweep

#### 4.3.1. Motivation

The injection pressure is changed while maintaining the baseline injection strategy. This sweep is performed to understand the effect it has on combustion noise, efficiency, and emissions. Higher injection pressure should decrease engine out soot [16, 17].  $\text{NO}_x$  should also decrease. As the prior sweeps have shown, less time spent at higher temperatures reduces  $\text{NO}_x$  formation. Higher injection pressures will require shorter injection durations, thus shortening the entire injection sequence. This will also alter the frequency content of the HRR and therefore the combustion noise. This should be reflected in the magnitude spectrum.

Due to the immature system model of the injector, while the intent was to maintain the baseline injection strategy across different injection pressures, that was achieved to varying degrees. Notable variations were limited to P3 in both mass and dwell after it. At the 700 and 800 bar levels the dwell after P3 was 30  $\mu\text{s}$  too short and at 1100 bar, 40  $\mu\text{s}$  too long. The mass of P3 was overshot by 1 mg at 700 and 800 bar, and undershot by 0.8 and 1.5 mg at 1000 and 1100 bar, respectively. This error arose from targeting constant HRR peaks as injection pressure was changed, having no better indicator for delivered mass at the time. It is known that in quasi-steady jets the combustion rate is mixing limited and that mixing rate increases with injection pressure [18]. However, it is not clear what should happen with multiple closely-coupled, relatively short injections. The assumption that injection pressure should not significantly effect the local peaks in the HRR was an appropriate assumption for P1 and P2. Their delivered masses only fluctuated a few tenths of a mg away from the baseline. The mixing controlled combustion rate did have an effect on P3 combustion, however. Maintaining the HRR peak value at P3 lead to the reduction in P3 mass as injection pressure rose. The takeaway is that for injections on the scale of P3, the higher mixing rates do lead to higher combustion rates for a given quantity of fuel. Prior work [9] shows that for similar injection strategies, P3 injection has ended well before the peak combustion of that fuel, so this mixing rate effect was not expected.

When interpreting the results, keep in mind there are two groupings with low fuel injection error within each group. One at 700/800 bar, the other at 900/1000 bar. Comparison within these levels will have the least obfuscation from fuel injection errors. Comparison between the levels is also possible, keeping in mind the early portions of the HRR will be comparable, less so with the later portions.

#### 4.3.2. Results for Sweeping Injection Pressure

A summary of results is presented in Table 8. The combustion noise tends towards lower values at lower injection pressures. It is difficult to comment on whether or not the spread would have been wider had P3 mass and dwell been on target. For example, at 700 bar, the HRR at P3 peak combustion would have decreased, but the HRR peak during the main combustion likely would have increased to compensate. The opposite can be said for the higher pressure levels. Once more, PPRR does

Table 8: Results from the injection pressure sweep.

Inj. Press. Sweep	700 bar	800	900	1000	1100
Comb. noise [dBA]	81.6	81.7	81.9	82.2	82.4
PPRR [bar/CAD]	4.2	4.2	4.4	4.4	4.3
CA10-CA90 [CAD]	23.8	23.1	22.0	21.2	20.1
Efficiency [p.p.]	-0.4%	-0.3%	-	0.2%	0.4%

not follow the trend in noise very well. Combustion duration is shortened by higher injection pressure. Compared with the variation in combustion duration in the sweep of all dwells, the gross indicated efficiency is affected much more strongly by injection pressure than the combustion duration would suggest. The reason for this improvement is that in the sweep of all dwells, the CA10-CA50 duration was primarily shortened with the CA50-CA90 duration remaining largely unchanged. At higher rail pressure, however, the opposite is true. Most of the reduction is in the CA50-CA90 duration. This allows for a more complete expansion of the burned gases, leading to higher efficiency.

The HRR traces shown in Figure 5a show a quite constant behavior. The shift is only due to the decreased injection durations at higher pressures (recalling also the P3 dwell error). V3 gets deeper at higher injection pressure. A small portion of this may be due to slower combustion rates at lower injection pressures, leaving more fuel to combust during the dwell. The largest portion, however, is likely due to the overshoot of P3 mass and undershoot of dwell at lower pressures. Nonetheless, the relative lack of variation in the HRRs is reflected in the weighted average RRHR values of Figure 5b. While the absolute dimensions of V1 and V2 don't substantially change across the different levels, their weighted RRHR values do since the absolute dimensions of V3 change.

The positioning of the  $f_0$ 's on the magnitude spectra in Figure 5c show that the trade-off of either higher or lower frequencies dominating is explained by the weighted RRHR values. When V1 and V2 become dominant portions in the weighted average RRHR, the strength of the frequency content in the combustion noise at those valley's  $f_0$ 's gets stronger as well.

The predicted increase in  $f_0$  due to the reduction of combustion durations at higher injection pressures does occur for V1 and V2. This has a smaller effect on combustion noise qualities than the relative size of each valley, however.

The behavior of the soot- $\text{NO}_x$  trade-off shows a near linear trend. This is shown in Figure 3. The color coding now reflects the injection pressure level and matches the coding in Figure 5. Lower injection pressures lead to more soot production. In contrast to the prior sweeps, longer combustion durations do not create higher  $\text{NO}_x$  levels. While the higher injection pressure levels had lower cylinder pressure (not shown) and temperature before peak pressure, they all have higher pressure (and therefore global temperature) values later in the cycle. It is likely that less time spent, but at higher peak pressures, increased the  $\text{NO}_x$  for the shorter combustion duration cases. Regarding the 1000 bar case, neither the pressure nor HRR traces explain the emissions behavior. This point was the first measured in this sweep

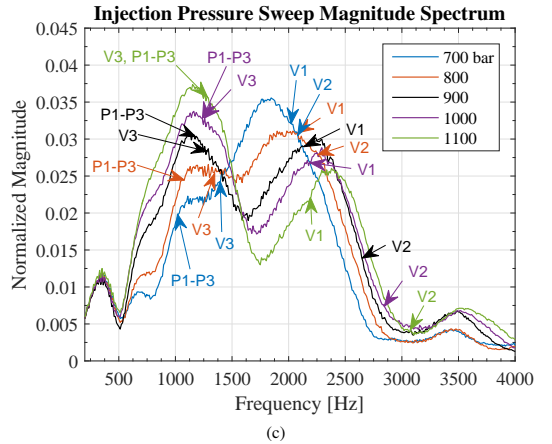
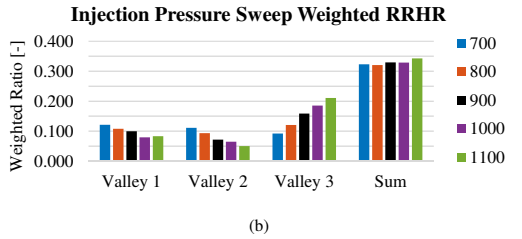
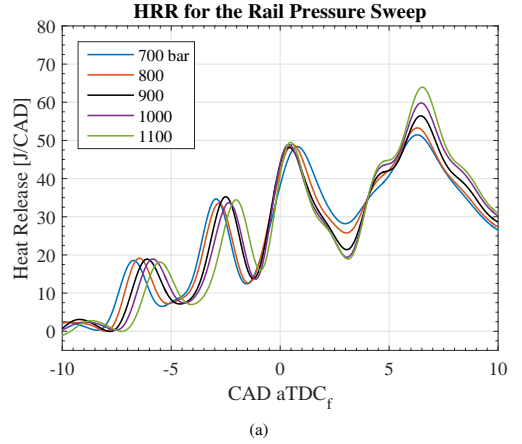


Figure 5: Ensemble averaged HRR, weighted RRHR values, and magnitude spectrum for the injection pressure sweep. The same injection strategy is implemented at all levels (with reduced dwells at higher pressure to maintain pilot fuel quantities). The black trace is the same point as those in the other sweeps, but re-run for each sweep.

Table 9: Results from the EGR sweep. The CO<sub>2</sub> concentration given is for inlet conditions.

EGR Sweep	2.15	2.49	2.81	3.28	3.75% CO <sub>2</sub>
Comb. noise [dBA]	83.1	82.3	81.9	81.4	83.0
PPRR [bar/CAD]	4.0	4.1	4.2	4.7	5.4
CA10-CA90 [CAD]	21.3	21.8	22.2	22.6	23.2
Efficiency [p.p.]	0.1%	0.2%	-	-0.2%	-0.1%

and it is possible the prior run had affected the captured emissions as a result of inadequate stabilization time before measurement.

#### 4.4. EGR Sweep

##### 4.4.1. Motivation

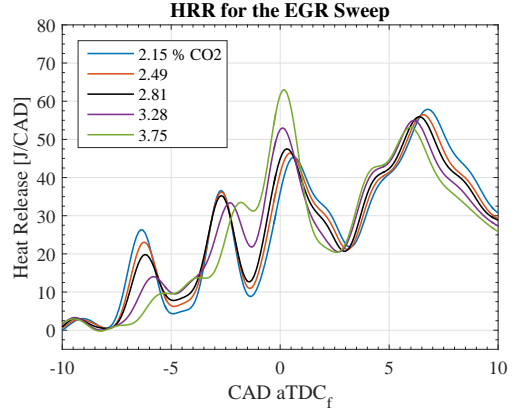
The intent behind changing the mixture dilution via EGR was to primarily investigate how combustion noise would change. The effect of EGR on engine emissions is well known, so that is not a point of investigation in itself. Rather, understanding how the combustion noise is affected by different dilution ratios is targeted. Higher dilution ratios should decrease the combustion rate of the early pilot injections, decreasing the local peak values which should lead to a smoother HRR. From one perspective, EGR may be useful for decreasing combustion noise. From another perspective, a transient change in EGR may provoke a change in combustion noise while all else is equal. The magnitude of this should be understood.

The baseline injection strategy summarized in Table 3 is kept constant as EGR levels are swept. No notable deviations in injected mass or dwells occurred.

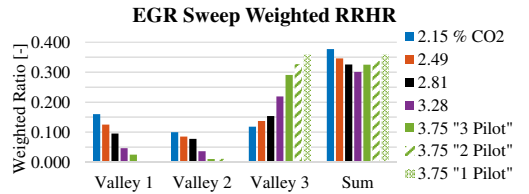
##### 4.4.2. Results for Sweeping EGR

A summary of the results for the EGR sweep is given in Table 9. Both combustion noise and PPRR are strongly dependent on dilution level. At more dilute levels (higher fractions of inlet CO<sub>2</sub>), noise tends to decrease and PPRR increases. One exception is at the highest dilution level where the noise level increases to nearly the loudest level. Combustion duration increases modestly with increasing dilution levels. Efficiency largely follows that trend, with shorter combustion durations being associated with improvements in gross indicated efficiency. The trend is not totally consistent, which is likely due to the change in values being on the same level as the resolution. Inspection of the combustion progression before and after CA50 does not lead to a more specific reasoning.

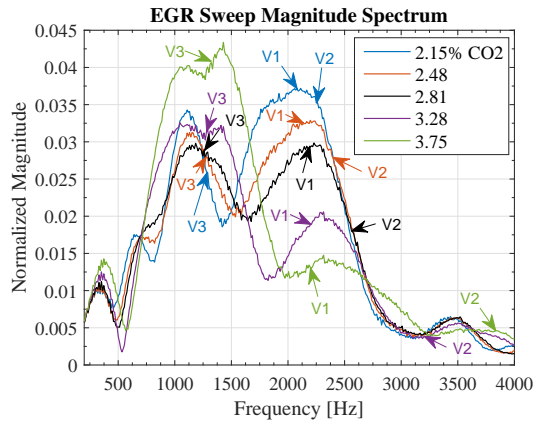
The HRR traces for this sweep are shown in Figure 6a. The first stage ignition of P1 (at approximately -9 CAD aTDC) is largely unaffected by the CO<sub>2</sub> concentration. The delay reflects the required shift of the entire injection strategy to maintain CA50 phasing. The onset of second stage ignition creating the P1 combustion peak is delayed at higher dilution levels, though. Additionally, the peak HRR value of P1 combustion decreases, with a significant change at the 3.28% level. The local minimum of V1 increases as the peak decreases. Through these two phenomena, the area of V1 is reduced from both its top and bottom. At the highest two dilution levels, the weak combustion of



(a)



(b)



(c)

Figure 6: Ensemble averaged HRR, weighted RRHR values, and magnitude spectrum for the EGR sweep. The same injection strategy is implemented at all levels. The black trace is the same point as those in the other sweeps, but re-run for each sweep.

P1 and P2 is compensated for by a strong P3 combustion. This is likely due to the contact ignition phenomenon observed in prior work [9]. By this point in the combustion progression, the prevailing combustion is likely developed enough to cause a rapid and strong ignition of the P3 injection. The combustion of P3 either interacts directly with the prior unburnt fuel, or increases the global temperature and pressure sufficiently such that it burns simultaneously. At the highest dilution level, significant portions of the first two pilot injections burn together. There is no inflection in the HRR up to approximately -2 CAD. This blending of combustion events is similar to what occurred in the all dwell sweep, but caused by a completely different phenomenon. Likewise, it is difficult to meet the requirements of the RRHR calculation which state that each pilot injection should have its own identifiable local peak in the HRR. The combustion blending is not as severe as before, though, so attempts to calculate the RRHR values are still made by manually defining where the peak combustion of P1 would likely occur had there been an inflection. This was selected as -5.5 CAD aTDC. P2 peak was selected as the local peak at -2 CAD aTDC.

These attempts are included along with the other weighted RRHR values in Figure 6b. By treating the injection strategy as if it had only a single pilot injection, the weighted average RRHR value most closely follows the trend in noise. Treating it as a double or the triple pilot strategy that it is leads to a worse correlation due to excessive blending of the individual HRR features.

The weighted RRHR values and their valley's placement on the magnitude spectrum, shown in Figure 6c, explain the change in noise level. The slower combustion rates caused by the higher dilution ratios reduce the size of both V1 and V2. While this does increase V3, the weighted RRHR values show that this is not enough to overcome the earlier reduction. The frequency content caused by the  $f_0$  of V1 and V2 decreases in magnitude with the size (and therefore weighted RRHR values) of those valleys. While the  $f_0$  of V1 remains quite consistent, higher dilution ratios cause the  $f_0$  of V2 to increase. This is further support of the stabilization of P3 combustion via contact ignition with prevailing combustion regions. P2 combustion is delayed from higher dilution, but since the injection dwell remains unchanged, contact ignition stabilizes the location of P3 combustion within the sequence. The consistency of the  $f_0$  of V3 also confirms that the higher dilution ratios did not affect the ignition delay of these later injections, stabilized by both higher in-cylinder temperature and pressure, and contact ignition of the subsequent injections on the prevailing combustion regions.

The magnitude spectrum at the highest dilution level shows that the delayed and fused combustion has a more narrow frequency spectrum, but with the highest peak values. The HRR trace becomes less complex and more similar to a pair of sinusoids. This requires less frequency content to be described than for combustion events with numerous peaks at irregular occurrences which create valleys that are only roughly sinusoidal. This is also different from the shape of the magnitude spectrum of the -3 level in the all dwell sweep and that of the reference

Table 10: Properties of each noise optimized injection strategy. Injection pressure is 700 bar and inlet CO<sub>2</sub> is 3.65%. \*The masses of these pilots are found by dividing the fused injection at the inflection point between the P3 and main injection.

3 Pilots				
	P1	P2	P3	
Dwell after [μs]	607	175	fused	
Mass [mg]	1.7	2.5	7.2*	
4 Pilots				
	P1	P2	P3	P4
Dwell after [μs]	481	183	69	fused
Mass [mg]	1.3	1.4	3.1	6.8*

strategy in prior work [8]. Those had a strong fundamental with cascading harmonics. They also had a single predominant HRR event, more similar to an impulse, which explains the cascading harmonics seen in their magnitude spectra.

The trend in emissions displayed in Figure 3 (noting the different axis) is expected when changing the dilution ratio of the mixture. What is interesting is the potential swing in noise within these EGR bounds compared to the emissions. An inlet CO<sub>2</sub> concentration of 3.28% produces similar combustion noise and soot levels as those achieved at 700 bar and the -2 and -1 levels of the final dwell sweep. The reduction in NO<sub>x</sub> far exceeds what was achieved in those other strategies, however, with absolute levels of 0.7 g/kWh as opposed to between 1.05-1.10 g/kWh. Efficiency is improved for the shorter dwell levels of the final dwell sweep, but worse for the 700 bar case.

## 4.5. Noise Optimization

### 4.5.1. Motivation

The intent is to build upon the learnings from above in order to create an injection strategy optimized for the lowest combustion noise.

Based on further investigation of dilution levels, 3.65% inlet CO<sub>2</sub> was found to be an acceptable upper limit which creates very smooth initial HRR behavior avoiding significant combustion blending. 700 bar injection pressure is selected since it will generate neither high air entrainment nor combustion rates. The high dilution rate will also help offset the smoke penalty which occurs at lower injection pressures. Understanding that the HRR should be as smooth and linear as possible, and seeing the gap to that with a triple pilot strategy, a quadruple pilot strategy is also developed. The injection parameters of these strategies are listed in Table 10.

### 4.5.2. Results for the Noise Optimization

A summary of the results for both noise optimized strategies is found in Table 11. The combustion noise for these optimized points show that by implementing all the learnings from the prior investigations, very low noise levels are possible. The triple-pilot strategy is over 5 dB quieter than the baseline, but it should be kept in mind that the baseline itself was not designed to minimize noise. Compared to the noise optimized triple-pilot strategy, the quadruple-pilot strategy achieved another 1.4 dB reduction. The PPRR values remain at the level

Table 11: Results from the noise optimization investigation. The efficiency are still relative to the baseline considered in the other sweeps.

Noise Optimization	3 Pilot	4 Pilot
Comb. noise [dBA]	76.7	75.3
PPRR [bar/CAD]	4.0	3.8
CA10-CA90 [CAD]	24.0	23.6
Efficiency [p.p.]	-0.3%	-0.8%

seen in the sweeps where combustion noise is much higher. Despite having a longer overall injection sequence, the quadruple-pilot strategy has a slightly shorter burn duration, but worse efficiency. This could partially be due to an imperfect CA50 target. The quadruple-pilot strategy is phased 0.3 CAD earlier. If the triple-pilot strategy is at or earlier than MBT timing, this further advancing would explain the drop in efficiency for the quadruple-pilot strategy.

The HRR profiles in Figure 7a both show a very smooth behavior, with the quadruple-pilot strategy producing a nearly linear behavior towards its maximum value. Comparatively, the first stage ignition of the P1 fuel has a very long delay in the triple-pilot strategy despite being phased closer to TDC. A possible explanation is the P1 mass is smaller in the quadruple-pilot strategy. This could lead to locally richer mixtures after P1 in the triple-pilot case. Due to the ignition delay behavior of diesel at these temperatures (about 780 K) higher local equivalence ratios will lead to longer ignition delays [19].

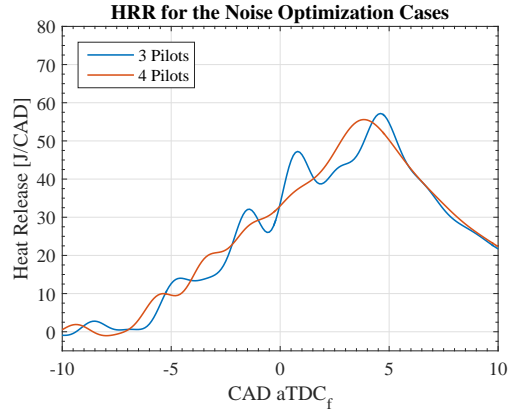
The HRR from the pilots in the quadruple-pilot case show that after the combustion of P1, there is no inflection in the HRR. Each individual pilot is small, and the dwell between the first and second is also much shorter than in the triple-pilot strategy. Small pilots close together lead to less intense peak HRR values, less delay before the next combustion event, and less extinguishing via shorter injection durations entering into relatively less developed combustion regions.

From the perspective of the x-axis in the HRR, the quadruple-pilot case does not have inflection points. This would mean that there are no local peaks to detect for the RRHR calculation. However, compared to the mean slope of the HRR, there are inflections. Therefore, in order to calculate the RRHR values, the bridges are placed at local maxima from the perspective of the mean slope, which appears as a tangential connection method from the perspective of the x-axis.

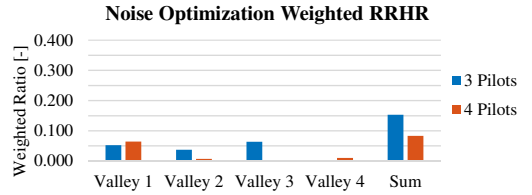
The weighted RRHR values in Figure 7b have very small values at all valleys in both injection strategies. The quadruple-pilot strategy is very near a true linear progression with a weighted average RRHR of 0.083.

The magnitude spectra in Figure 7c show an unprecedented behavior; the strongest peak for both strategies is the one which represents the combustion duration itself, just below 500 Hz. The quadruple-pilot case appears to have a small harmonic cascade, but these local maxima are actually the result of the  $f_0$  of non-adjacent peaks in the HRR being significant contributors. For both strategies, non-adjacent  $f_0$ 's are significant between 750 and 2000 Hz.

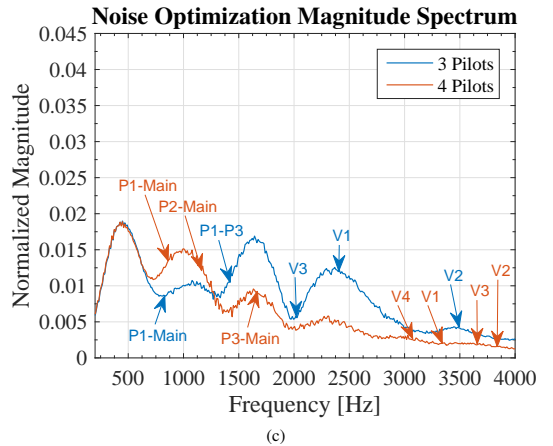
For the triple-pilot strategy, the source of the bump at about



(a)



(b)



(c)

Figure 7: Ensemble averaged HRR, weighted RRHR values, and magnitude spectrum for the noise optimization case.

1650 Hz cannot be identified as some  $f_0$  in the HRR. The positioning of V3 in the magnitude spectrum is also odd considering its weighted RRHR value. However, it is helpful to recall that the  $f_0$ 's are an estimates of the frequency defining a valley between adjacent peaks. Considering the shape of V3 in the HRR at 3 CAD aTDC, it is clear that higher frequency content is also required to describe it. This will push the true frequency content of V3 upwards, and it is likely that V1 and V3 share similar frequency content.

Unfortunately, due to technical difficulties, the FSN measurement for each of these strategies was not captured. A backup opacimeter can give some insight between them, but not also with relation to the baseline strategy. The results from the opacimeter show a 100% increase in soot for the quadruple-pilot strategy.  $\text{NO}_x$  levels are identical for both cases at 0.5 g/kWh.

#### 4.6. Consideration of other HRR profiles

In additional investigations, the mass of the pilots was changed to produce different HRR profiles. The intent was to search for further evidence that the HRR should tend towards a linear progression for minimum noise. One sweep targeted equal HRR peaks for the pilot combustion events. When running online with a 2-period HRR calculation, this was largely achieved. However, due to the poor control over the injector behavior, the dwells varied too much for direct comparisons to be drawn. Another sweep had different levels of sequentially increasing peaks during the pilot combustion phase. This was referred to as the stair peaks sweep. Again, due to large errors in both delivered mass and dwell, too many confounding errors precludes in-depth analyses. The HRR profiles for these sweeps are found in the appendix in Figures A.9 and A.10. The strategies themselves, however, are valid for further testing of the weighted average RRHR and PPRR as predictors of noise. They are included only for more stringent vetting of those metrics.

#### 4.7. Predictors of Combustion Noise

As found throughout the detailed investigations of the injection strategies and boundary conditions considered, weighted average RRHR values are found to follow the changes in combustion noise, while PPRR values do not. Figures 8a and 8b show linear regressions of these metrics for prediction of combustion noise levels. The model for weighted average RRHR has a coefficient of determination of 0.934, while the one for PPRR is less than half that at 0.434. The scatter of the data does not suggest a higher order model would be more appropriate. Considering the y-intercept of the weighted average RRHR model, a truly linear HRR (weighted RRHR = 0) should produce a combustion noise level of 73.2 dB. Based on the noise optimized cases, this is a fairly reasonable lower noise limit at this speed-load point. Trying to understand the minimum achievable noise based on PPRR in a similar manner is not possible.

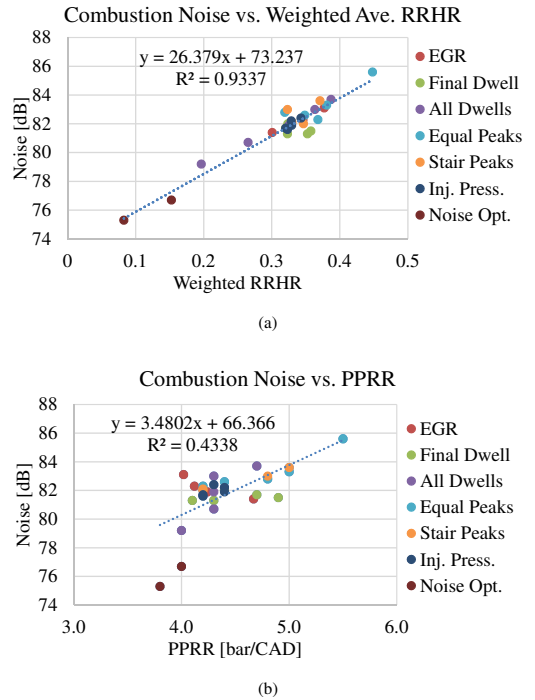


Figure 8: Weighted average RRHR and PPRR as predictors of combustion noise for the operating points in this study.

## 5. Conclusions

Several variations of closely-coupled multiple-pilot diesel injection strategies have been experimentally investigated. Pilot injection timing, mixture dilution, and injection pressure have been investigated to understand the effects on the combustion progression, emissions, and combustion noise levels. Then, utilizing those learnings, triple and quadruple pilot injection strategies have been created to achieve minimum combustion noise at the same speed-load point and combustion phasing. The main conclusions are as follows.

In order to minimize noise, dwell should be reduced and dilution increased without causing excessive blending of individual pilot combustion events. Extremes of either cause the bulk portions of separate injections to combust as a group, leading to more aggressive combustion.

Minimum noise is achieved by shaping the HRR to as linear a progression as possible. This was achieved in part through injection rate shaping, which occurs when there is no hydraulic separation between injections but the flow rate still changes.

For a better balance of combustion noise and emissions, higher rail pressure can significantly decrease soot emissions without significantly increasing combustion noise. This is beneficial since high dilution ratios are desired to achieve both lower NO<sub>x</sub> and noise levels.

PPRR is not a good predictor of combustion noise for the injection strategies studied, leading to a coefficient of determination of only 0.434. The pressure traces of closely-coupled multiple-pilot injection strategies are too complex to be described by such a simple metric.

As shown in prior works, individual RRHR values are good indicators for what potential is left for achieving a linear HRR within that specific HRR valley. Weighting those values based on the areas of each valley, however, is an improvement since they also indicate which valleys are significant contributors to combustion noise and which are not. Another benefit is the sum of those individual values to create the overall weighted average RRHR. This single value is a very good predictor of combustion noise at a constant load-speed point. This metric led to a coefficient of determination of 0.934 for predicting combustion noise.

The fundamental frequencies of the valleys are overlaid onto the magnitude spectrum plots. These indicate what specific valley should be modified in order to reduce the sound power of that valley (by shifting the frequency and/or decreasing the magnitude of the valley). However, the individual weighted RRHR values are also necessary in order to not be misled by coincidences of a specific valley aligning with a strong frequency range in the magnitude spectrum.

In rare occasions, considering the fundamental frequency of the peaks the HRR can identify important frequency content. However, these frequencies were not found to consistently correlate with important frequency in the pressure trace. Studying the valleys rather than the peaks leads to a better identification of strong frequency content in the combustion noise.

An overview of the magnitude spectrum plots shows that as the HRR becomes more complex and less sinusoidal, the com-

bustion noise will also be characterized by a broader, more complex spectrum. The opposite also holds true. When the fundamental frequencies of the valleys are all very similar, or combustion blending causes a more sinusoidal HRR, the frequency content of the combustion noise also narrows.

### Funding

This work was performed as a collaboration between Volvo Car Corporation and Lund University. It was funded through the KCFP Engine Research Center (Swedish Energy Agency project number 22485-3).

### Acronyms

$f_0$  fundamental frequency

**a** after

**CAD** crank angle degrees

**CAXX** crank angle at XX% of released heat

**EGR** exhaust gas recirculation

**HRR** heat release rate

**IMEP** indicated mean effective pressure

**LD** light duty

**MBT** maximum brake torque

**P1,2,...** peak 1, 2, etc. in the HRR

**RRHR** ratio of reduced heat release

**TDC** top dead center

**V1,2,...** valley 1, 2, etc. in the HRR



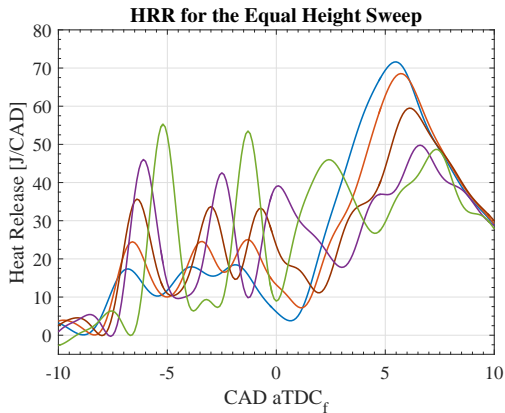


Figure A.9: Ensemble averaged HRR profiles for the different strategies investigated in the sweep intended to have even HRR peaks from the pilot injections. When using a 2-period HRR calculation, the HRR peaks are very close to level. However, due to large deviations in dwells, detailed conclusions are not drawn but the weighted average RRHR values are compared against combustion noise.

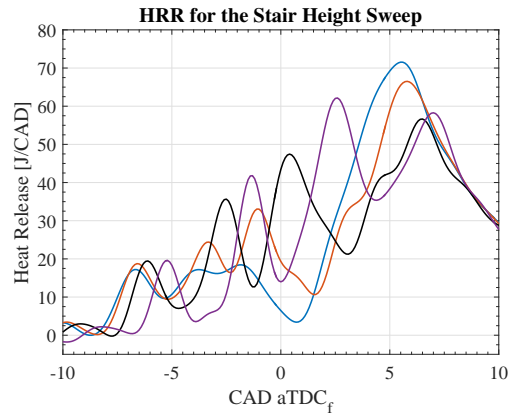


Figure A.10: Ensemble averaged HRR profiles for the different strategies investigated in the sweep intended to have a stair shaped progression in HRR peaks values. Due to large deviations in both delivered mass and dwells, detailed conclusions are not drawn but the weighted average RRHR values are compared against combustion noise.

## Appendix A.

## References

- [1] Delphi, Worldwide emissions standards, passenger cars and light duty vehicles, Booklet, G.D. of Luxembourg (2019).
- [2] D. Schöppe, F. Atzler, O. Kastner, F. Kapphan, High Performance Diesel Direct Driven Piezo Common Rail Injection System, in: 23rd Aachen Colloquium Automobile and Engine Technology 2014, Aachen, 2014, pp. 773–790.
- [3] J. Hagen, O. E. Herrmann, J. Weber, D. Queck, Diesel Combustion Potentials by Further Injector Improvement, MTZ (2016) 16–21.
- [4] D. Zeh, J. Hammer, C. Uhr, M. Rückle, A. Rettich, B. Grota, W. Stöcklein, J. Gerhardt, D. Naber, M. Raff, Bosch Diesel Injection Technology - Response for Every Vehicle Class Production, 23rd Aachen Colloquium Automobile and Engine Technology 2014 (2014) 757–772.
- [5] S. Busch, K. Zha, P. C. Miles, A. Warey, F. Pesce, R. Peterson, A. Vassallo, Experimental and Numerical Investigations of Close-Coupled Pilot Injections to Reduce Combustion Noise in a Small-Bore Diesel Engine, SAE Int. J. Engines 8 (2015) 660–678. doi:10.4271/2015-01-0796.
- [6] T. Tanaka, A. Ando, K. Ishizaka, Study on pilot injection of DI diesel engine using common-rail injection system, JSAE Review (3) (2002) 297–302. doi:10.1016/S0389-4304(02)00195-9.
- [7] S. Mendez, B. Thirouard, Using Multiple Injection Strategies in Diesel Combustion: Potential to Improve Emissions, Noise and Fuel Economy Trade-Off in Low CR Engines, SAE Int. J. Fuels Lubr. (2008) 662–674doi:10.4271/2008-01-1329.
- [8] M. Denny, F. Holst, A. Helmantel, H. Persson, P. Tunestål, Ö. Andersson, Impact of closely-coupled triple-pilot and conventional double-pilot injection strategies in a LD diesel engine, Fuel 246 (February) (2019) 141–148. doi:10.1016/j.fuel.2019.02.101.
- [9] M. Denny, A. Matamis, Z. Wang, H. Persson, P. Tunestal, M. Richter, Ö. Andersson, Optical Investigation on the Combustion Process Differences between Double-Pilot and Closely-Coupled Triple-Pilot Injection Strategies in a LD Diesel Engine, no. 2019-01-0022, 2019. doi:10.4271/2019-01-0022.
- [10] M. Denny, A. Matamis, H. Persson, M. Richter, Ö. Andersson, Interaction between Fuel Jets and Prevailing Combustion during Closely-Coupled Injections in an Optical LD Diesel Engine, no. 2019-01-0551, 2019.
- [11] T. Husberg, I. Denbratt, A. Karlsson, Analysis of Advanced Multiple Injection Strategies in a Heavy-Duty Diesel Engine using Optical Measurements and CFD-Simulations, SAE Technical Paperdoi:10.4271/2008-01-1328.
- [12] J. Lee, J. Jeon, J. Park, C. Bae, Effect of Multiple Injection Strategies

on Emission and Combustion Characteristics in a Single Cylinder Direct- Injection Optical Engine, SAE Technical Paper.

- [13] N. Möller, M. Fleiss, S. Rengmyr, J. Somhorst, VEA the new engine architecture from Volvo, MTZ Available at [http://link.springer.com/10.1007/978-3-658-05016-0\\_4](http://link.springer.com/10.1007/978-3-658-05016-0_4).
- [14] A. J. Shahlari, C. Hocking, E. Kurtz, J. Ghandhi, Comparison of Compression Ignition Engine Noise Metrics in Low-Temperature Combustion Regimes, SAE Int. J. Engines (2013) 541–552 doi:10.4271/2013-01-1659.
- [15] J. B. Heywood, Internal Combustion Engine Fundamentals, McGraw-Hill, New York, 1988.
- [16] S. Fischer, J.-O. Stein, Investigation on the Effect of Very High Fuel Injection Pressure on Soot-NOx Emissions at High Load in a Passenger Car Diesel Engine, SAE International Journal of Engines 2 (1) (2010) 1737–1748. doi:10.4271/2009-01-1930.
- [17] H. Dembinski, H.-E. Angstrom, Swirl and Injection Pressure Impact on After-Oxidation in Diesel Combustion, Examined with Simultaneous Combustion Image Velocimetry and Two Colour Optical Method, in: SAE Technical Paper Series, Vol. 1, 2013. doi:10.4271/2013-01-0913.
- [18] C. A. Idicheria, L. M. Pickett, Formaldehyde Visualization Near Lift-off Location in a Diesel Jet, SAE Technical Paper doi:10.4271/2006-01-3434.
- [19] Ö. Andersson, P. C. Miles, Diesel and Diesel LTC Combustion, Wiley, 2014, pp. 1–36. doi:10.1002/9781118354179.auto120.

# Notes

---

# Notes

---

# Notes

---